École doctorale 209 : Sciences physiques et de l'ingénieur

THÈSE

pour obtenir le grade de docteur délivré par

Université de Bordeaux

Spécialité doctorale "Laser, Matière, Nanosciences"

présentée et soutenue publiquement par

Paul Gersberg

le 20 juillet 2020

Confinement and driving effects on continuous and discrete model interfaces

Directeur de thèse : **David S. Dean**
Co-directeur de thèse : **Peter C.W. Holdsworth**

Jury

Steve Bramwell, University College London,	Professeur	Rapporteur
Jorge Kurchan, ENS Paris,	Directeur de recherche	Rapporteur
Pierre Pujol, LPT Toulouse ,	Professeur	Examinateur
Jérôme Cayssol, LOMA,	Professeur	Examinateur

Université de Bordeaux
Laboratoire Onde Matière d'Aquitaine
351 Cours de la Libération, Talence, France

Effets d'écoulements et de confinement dans les modèles discrets et continus d'interfaces

Cette thèse examine les propriétés de l'interface entre deux phases dans un système avec des phases séparées. Nous regardons comment les effets de taille finis modifient les propriétés statistiques de ces interfaces, en particulier comment la dépendance de l'énergie libre par rapport à la taille du système donne lieu à des interactions de Casimir critique à longue portée proche du point critique. Souvent, les interfaces sont décrites par des modèles simplifiés ou coarse-grained dont les seuls degrés de liberté sont les hauteurs de l'interface. Nous rappelons comment les propriétés statiques et dynamiques de ces interfaces sont retrouvées à partir de modèles microscopiques de spins et de théorie statistique des champs. Nous étudions ensuite les effets de taille finie pour les interfaces continues comme le modèle Edwards-Wilkinson ou discrètes comme le modèle Solid-On-Solid, et discutons leur pertinence dans le cadre de l'effet Casimir critique.

Dans la seconde partie de la thèse, nous examinons des modèles d'interfaces sous écoulement qui possède des états stationnaires hors-équilibres. Nous développons ces équations dans le cadre du modèle C d'une interface, qui a un état stationnaire hors-équilibre lorsque soumis à un écoulement uniforme. L'état stationnaire hors-équilibre résultant exhibe des propriétés retrouvées dans les expériences sur des colloïdes sous cisaillement, notamment la suppression des fluctuations de la hauteur de l'interface et une augmentation de la longueur de corrélation des fluctuations. Finalement, nous proposons un nouveau modèle pour des interfaces uni-dimensionnelles qui est une modification du modèle Solid-on-Solid qui contient un terme supplémentaire d'entropie, ce qui le rend plus approprié pour l'étude de la diffusion et du cisaillement.

Keywords : Modèles d'interface, Théorie d'ordonnancement des phases, Modèle d'Ising, Modèle Solid-On-Solid, Force de Casimir, Écoulements stationnaires hors-équilibre

Confinement and driving effects on continuous and discrete model interfaces

This thesis examines the properties of the interface between two phases in phase separated systems. We are interested in how finite size effects modify the statistical properties of these interfaces, in particular the dependence of the free energy on the system size gives rise to long range critical Casimir forces close to the critical point. Often the interfaces in phase separated systems are described by simplified or coarse grained models whose only degrees of freedom are the interface height. We review how the statics and dynamics of these interface models can be derived from microscopic spin models and statistical field theories. We then examine finite size effects for continuous interface models such as the Edwards Wilkinson model and discrete models such as the Solid-On-Solid model and discuss their relevance to the critical Casimir effect. In the second part of the thesis we examine models of driven interfaces which have nonequilibrium steady states. We develop a model C type model of an interface which shows a nonequilibrium steady state even with constant driving. The resulting nonequlibrium steady state shows properties seen in experiments on sheared colloidal systems, notably the suppression of height fluctuations but a increase in the correlation length of the fluctuations. Finally we propose a new model for one dimensional interfaces which is a modification of the solid-on-solid model and which contains extra entropic terms which make it more appropriate to study diffusive dynamics and driving.

Keywords : Interface models, phase ordering dynamics, Ising model, Solid-On-Solid model, Casimir force, driven nonequilibrium steady states

Résumé en français

La majorité des systèmes statistiques peuvent être décrits par un paramètre d'ordre, comme la magnétisation moyenne dans les systèmes magnétiques, la densité dans un fluide ou l'orientation moyenne des polymères dans les cristaux liquides. Les propriétés statiques et dynamiques de tels systèmes est bien décrite par la théorie statistique des champs. Dans cette théorie, le champ ϕ est soumis à un hamiltonien $H(\phi)$, et ses propriétés peuvent être dérivée de la fonction de partition Z. Lorsque ces systèmes possèdent une transition de phase au point critique, il y a une discontinuité de l'énergie libre due à la modification des micro-configurations possibles. Dans les systèmes magnétiques, on passe ainsi d'une magnétisation nulle à une magnétisation finie, les liquides qui étaient auparavant mélangés se séparent, et les polymères adoptent une direction moyenne commune. Dans la phase ordonnée on retrouve alors des composantes connexes où la valeur de ϕ est quasi-constante. Entre ces composantes connexes se situe l'interface entre les phases. Dans cette thèse, nous nous intéressons particulièrement aux propriétés statiques et dynamiques des interfaces dans des modèles continus et discrets avec des contraintes telles que le confinement ou le cisaillement.

Description d'une interface

La première partie de cette thèse est consacrée à la description des interfaces à partir de la théorie statistique des champs. L'utilisant un champ externe ϕ^4 dans l'Hamiltonien induit une séparation de phase en dessous de la température critique, ce qui donne une interface dont le profil peut-être calculé grâce aux équations dynamiques du modèle A dans le cas stationnaire. L'énergie libre associée à cette interface est directement reliée à la tension superficielle σ par la relation de Cahn-Hilliard. Depuis les équations de théorie statistique des champs, en considérant une interface d'épaisseur nulle, on retrouve les équations d'Edwards-Wilkinson pour le modèle A et le modèle B. La réduction du nombre de degrés de liberté par cette transformation d'un volume en surface permet leur étude grâce à des intégrales de chemin, qui seront détaillées plus tard.

Ensuite nous expliquons le modèle le plus simple sur réseaux, le modèle d'Ising, qui décrit un réseau orthogonal de spins avec une interaction uniquement entre les plus proches voisins et un champ externe. Ce modèle, où chaque site du réseau prend la valeur $\sigma_1 = \pm 1$, permet également de modéliser un système de gaz sur réseau ou de liquides binaires en faisant un changement de variable sur σ_i. En appliquant la même approximation d'interface d'épaisseur nulle que précédemment, on trouve cette fois-ci le modèle Solid-On-Solid. La fonction de partition SOS a l'avantage d'être diagonalisée grâce à la matrice de transfert, dont le formalisme est développé. Dans la limite thermodynamique, seul l'état fondamental (qui possède la plus grande valeur propre de la matrice de transfert) est nécessaire pour obtenir toutes les observables du système.

Dans ce premier chapitre, une grande importance est également donnée quant à la différence entre les différents ensembles statistiques. La complexité de l'ensemble canonique provient de la contrainte sur la hauteur totale de l'interface qui ne peut être intégrée au formalisme des matrices de transfert. Pour étudier ces différences, il faut donc utiliser des méthodes numériques. Dans l'ensemble canonique, il est également possible d'introduire des états stationnaires hors-équilibre

grâce à l'advection d'un champ de vitesse, que nous introduisons ici mais discuterons dans le dernier chapitre.

Méthodes numériques

Dans ce chapitre, nous développons le fonctionnement des simulations de Monte Carlo Métropolis, qui permettent d'explorer l'espace des configurations et ainsi obtenir les valeurs moyennes d'observables. Ces méthodes sont particulièrement adaptées aux systèmes sur réseau comme le modèle d'Ising ou Solid-On-Solid, et on utilise alors l'algorithme de Glauber ou de Kawasaki selon l'ensemble thermodynamique dans lequel on se place.

Néanmoins, l'énergie libre n'est pas une valeur mesurable directement dans les simulations de Monte Carlo, et il faut alors utiliser des méthodes indirectes. La méthode de Vasilyev consiste à découpler progressivement une rangée du système afin d'obtenir la dérivée de l'énergie libre par rapport à la taille du système. Cette méthode ne fonctionnant pas dans le cas du modèle SOS à cause de l'absence de terme de volume dans son hamiltonien, on utilise alors la méthode Lopes-Jacquin-Holdsworth, qui a été développée dans le cas d'un champ magnétique uniforme. Puisque l'intensité du champ magnétique est la valeur conjuguée de la magnétisation totale, on calcule alors l'intégrale de la magnétisation entre deux intensités afin d'obtenir la différence entre l'énergie libre des deux systèmes. Puisque cette méthode utilise la magnétisation, elle ne peut donc pas être utilisée lorsque le paramètre d'ordre est conservé, ce qui nous mène à une conclusion : il n'existe pas de méthode pour la mesure de l'énergie libre dans des simulations numériques de Kawasaki pour le modèle SOS.

Le chapitre se termine avec une petite liste d'astuces à connaître pour celui qui désirerait reproduire mes résultats numériques, principalement sur l'optimisation du code et la parallélisation.

Interfaces à l'équilibre et effets de taille finie

Lorsque la longueur de corrélation est du même ordre de grandeur que la taille du système, la contrainte imposée sur les modes mous de fluctuations ajoute une partie singulière à l'énergie libre. Cette dépendance de l'énergie libre en fonction de la taille du système implique une force thermodynamique qui s'appelle force de Casimir dans le cas des fluctuations du champ électromagnétique entre deux plaques diélectriques parfaitement conductrices, ou effet Casimir critique dans les systèmes critiques. Après avoir exposé ces deux effets grâce à la mécanique quantique et le groupe de renormalisation, nous étudions cette force de confinement dans le cas des interfaces confinées.

En utilisant le formalisme de Matsubara pour l'équation du propagateur de l'hamiltonien dans le cas d'une interface continue soumise à champ externe, nous explicitons la distribution de probabilité de l'interface, l'énergie libre, la fonction de corrélation à deux points et la longueur de corrélation en fonction de l'énergie de l'état fondamental et du premier état excité. En appliquant ce formalisme à une interface libre et confinée, on retrouve des résultats connus sur la force thermodynamique. Dans le cas où cette interface ne possède pas de tension superficielle (comme c'est le cas dans les systèmes critiques), la correction de taille finie à la tension superficielle proposée par Privman nous permet de retrouver quantitativement le même comportement que pour la force de Casimir critique. Nous utilisons également ce formalisme dans le cas où l'interface est confinée à cause d'une pression afin de trouver la hauteur de moyenne de l'interface et sa variance.

Puisque la méthode Lopes-Jacquin-Holdsworth de calcul de l'énergie libre dans les simulations de Monte Carlo n'est pas utilisable dans la dynamique de Kawasaki et que la méthode de Vasilyev ne l'est pas non plus pour les modèles SOS, nous généralisons la méthode LJH pour des champs externes non-uniformes, ce qui permet l'intégration sur une magnétisation généralisée qui n'est plus conservée dans une dynamique de Kawasaki. Nous montrons que cette généralisation est en accord avec la

matrice de transfert SOS, et observons le même comportement de l'énergie libre pour les dynamiques de Glauber et de Kawasaki.

Ce troisième chapitre s'achève par la diagonalisation exacte de la matrice de transfert du modèle SOS en absence de potentiel externe, généralisant ainsi les résultats de Privman, et nous étudions les limites à faible et haute température ainsi que dans la limite thermodynamique.

Le modèle Particles-Over-Particles

Le modèle SOS est un modèle d'interface provenant de l'approximation à basse température du modèle d'Ising. Nous développons dans ce quatrième chapitre un nouveau modèle : le modèle POP. Ce nouveau modèle prend en compte le terme d'entropie associé au modèle d'Ising et qui se retrouve aisément lorsque l'on fait des simulations numériques sur Ising, mais qui font défaut dans SOS. Ce terme d'entropie apparaît lorsque l'on considère non plus juste la hauteur de l'interface (comme dans SOS), mais également le nombre de particules en dessous. En labellisant ainsi les particules, il devient possible de créer des modèles avec M types différents de particules, chacune étant régie par un coefficient cinétique ou un coefficient de diffusion dans le cas où elles appartiennent à des ensembles thermodynamiques différents. Nous finissons le chapitre en montrant comment procéder aux simulations numériques dans ce modèle, que nous comparons à la matrice de transfert.

Interfaces stationnaires hors-équilibre

Lorsqu'une interface est advectée par un champ de vitesse, sa largeur et sa longueur de corrélation sont modifiées. Le cinquième et dernier chapitre s'intéresse à un écoulement uniforme et constant.

À cause de l'invariance galiléenne de translation dans le référentiel de l'écoulement, l'équation dynamique du modèle B reste inchangée. Le cas d'un champ soumis au modèle B et couplé à un autre champ soumis au modèle A (afin de briser l'invariance galiléenne) a été l'objet d'un article publié dans **Journal of Statistical Mechanics: Theory and Experiment** en mars 2020, et la première partie de ce chapitre est une reproduction de l'article original. À partir des équations couplées donnant le modèle C, on trouve une relation fermée pour la dynamique d'une interface soumis à un écoulement uniforme et constant dans l'espace de Fourrier. Cette méthode donne est valable pour une théorie gaussienne de l'interface, et l'écoulement introduit de la nouvelle physique, principalement que la tension de surface effective du système ainsi que la longueur de corrélation des fluctuations de l'interface sont augmentées. Ces résultats sont en accord qualitative avec les expériences de cisaillement sur les colloïdes. Tandis que la théorie sur les grandes longueurs d'onde que nous trouvons se comporte comme celles d'une onde capillaire, nous trouvons les ordres suivants qui sont générés par le spectre de la hauteur des fluctuations. De plus, nous montrons comment ce modèle permet de décrire l'interface entre deux phases de colloïdes ayant une activité différente en jouant sur la température de chaque phase, ce qui nous donne de nouveaux résultats que nous ne pourrions trouver dans le cas à l'équilibre.

Nous passons ensuite aux modèles sur réseau, et étudions la dépendance de la variance des hauteurs et de la tension superficielle de l'interface SOS en fonction de l'écoulement. Dans le cas POP à deux types de particules, nous développons un formalisme très similaire à celui de l'article publié qui montre comment l'augmentation de l'écoulement induit un découplage dans la fonction de corrélation entre les différents types de particules dans la limite où l'écoulement est infini.

Contents

Introduction

Most statistical mechanical models can be described using an order parameter, such as the mean magnetization in a magnetic system, the density of a liquid or gas or the average orientation of liquid crystals [1]. During a continuous phase transition, the correlation length diverges [2]. When the correlation length becomes of the same order of magnitude as the experimental or numerical system size, finite size effect become stronger, leading to interesting new physics, for example the critical Casimir effect [3].

In a system where the order parameter is conserved, or when it is fixed at values corresponding to two different phases, an interface is formed between the two phases. In systems with a rectangular geometry this interface is at a first order of approximation flat as the system tends to minimise the area between the two phases to minimize the interfacial energy generated by the surface tension. However thermal fluctuations induce fluctuations of the interface. From a theoretical point of view, one can study the statistical properties, both static and dynamic, of interfaces between two phases through different though complementary methods. Historically, the first method was through lattice models, and more precisely the Ising model [4]. Those models are well-suited for numerical analysis due to their discrete nature, while posing analytical challenges due to the large number of degrees of freedom. Analytic studies of the interface are limited to two dimensional systems [5]. Numerical simulations of phase separated Ising models are straightforward, however the identification of the interface and even an unambiguous definition of the position of the interface are not obvious. For this reason coarse grained models of the interface have been proposed.

For instance, the Solid-On-Solid model [6] is an approximation of the Ising model in d dimensions which describes the position of an interface under certain simplifying circumstances. For two dimensional Ising systems this means that the transfer matrix method can be applied either analytically or numerically and the results are directly comparable with numerical simulations. Coarse graining the Ising model leads the Landau-Ginzburg Hamiltonian description in terms of a continuous field [7]. Using this description on can derives approximate descriptions for both the dynamics and statics of the interface. In particular within this formalism the effective partition function of the interface describes a random walker in a potential, then using path integrals [8] two dimensional systems can be analysed using a quantum mechanical treatment.

When modeling experiments using statistical mechanics it is important to identify the correct thermodynamic ensemble to describe the system. For instance in an Ising spin which describes interacting spins with $s = \pm 1$ the total magnetisation is not necessarily conserved as a single spin can change its sign. However if the spins are regarded as fixed but can exchange with each other by swapping sites (to describe a lattice gas for example), the overall all magnetization is fixed. In the latter case the magnetization is thus fixed and so the two ensembles are clearly different. It is thus interesting to study how ensemble differences in the underlying lattice model affect the statics and dynamics of interfaces in these models.

The thesis' outline is as following :

- In the first chapter we discuss interface. We explain how there statics can be modeled in terms of various discrete and continuous interface models. In particular we review phase ordering kinet-

ics for the evolution of the order parameter in coarse grained systems. From this one can deduce using a method introduced by Bray and coworkers [9] to derive the equilibrium dynamics of the interface. We then discuss discrete models and discuss the links between Ising and lattice gas models and the appropriate thermodynamic ensembles. The approximate description of these systems in terms of Solid-On-Solid type models is then addressed as well as their solution via the transfer matrix method. Finally we discuss the case of interfaces which are driven and whose steady states are non-equilibrium ones, giving some examples of numerical simulations and experimental results which motivate our later study of driven interface models for model C type systems.

- In the second chapter we discuss the basis of numerical simulations [10] for lattice systems, and in particular two methods to compute the free energy for equilibrium systems. In the first method by Vasiliyev et al, we compute its derivative with respect to the system size by decoupling a layer of the system [11], which for SOS models does not work. For interface models, we thus have to use the Lopes-Jacquin-Holdsworth method [12] which gives the difference of free energy between two points in parameter-space by integrating over the total magnetization. We also discuss some numerical tips we have found particularly useful.

- The third chapter is devoted to finite size effects for various models. A particularly interesting manifestation of finite size effects is the so called Casimir interaction [13]. For completeness we describe the original quantum calculation of Casimir for two perfectly conducting plates at zero temperature [14]. Then we discuss the generalization to arbitrary dielectric materials,the so called Lifshitz theory [15]. We then explain the critical Casimir effect which was first predicted by Fisher and de Gennes, this due to thermal, rather than quantum, fluctuations in critical or near critical systems. A natural question to ask is whether interface models can capture the same finite size scaling as predicted by Fisher and de Gennes. To this end we analyse finite size effects for an number of interface models for two dimensional systems. First we analyse continuous elastic line models where the underlying interface is described by a Brownian motion in an external potential. These models have been studied extensively in the literature but we find a number of new results. First we consider an elastic surface (corresponding to the Edwwards-Wilkinson model) confined between two hard walls. The resulting free energy is well known and does not correspond to what is expected from the critical Casimir effect. However we show that by including a phenomenological finite size correction to the surface tension (or line stiffness) proposed by Privman [16] one can recover the quantitative form predicted by the critical Casimir effect. We also derive the statistics of the equilibrium interface, in particular the fluctuations of the integrated height (corresponding to the average magnetisation in a spin model). Then we analyse the so called Airy line, corresponding to an interface above a hard wall but with a linear potential (corresponding to an applied pressure in the constant pressure ensemble) pushing the interface toward the wall.

  Then, we generalize the LJH method [12] for the free energy's measurement in numerical simulations for any external field, which allows to use it in conserved dynamics. The method is used in the case of an exotic potential in SOS, both in Glauber and Kawasaki dynamics, in agreement with transfer matrix results.

  Finally we examine finite size effects in the Solid-on-Solid model. These were first analysed in [16], however we give an alternative derivation which allows one to compute the correlation length and also show that for large systems the physics is essentially the same as for continuum Brownian models and determine the effective surface tension.

- In the fourth chapter we introduce a new $d-1$ lattice model similar to SOS in which we have taken into account the entropy. This model, that we call Particles-Over-Particles, takes the lit-

teral definition of the height of the interface by assuming the existence of particles under it. Through this lens, we are able to form systems with many different types of particles which are in different statistical ensembles and different activities, and we develop the mixed Glauber-Kawasaki dynamics in such case.

- The last chapter is explains how uniform driving alters the properties of the interface. The first section is essentially a published paper [17], where we consider an interface model which can be driven out of equilibrium by a uniform driving field. In order for a uniform field to have an effect on the system we introduce two fields, a colloidal field with model B conserved dynamics and a solvent field with model A dynamics. This combination of dynamics is called model C dynamics [18]. The system is driven out of equilibrium by assuming that the driving acts only on the colloidal field. Using the method of Bray et al [9] we derive the interface dynamics and compute its correlation function in the resulting non-equilibrium steady state. The properties are considerably different to the standard capillary wave properties of equilibrium surfaces and some of the results can be interpreted in terms of an effective surface tension. The calculations exhibit some of the phenomenology seen in experiments on sheared interface [19]. Finally we discuss the same model without driving but with different temperatures for the two fields to simulate active colloid systems, again a rich phenomenology of non-equilibrium states emerges. Afterwards we discuss uniform driving in SOS and POP models and their likeness with model C dynamics stated prior.

Chapter 1

Equilibrium interface dynamics

In this chapter we will analyse the dynamics of statistical systems. The analysis will allow us to understand how phase transitions - in particular those who possess a phase separation - occur dynamically [18]. The most famous example is the Ising model without any external field, its order parameter being the total magnetization.

In the high temperature phase, the system is homogeneous and its total magnetization is zero. Below the critical temperature, when the order parameter is conserved (for example with a Kawasaki dynamic or Model B), the system will locally separate into two phases of opposite mean magnetization separated by and interface, this interface minimizing the surface energy between both phases. When the order parameter is not conserved (for example Glauber dynamics or Model A), a spontaneous symmetry breaking will make one of the two phases take over the whole system. In a continuous phase transition where the critical point is reached from the disordered state to the ordered stated, the domain size, which is equal to the system's correlation length, diverges close to the critical temperature T_C. In a thermodynamical system, it becomes infinite, implying that the system takes an infinite amount of time to reach equilibrium : it's the critical slowing down. The process of domain growth is known as coarsening and phase ordering kinetics is the theory that has been developed to understand the phenomenon of coarsening[22]. In Fig 1.1, we show an example of coarsening in the Ising model with respect to time.

Furthermore, for systems with a conserved order parameter which separate into two phases, the two phases will be separated by an interface. This interface will be characterised by a surface tension, its average position will be fixed but it will exhibit fluctuations. Later we will see how model of phase ordering kinetics and be used to determine the static and dynamical properties of interfaces between two coexisting phases.

While the phase diagram of a system can be determined via its Hamiltonian and equilibrium statistical mechanics, the dynamics of coarsening depends on the details of the systems dynamics that do not show up in single time thermodynamic observables. Therefore, one needs to construct dynamical models that capture the underlying evolution of the state of the system. In particular, there is a big difference between systems where the order parameter is conserved and those where it is not conserved.
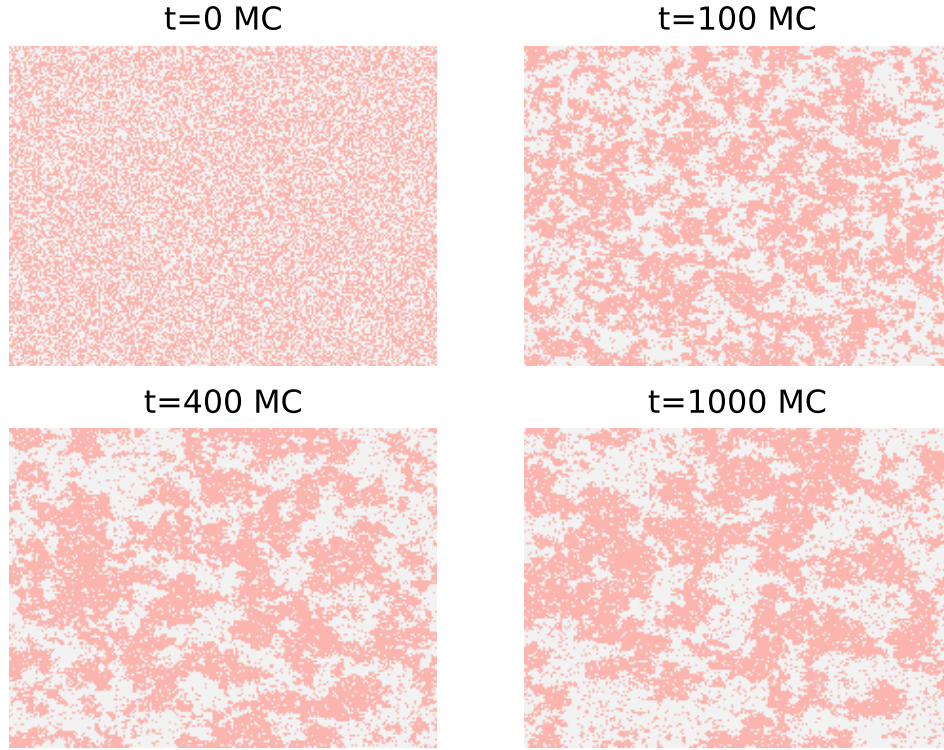
Figure 1.1: Numerical simulations of coarsening from a quench from a disordered state T = ∞ to an ordered state T = $T_{2D,C}$ [23] for different times, in Monte Carlo steps, for a 600 × 600 system with non-conserved Glauber dynamics.

1.1 Models for equilibrium fields

1.1.1 Statics of systems with a finite number of degrees of freedom

Thermodynamic systems are naturally described in terms of fields, for example densities.

Measuring observables in experimental setups means to measure the derivative of the partition function Z with respect to its conjugate variable. This measure is done with a certain degree of spatial and temporal resolution, which means in a statistical language that they measure the average of the observable over some space and time. If $\Phi(\mathbf{x}, t)$ is the physical field of our system, our device having a temporal resolution of Δt and a spatial resolution over a volume V will measure

$$\phi(\mathbf{x}, t) = \frac{1}{V\Delta t} \int_{t-\Delta t}^{t} dt' \int_{V} d\mathbf{x}' \Phi(\mathbf{x}', t') \tag{1.1}$$

This means that one is naturally lead to consider statistical field theories where the system is described in terms of a local field $\phi(\mathbf{x}, t)$. Statistical field theories can be applied to both statics, to understand phase diagrams, and dynamics to understand phase ordering. However to start with we will examine the case of systems with a finite number of degrees of freedom.

Consider a system in the canonical ensemble with a Hamiltonian H(**q**) where q_i for $1 \leq i \leq$ N represent a finite number of continuous spatial degrees of freedom and where in a classical system

we have already integrated over the corresponding momenta. The partition function for the system is given by

$$Z = \int d\mathbf{q} \exp\left(-\beta H(\mathbf{q})\right) \tag{1.2}$$

In general the integral which gives the partition function cannot be computed analytically. In equilibrium, the probability density function $P_{eq}(\mathbf{q})$ of the degrees of freedom is given by

$$P_{eq}(\mathbf{q}) = \frac{\exp\left(-\beta H(\mathbf{q})\right)}{Z} \tag{1.3}$$

The simplest approximation to compute Z is the mean field approximation where the integral is approximated by the integrand at its largest value - in mathematics this is the Laplace method for approximating an integral and in this context it is just an expansion about the minimum energy configuration of the system. The mean field approximation is thus

$$Z_{\mathrm{MF}} = \exp\left(-\beta H(\mathbf{q}^*)\right) \tag{1.4}$$

where $\mathbf{q}^*$ is the value of $\mathbf{q}$ which minimises H (note that the approximation becomes exact in the zero temperature limit - $\beta \to \infty$ - as the system will minimise its energy). The values q_i^* are determined from

$$\frac{\partial H}{\partial q_i}\big|_{\mathbf{q}=\mathbf{q}^*} = 0 \tag{1.5}$$

Within this approximation any thermodynamic observable is given by

$$\langle f(\mathbf{q})\rangle = f(\mathbf{q}^*) \tag{1.6}$$

We now consider how one can model dynamics of such systems. We will look for a Langevin equation which is chosen to give the correct equilibrium Gibbs-Boltzmann distribution. We write

$$\frac{dq_i}{dt} = -L_{ij}\frac{\partial H(\mathbf{q})}{\partial q_j} + \eta_i(t) \tag{1.7}$$

where L_{ij} is a matrix which discuss later and $\eta_i(t)$ is zero mean Gaussian white noise with correlation function

$$\langle \eta_i(t)\eta_j(t')\rangle = \Gamma_{ij}\delta(t-t') \tag{1.8}$$

The Gaussian white noise represents the effects of thermal fluctuations on the system we assume that the correlation time of these fluctuations is extremely short with respect to the dynamics of the degrees of freedom q_i (in fact in critical systems the dynamics become very slow, critical slowing down, and this approximation becomes better and better as one approaches the critical point). There is no momentum term in this Langevin equation and for this reason it is often called the overdamped Langevin equation. Overdamped Langevin equations can also be derived staring from Newton's laws in the presence of friction, due to a solvent, and again white noise (again due to molecular collisions with the solvent) and by taking the limit where the frictional forces are greater than the acceleration term in Newton's equations (equivalent to setting the particle masses to zero).

As Eq. (1.8) is for a correlation function the matrix Γ_{ij} must be symmetric and cannot have any negative eigenvalues.

In the absence of noise or thermal fluctuations, so at zero temperature, the system will simply minimise its energy. Therefore if

$$\frac{\partial H(\mathbf{q})}{\partial q_j} = 0 \tag{1.9}$$

with no noise we have $\frac{dq_i}{dt} = 0$, that is to say it is the term $\frac{\partial H(\mathbf{q})}{\partial q_j}$ that drives the dynamics if there is no noise. As long as the matrix L_{ij}^{-1} exists the zero temperature dynamics will take the system to the local minimum of H and to the absolute minimum if there are no metastable configurations.

Under these assumptions, the Fokker-Planck equation for the probability density function of the degrees of freedom is

$$\frac{\partial p(\mathbf{q}, t)}{\partial t} = \frac{\partial}{\partial q_i} \left[\frac{1}{2} \Gamma_{ij} \frac{\partial p(\mathbf{q}, t)}{\partial q_i} + p(\mathbf{q}, t) L_{ij} \frac{\partial H(\mathbf{q})}{\partial q_j} \right] \tag{1.10}$$

This can be written as

$$\frac{\partial p(\mathbf{q}, t)}{\partial t} + \frac{\partial}{\partial q_i} J_i(\mathbf{q}, t) = 0 \tag{1.11}$$

where the $\mathbf{J}(\mathbf{q}, t)$ is the probability current. We now insist that the system is in equilibrium with zero current when $p(\mathbf{q}, t) = P_{eq}(\mathbf{q})$ as given by Eq. (1.3), this gives

$$\left[-\frac{\beta}{2} \Gamma_{ij} + L_{ij} \right] \frac{\partial H(\mathbf{q})}{\partial q_j} \tag{1.12}$$

and this holds for any choice of H is we chose

$$\Gamma_{ij} = 2TL_{ij} \tag{1.13}$$

where we have taken units where Boltzmann's constant $k_B = 1$.

1.1.2 Statistical field theory

We now consider a system with Hamiltonian $H[\phi]$ which depends on a continuous field $\phi(\mathbf{x})$. The partition function is given by a functional integral

$$Z = \int d[\phi] \exp(-\beta H[\phi]), \tag{1.14}$$

the functional integral over all possible fields ϕ can be taken as a limit where ϕ is defined at a finite number of points on a lattice and then the lattice spacing is taken to zero. In many cases, the system has been coarse grained and ϕ represents a spatially varying order parameter, for instance the local density averaged over some small volume. In this case the Hamiltonian H is strictly speaking a free energy and contains terms that depend on the temperature.

The mean field approximation to partition function is then given by

$$Z_{MF} = \exp(-\beta H[\phi_{MF}]) \tag{1.15}$$

where ϕ_{MF} is the mean field solution which minimises H. The definition of a functional derivative of a functional is

$$F[\phi + \delta\phi] - F[\phi] = \int d\mathbf{x} \frac{\delta F}{\delta\phi(\mathbf{x})} \delta\phi(\mathbf{x}) \tag{1.16}$$

Therefore if a field ϕ maximises H we must have

$$\frac{\delta H}{\delta\phi(\mathbf{x})} = 0 \tag{1.17}$$

We now consider the standard Landau-Ginzburg Hamiltonian [1] describing Ising like systems where

$$H[\phi] = \int d\mathbf{x} \frac{\kappa}{2} [\nabla\phi]^2 + V(\phi) \tag{1.18}$$
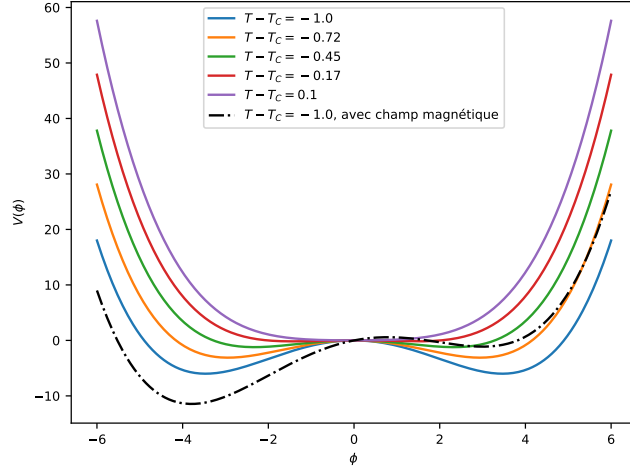
Figure 1.2: Double-well potential (1.19) for $\lambda = 1$ in function of the temperature difference with respect to the critical temperature with $m^2 = T - T_C$. In the ordered phase, the minima are at $\phi_C = \pm\sqrt{-\frac{6m^2}{\lambda}}$, while for the ordered phase it is at $\phi_C = 0$. In black, the addition of a uniform magnetic field $h(\mathbf{x}) = 1$ makes the positive phase metastable.

The first term represents an energetic cost of varying the field ϕ. The second potential term has two minima at $\phi = \pm\phi_c$, and, in the low temperature or phase separated phase, without loss of generality we can chose $V(\phi_c) = V(-\phi_c)$, while it has a single minimum at $\phi = 0$ in the high temperature phase.

The standard potential for phase separations, called the ϕ^4 model, is given by the double-well

$$V(\phi) = \frac{1}{2}m^2\phi^2 + \frac{\lambda}{4!}\phi^4 \tag{1.19}$$

where $m^2 = T - T_C$. For $m^2 < 0$, the minima are at $\phi_C = \pm\sqrt{-\frac{6m^2}{\lambda}}\pm$, while at $m^2 \geq 0$, the single minimum is at $\phi_C = 0$. We can also couple our system with the magnetic field of Hamiltonian

$$H_1 = -\int d^d x\, h(\mathbf{x})\phi(\mathbf{x}) \tag{1.20}$$

As we in Fig 1.2, the addition of an uniform external field does favour one phase over the other one.

It is easy to see that

$$\frac{\delta H}{\delta\phi(\mathbf{x})} = -\kappa\nabla^2\phi(\mathbf{x}) + V'(\phi) \tag{1.21}$$

If we compare with systems with a discrete number of variables we should have a Langevin equation of the form

$$\frac{\partial\phi(\mathbf{x})}{\partial t} = -L\frac{\delta H}{\delta\phi(\mathbf{x})} + \eta(\mathbf{x}, t) \tag{1.22}$$

The white noise correlator should have the form

$$\langle\eta(\mathbf{x}, t)\eta(\mathbf{x}', t)\rangle = \delta(t - t')\Gamma(\mathbf{x}, \mathbf{x}'), \tag{1.23}$$

where here $\Gamma(\mathbf{x}, \mathbf{x}')$ is an operator (before it was a matrix) defined by its action on functions f as

$$\Gamma f(\mathbf{x}) = \int d\mathbf{x}'\Gamma(\mathbf{x}, \mathbf{x}')f(\mathbf{x}') \tag{1.24}$$

and L is also an operator with

$$Lf(\mathbf{x}) = \int d\mathbf{x}' L(\mathbf{x}, \mathbf{x}') f(\mathbf{x}') \tag{1.25}$$

Following the same arguments for systems with a finite number of degrees of freedom we thus have the relation (which is sometimes called the fluctuation dissipation theorem as it essentially is equivalent)

$$\Gamma(\mathbf{x}, \mathbf{x}') = 2TL(\mathbf{x}, \mathbf{x}') \tag{1.26}$$

The simplest form of dynamics is given by $L(\mathbf{x}, \mathbf{x}') = \alpha\delta(\mathbf{x} - \mathbf{x}')$ which gives the **model A dynamics**

$$\frac{\partial\phi(\mathbf{x})}{\partial t} = -\alpha\frac{\delta H}{\delta\phi(\mathbf{x})} + \eta(\mathbf{x}, t) \tag{1.27}$$

with the noise correlator

$$\langle\eta(\mathbf{x}, t)\eta(\mathbf{x}', t)\rangle = 2T\alpha\delta(t - t')\delta(\mathbf{x} - \mathbf{x}') \tag{1.28}$$

The average value of ϕ

$$\overline{\phi}(t) = \frac{1}{V}\int d\mathbf{x}\,\phi(\mathbf{x}, t) \tag{1.29}$$

is clearly not generally conserved by this dynamics. Model A corresponds to a system in the grand-canonical ensemble, where α is the kinetic coefficient related to the relaxation time of the system [18].

Model B dynamics amounts to choosing

$$L(\mathbf{x} - \mathbf{x}') = -D\nabla^2\delta(\mathbf{x} - \mathbf{x}') \tag{1.30}$$

The fact that L is a positive semi-definite operator can be seen by taking its Fourier transform. The evolution equation here is

$$\frac{\partial\phi(\mathbf{x})}{\partial t} = D\nabla^2\frac{\delta H}{\delta\phi(\mathbf{x})} + \eta(\mathbf{x}, t) \tag{1.31}$$

where

$$\langle\eta(\mathbf{x}, t)\eta(\mathbf{x}', t)\rangle = -2TD\delta(t - t')\nabla^2\delta(\mathbf{x} - \mathbf{x}') \tag{1.32}$$

We notice that if we introduce the vectorial white noise with components $\eta_i(\mathbf{x}, t)$ such that

$$\langle\eta_i(\mathbf{x}, t)\eta_i(\mathbf{x}', t')\rangle = \delta_{ij}\delta(\mathbf{x} - \mathbf{x}')\delta(t - t) \tag{1.33}$$

where $\delta_{ij} = 1$ for $i = j$ and is zero otherwise, we can write

$$\eta(\mathbf{x}, t) = \nabla \cdot \boldsymbol{\eta}(\mathbf{x}, t) \tag{1.34}$$

as one can verify the two noises have the same correlation function. In this way Eq. (1.31) becomes

$$\frac{\partial\phi(\mathbf{x})}{\partial t} = \nabla \cdot [D\nabla\frac{\delta H}{\delta\phi(\mathbf{x})} + \boldsymbol{\eta}(\mathbf{x}, t)] \tag{1.35}$$

From this it is easy to see that the order parameter is conserved - thus model B describes conserved phase ordering dynamics. This model corresponds to the canonical ensemble, and is useful to describe diffusion or accretion systems.

Without the noise fluctuations, equations (1.27) and (1.31) are called the Time Dependant Ginzburg-Landau equation [24] and the Cahn-Hilliard equation[25] equations, which give the mean field's dynamics.

1.1.3 Surface tension

In order to minimize the free energy in a non-conserved system, we can simply choose $\phi(\mathbf{x}) = \phi_c$ or $\phi(\mathbf{x}) = -\phi_c$ everywhere, which corresponds to a free energy $F = H[\phi_c] = 0$. However in a system with a conserved order parameter

$$\int d\mathbf{x}\,\phi(\mathbf{x}) = 0 \tag{1.36}$$

the solutions $\phi = \pm\phi_c$ cannot hold. In this case the system will separate into two homogeneous phases where $\phi(\mathbf{x}) = \pm\phi_c$. We therefore choose an interface at $z = 0$ and take $\phi(\mathbf{x}) = \phi_K(z)$ (K standing for kink as it is known as the kink solution in the literature) where $\lim_{z\to\infty} = -\phi_c$ and $\lim_{z\to\infty} = -\phi_c$. We therefore find from Eq. (1.21) that

$$-\kappa\frac{d^2}{dz^2}\phi_K(z) + V'(\phi_K) = 0 \tag{1.37}$$

We can write

$$H[\phi_K] = A\int dz\,\frac{\kappa}{2}\left(\frac{d\phi_K(z)}{dz}\right)^2 + V(\phi_K(z)) \tag{1.38}$$

where A is the surface area of the system in the plane perpendicular to the direction z. However, if we multiply Eq. (1.37) by $d\phi/dz$ and integrate we find

$$-\frac{\kappa}{2}(\frac{d\phi_K}{dz})^2 + V(\phi_K) = C \tag{1.39}$$

where C is a constant. However as $\phi_K(z) \to \pm\phi_c$ as $z \to \pm\infty$ and $V(\pm\phi_c) = 0$ we find that $C = 0$. Using this, we obtain

$$H[\phi_K] = A\int dz\,\kappa\left(\frac{d\phi_K(z)}{dz}\right)^2 \tag{1.40}$$

If the interface has a free energy per unit area of σ then we have the Cahn-Hillard estimate of the surface tension [25]

$$\sigma = \int dz\,\kappa\left(\frac{d\phi_K(z)}{dz}\right)^2 \tag{1.41}$$

In the case of the ϕ^4 model defined at Eq (1.19), the equation (1.37) becomes

$$\kappa\phi_K''(z) = m^2\phi_K(z)\left(1 + \phi_C\phi_K(z)^2\right) \tag{1.42}$$

This potential is only defined by the ratio between m^2 and λ, so without loss of generality we set $\phi_C = 1$. The solution becomes

$$\phi_K(z) = \tanh\left(\frac{z}{\xi}\right) \tag{1.43}$$

where $\xi = \sqrt{\frac{-2\kappa}{m^2}}$. This correlation length diverges when $T \to T_C$. From Fig 1.3 we see that the bigger the correlation length of the system, the smaller the surface tension is. The experimental study of quasi-critical systems, which have fluctuations at a macroscopic length scale, is a good way to probe the properties of ultra-low surface tension systems [26]. Such systems are very susceptible to hydrodynamic instabilities caused by thermal noise, as in microfluidics for example [27].
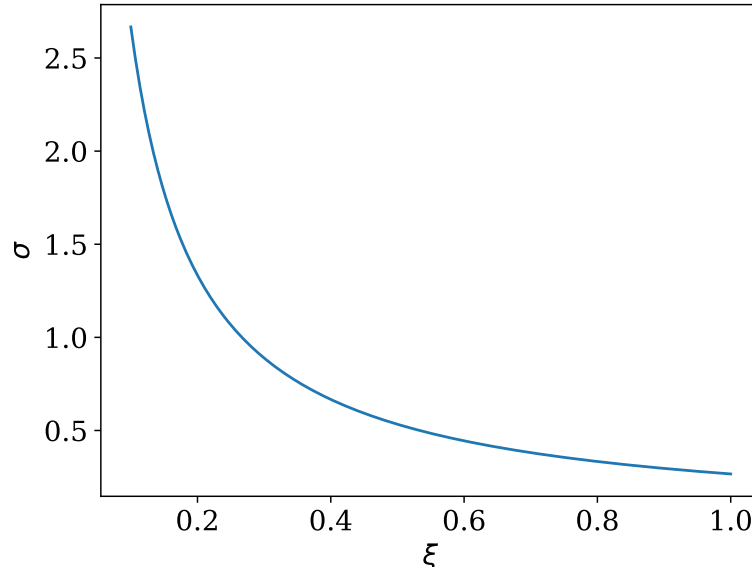
Figure 1.3: Surface tension (1.41) versus ξ for the ϕ^4 solution (1.43).

1.2 Models for equilibrium interfaces

1.2.1 Basic continuous model

Here we discuss effective models of interfaces. The simplest model is to assume that the interface is parameterised by a height profile $h(\mathbf{r})$, where $\mathbf{x} = (\mathbf{r}, z)$ however one also has to assume that $h(\mathbf{r})$ is a single-valued function of $\mathbf{r}$. Given this one can write

$$H[h] = \sigma A[h] \tag{1.44}$$

where $A[h]$ is the area of the interface. The interface area is given by

$$A[h] = \int_A d\mathbf{r} \sqrt{1 + [\nabla h]^2} \tag{1.45}$$

where the integral is over the plane perpendicular to the z axis which is taken to be of area A. When the fluctuations of the interface are small, we can expand the above to quadratic order in h to obtain

$$H[h] = A\sigma + \frac{\sigma}{2} \int_A d\mathbf{r} \, [\nabla h]^2 \tag{1.46}$$

The first term is independent of the height, so we can write the effective Hamiltonian for the surface as

$$H_{eff}[h] = \frac{\sigma}{2} \int_A d\mathbf{r} \, [\nabla h]^2 \tag{1.47}$$

The basic model describing the height of an interface at $z = h(\mathbf{r})$ above a plane with coordinates $\mathbf{r}$ has the Hamiltonian

$$H[h] = \int d\mathbf{x} \frac{\sigma}{2} [\nabla h(\mathbf{x})]^2 + V(h(\mathbf{x})) \tag{1.48}$$

The first term corresponds to the surface energy. In principle surfaces can also have bending energies, while surface energies correspond to stretching the surface to increase its size, bending energies correspond to curving the surface. The standard bending energy for small surface energies [28] is given

by

$$H_b[h] = \int d\mathbf{r} \frac{\kappa_b}{2} [\nabla^2 h(\mathbf{r})]^2 \tag{1.49}$$

where κ_b is called the bending rigidity. The term $V(h)$ represents the potential energy of the surface per unit area. For instance if the surface interacts via an infinite hard-core potential with a solid surface at $z = 0$, this can be modelled by the potential $V(z) = 0$ for $z > 0$ and $V(z) = \infty$ for $z \leq 0$. Another example is where the surface describes the surface of a liquid such as water, again with a solid surface at $z = 0$, in the presence of gravity the potential energy of the water column above the area element $d\mathbf{x}$ is given by

$$\delta V = \int_0^{h(\mathbf{r})} dz\, \rho g z = \frac{1}{2} \rho g h^2(\mathbf{r}) \tag{1.50}$$

where ρ is the (mass) density of the liquid. This then gives

$$H[h] = \int d\mathbf{r} \frac{\sigma}{2} [\nabla h(\mathbf{r})]^2 + \frac{1}{2} \rho g h^2(\mathbf{r}) \tag{1.51}$$

We see that the correlation length of the interface is given by

$$\xi = \left(\frac{\sigma}{\rho g} \right)^{\frac{1}{2}} \tag{1.52}$$

In the more general context, if $V(h)$ has a minimum at some point h_m we can write $h = h_f(\mathbf{x}) + h_m$, where $h_f(\mathbf{x})$ represents the height fluctuations about the mechanically stable flat interface $h(\mathbf{x}) = h_m$. Now expand assuming that $h_f(\mathbf{x})$ is small we find the effective Hamiltonian for the fluctuations

$$H_{eff}[h_f] = \int d\mathbf{r} \frac{\sigma}{2} [\nabla h_f(\mathbf{r})]^2 + \frac{1}{2} V''(h_m) h_f^2(\mathbf{r}) \tag{1.53}$$

where we have dropped the constant term $AV(h_m)$. The above field theory is Gaussian and so, when the approximations made to derive it are valid, all of the statistical properties of the height fluctuations can be deduced. However for general potentials $V(h)$ the model cannot be solved exactly in two dimensions but can in principle be solved in one dimension as we will see below.

1.2.2 Effective dynamics of interface heights

We will now try and derive an approximation for the dynamics of the height of the interface from the original phase ordering kinetics. Here we use the method of Bray and Cavagnha [9, 29], which was used to study the dynamics of sheared interfaces, in the absence of shear to determine the dynamical properties of interfaces in phase separated systems for both model A and model B dynamics.

   We imagine that the system is phase separated in the direction z, on average the interface is taken to be at $z = 0$, and we write

$$\phi(z, \mathbf{r}, t) = f(z - h(\mathbf{r}, t)) \tag{1.54}$$

where $f(z) = \phi_K(z)$ is the kink solution from mean field theory.

1.2.2.1 Model A dynamics

For model A dynamics, we substitute Eq. (1.54) into Eq. (1.27) and make use of the following results

$$\frac{\partial f(z - h(\mathbf{r}, t))}{\partial t} = - f'(z - h(\mathbf{r}, t)) \frac{\partial h(\mathbf{r}, t)}{\partial t} \tag{1.55}$$

$$\nabla f(z - h(\mathbf{r}, t) = [\mathbf{e}_z - \nabla h(\mathbf{r}, t)] f'(z - h(\mathbf{r}, t)) \tag{1.56}$$

$$\nabla^2 f(z - h(\mathbf{r}, t)) = f''(z - h(\mathbf{r}, t)) - \nabla^2 h(\mathbf{r}, t) f'(z - h(\mathbf{r}, t)) + [\nabla h(\mathbf{r}, t)]^2 f''(z - h(\mathbf{r}, t)) \tag{1.57}$$

and thus find

$$-f'(z - h(\mathbf{r}, t)) \frac{\partial h(\mathbf{r}, t)}{\partial t} = \alpha \kappa \left[f''(z - h(\mathbf{r}, t)) - \nabla^2 h(\mathbf{r}, t) f'(z - h(\mathbf{r}, t)) + [\nabla h(\mathbf{r}, t)]^2 f''(z - h(\mathbf{r}, t)) \right] \quad (1.58)$$

$$- \alpha V'(f'(z - h(\mathbf{r}, t))) + \eta(\mathbf{r}, z, t) \quad (1.59)$$

We now multiply both sides of this equation by $f'(z - h(\mathbf{r}, t))$ and defining $\zeta = z - h(\mathbf{r}, t)$, we integrate ζ over $[-\infty, \infty]$ while using the following identities

$$\int_{-\infty}^{\infty} d\zeta f'(\zeta) f''(\zeta) = [\frac{1}{2} f'^2(\zeta)]_{-\infty}^{\infty} = 0$$

$$\int_{-\infty}^{\infty} d\zeta f'(\zeta) V'(f) = \int_{-\infty}^{\infty} d\zeta \frac{dV(f)}{d\zeta} = [V(f(\zeta))]_{-\infty}^{\infty} = 0$$

Note that the first relation above holds as $f(\zeta) = \pm \phi_c$ as $\zeta \to \pm \infty$ and the second as $V(\phi_c) = V(-\phi_c) = 0$. The terms that are left then give

$$-\int_{-\infty}^{\infty} f'^2(\zeta) d\zeta \frac{\partial h(\mathbf{r}, t)}{\partial t} = -\alpha \int_{-\infty}^{\infty} f'^2(\zeta) d\zeta \, \kappa \nabla^2 h(\mathbf{r}, t) + \int_{-\infty}^{\infty} d\zeta \eta(\mathbf{r}, \zeta + h(\mathbf{r}, t)) f'(\zeta) \quad (1.60)$$

Now using the Cahn-Hillard estimate of the surface tension, Eq. (1.41) thus becomes

$$\frac{\sigma}{\kappa} \frac{\partial h(\mathbf{r}, t)}{\partial t} = \alpha \sigma \nabla^2 h(\mathbf{r}, t) + \xi(\mathbf{r}, t) \quad (1.61)$$

where the noise term is given by

$$\xi(\mathbf{r}, t) = -\int_{-\infty}^{\infty} d\zeta \eta(\mathbf{r}, \zeta + h(\mathbf{r}, t)) f'(\zeta) \quad (1.62)$$

The noise term has zero mean and correlation function

$$\langle \xi(\mathbf{r}, t) \xi(\mathbf{r}', t') \rangle = 2\alpha T \delta(t - t') \delta(\mathbf{r} - \mathbf{r}') \int_{-\infty}^{\infty} d\zeta d\zeta' \delta(\zeta - \zeta') f'(\zeta) f'(\zeta')$$

$$= 2\alpha T \delta(t - t') \delta(\mathbf{r} - \mathbf{r}') \int_{-\infty}^{\infty} d\zeta f'^2(\zeta) = \frac{2\alpha T \sigma}{\kappa} \delta(t - t') \delta(\mathbf{r} - \mathbf{r}') \quad (1.63)$$

This now gives

$$\frac{\partial h(\mathbf{r}, t)}{\partial t} = \kappa \alpha \nabla^2 h(\mathbf{r}, t) + \eta(\mathbf{r}, t) \quad (1.64)$$

where

$$\langle \eta(\mathbf{r}, t) \eta(\mathbf{r}', t') \rangle = \frac{2\alpha T \kappa}{\sigma} \delta(t - t') \delta(\mathbf{r} - \mathbf{r}') \quad (1.65)$$

Now defining $\alpha' = \frac{\kappa \alpha}{\sigma}$ we can write

$$\frac{\partial h(\mathbf{r}, t)}{\partial t} = \alpha' \sigma \nabla^2 h(\mathbf{r}, t) + \eta(\mathbf{r}, t) \quad (1.66)$$

This has the form of model A dynamics (as in Eq. (1.27)) for the height profile with Hamiltonian H_{eff} as given in (1.47), that is to say we can write

$$\frac{\partial h(\mathbf{r}, t)}{\partial t} = -\alpha' \frac{\delta H_{eff}[h]}{\delta h(\mathbf{r})} + \eta(\mathbf{r}, t) \quad (1.67)$$

with

$$\langle \eta(\mathbf{r}, t) \eta(\mathbf{r}', t') \rangle = 2T\alpha' \delta(t - t') \quad (1.68)$$

This dynamical calculation is thus consistent with the idea of describing the surface in terms of a height variable with an energy given by the surface tension. The equation (1.67) is known as the Edwards-Wilkinson equation [30, 31]. We can use this equation to determine how the domains of a coarsening system grow at low temperatures. To do this we ignore the noise term and assume that at $t = 0$ the correlations of the height are short range. so

$$C(\mathbf{r} - \mathbf{r}', 0) = \langle h(\mathbf{r}, 0) h(\mathbf{r}', 0) \rangle = C_0 \delta(\mathbf{r} - \mathbf{r}') \tag{1.69}$$

In Fourier space the noiseless Edwards-Wilkinson equation becomes

$$\frac{\partial \tilde{h}(\mathbf{k}, t)}{\partial t} = -\alpha' \sigma k^2 \tilde{h}(\mathbf{k}, t) \tag{1.70}$$

and so we find

$$\tilde{h}(\mathbf{k}, t) = h(\mathbf{k}, 0) \exp(-\alpha' \sigma \mathbf{k}^2 t) \tag{1.71}$$

The two point correlation function becomes

$$\langle \tilde{h}(\mathbf{k}, t) \tilde{h}(\mathbf{k}', t') \rangle = \langle h(\mathbf{k}, 0) h(\mathbf{k}', 0) \rangle \exp(-\alpha' \sigma [k^2 + k'^2] t). \tag{1.72}$$

Now recall that if

$$\langle h(\mathbf{r}, t) h(\mathbf{r}', t') \rangle = C(\mathbf{r} - \mathbf{r}', t) \tag{1.73}$$

then

$$\langle \tilde{h}(\mathbf{k}, t) \tilde{h}(\mathbf{k}', t') \rangle = (2\pi)^d \delta(\mathbf{k} + \mathbf{k}') \tilde{C}(\mathbf{k}, t) \tag{1.74}$$

where

$$\tilde{C}(\mathbf{k}, t) = \int d\mathbf{r} \exp(-i\mathbf{k} \cdot \mathbf{r}) C(\mathbf{r}, t) \tag{1.75}$$

is the Fourier transform of the correlation function, which is a function of a single position due to invariance by translation in space, and d is the dimension of space (so here $d = 2$ for a surface in 3d space and $d = 1$ for a surface in a 2d space). Putting all this together gives

$$\tilde{C}(\mathbf{k}, t) = C_0 \exp(-2\alpha' \sigma k^2 t) \tag{1.76}$$

Inverting the Fourier transform, we have

$$C(\mathbf{r}, t) = \frac{C_0}{(8\pi \alpha' \sigma t)^{\frac{d}{2}}} \exp(-\frac{\mathbf{r}^2}{16\pi \alpha' \sigma t}) \tag{1.77}$$

From this we see that if $C(\mathbf{r}, t) \sim g(\frac{\mathbf{r}}{\ell(t)}) r(t)$ then the length scale $\ell(t) \sim t^{\frac{1}{2}}$, this agrees with what is found in the Ising model under Glauber dynamics, where the growth exponent is also given by $z = \frac{1}{2}$ [32].

1.2.2.2 Model B dynamics

For model B dynamics, we take the same ansatz as in Eq. (1.54) but we rewrite the model B dynamics as

$$-\nabla^{-2} \frac{\partial \phi(\mathbf{x}, t)}{\partial t} = -D \frac{\delta H}{\delta \phi(\mathbf{x})} + \theta(\mathbf{x}, t) \tag{1.78}$$

here $-\nabla^{-2}$ represents the Green's function G which obeys

$$\nabla^2 G(\mathbf{x} - \mathbf{x}') = -\delta(\mathbf{x} - \mathbf{x}') \tag{1.79}$$

and

$$\theta(\mathbf{x}, t) = -\nabla^{-2}\eta(\mathbf{x}, t) = \int d\mathbf{x}' G(\mathbf{x} - \mathbf{x}')\eta(\mathbf{x}, t) \tag{1.80}$$

The correlation function of $\theta(\mathbf{x}, t)$ is given by

$$\begin{aligned}
\langle \theta(\mathbf{x}, t)\theta(\mathbf{y}, t') \rangle &= -2DT\delta(t - t')\int d\mathbf{x}' G(\mathbf{x} - \mathbf{x}')d\mathbf{y}' G(\mathbf{y} - \mathbf{y}')\nabla^2\delta(\mathbf{x}' - \mathbf{y}') \\
&= -2DT\delta(t - t')\int d\mathbf{x}' G(\mathbf{x} - \mathbf{x}')d\mathbf{y}'\nabla^2 G(\mathbf{y} - \mathbf{y}')\delta(\mathbf{x}' - \mathbf{y}') \\
&= 2DT\delta(t - t')G(\mathbf{x} - \mathbf{y})
\end{aligned} \tag{1.81}$$

where we have integrated by parts in the second line and used

$$-\nabla^2 G(\mathbf{y} - \mathbf{y}') = \delta(\mathbf{y} - \mathbf{y}') \tag{1.82}$$

in the third.

Now multiplying by $f'(z - h(\mathbf{r}, t))$ and integrating z over $[-\infty, \infty]$, we find

$$-\int dz f'(z - h(\mathbf{r}, t))\int dz' d\mathbf{r}'\, G(z - z', \mathbf{r} - \mathbf{r}')f'(z' - h(\mathbf{r}', t))\frac{\partial h(\mathbf{r}', t)}{\partial t} = -D\sigma\nabla^2 h(\mathbf{r}, t) + \chi(\mathbf{r}, t), \tag{1.83}$$

with the noise

$$\chi(\mathbf{r}, t) = \int dz f'(z - h(\mathbf{r}, t))\theta(\mathbf{r}, z, t). \tag{1.84}$$

As we assume that the height fluctuations are small, we keep only the lowest order terms in h in the deterministic terms and the noise, we will see later that this is compatible thermodynamically. We thus have

$$-\int dz\, f'(z)\int dz' d\mathbf{r}'\, G(z - z', \mathbf{r} - \mathbf{r}')f'(z')\frac{\partial h(\mathbf{r}', t)}{\partial t} = -D\sigma\nabla^2 h(\mathbf{r}, t) + \chi(\mathbf{r}, t) \tag{1.85}$$

and now the noise is given by

$$\chi(\mathbf{r}, t) = \int dz\, f'(z)\theta(\mathbf{r}, z', t) \tag{1.86}$$

This equation which is linear in h can now be Fourier transformed in the plane $\mathbf{r}$. In terms of the Fourier transform of h we find

$$-\int dz\, f'(z)\int dz' d\mathbf{r}'\, \tilde{G}(z - z', \mathbf{k})f'(z')\frac{\partial \tilde{h}(\mathbf{k}, t)}{\partial t} = Dk^2\sigma\tilde{h}(\mathbf{k}, t) + \tilde{\chi}(\mathbf{k}, t) \tag{1.87}$$

The Fourier transform of G in the $\mathbf{r}$ plane obeys

$$\frac{d^2\tilde{G}(z - z', \mathbf{k})}{dz^2} - k^2\tilde{G}(z - z', \mathbf{k}) = -\delta(z - z') \tag{1.88}$$

and the solution to this equation (with the boundary condition that $\tilde{G}(z - z', \mathbf{k}) \to 0$ as $|z - z'| \to \infty$) is

$$\tilde{G}(z - z', \mathbf{k}) = \frac{\exp(-k|z - z'|)}{2k} \tag{1.89}$$

where we have used the notation $k = |\mathbf{k}|$, so k is positive. Next we make the sharp interface approximation where we write

$$f(z) = 2\phi_c\delta(z) \tag{1.90}$$

that is to say we have replaced the smooth kink solution with a step like solution $f(z) = \phi_c \, \text{sgn}(z)$. This then gives

$$-4\phi_c^2 \tilde{G}(0, k) \frac{\partial h(\mathbf{k}, t)}{\partial t} = D k^2 \sigma \tilde{h}(\mathbf{k}, t) + \tilde{\chi}(\mathbf{k}, t) \tag{1.91}$$

which we rewrite as

$$\frac{\partial \tilde{h}(\mathbf{k}, t)}{\partial t} = -\frac{D k^3 \sigma}{2\phi_c^2} \tilde{h}(\mathbf{k}, t) + \tilde{\xi}(\mathbf{k}, t) \tag{1.92}$$

with

$$\tilde{\xi}(\mathbf{k}, t) = -\frac{k}{2\phi_c^2} \tilde{\chi}(\mathbf{k}, t) \tag{1.93}$$

where

$$\tilde{\chi}(\mathbf{k}, t) = \int dz \, f'(z) \tilde{\theta}(\mathbf{k}, z, t) \tag{1.94}$$

The correlation function of $\tilde{\theta}(\mathbf{k}, t)$ is

$$\langle \theta(\mathbf{k}, t) \theta(\mathbf{k}', t') \rangle = 2 D T (2\pi)^d \delta(t - t') \delta(\mathbf{k} + \mathbf{k}') \tilde{G}(z - z', k) \tag{1.95}$$

From this we find

$$\langle \chi(\mathbf{k}, t) \chi(\mathbf{k}', t') \rangle = 2 D T (2\pi)^d \delta(t - t') \delta(\mathbf{k} + \mathbf{k}') \int dz dz' f(z) f(z') \tilde{G}(z - z', k) \tag{1.96}$$

Now, using the sharp interface approximation Eq. (1.90), we obtain

$$\langle \chi(\mathbf{k}, t) \chi(\mathbf{k}', t') \rangle = 2 D T (2\pi)^d \delta(t - t') \delta(\mathbf{k} + \mathbf{k}') \frac{2\phi_c^2}{k} \tag{1.97}$$

and consequently

$$\langle \xi(\mathbf{k}, t) \xi(\mathbf{k}', t') \rangle = 2 D T (2\pi)^d \delta(t - t') \delta(\mathbf{k} + \mathbf{k}') \frac{k}{2\phi_c^2} \tag{1.98}$$

Finally in we find the interface dynamics for model B in Fourier space is

$$\frac{\partial h(\mathbf{k}, t)}{\partial t} = -\frac{D k^3 \sigma}{2\phi_c^2} \tilde{h}(\mathbf{k}, t) + \tilde{\xi}(\mathbf{k}, t) \tag{1.99}$$

In real space this has the form

$$\frac{\partial h(\mathbf{r})}{\partial t} = -L \frac{\delta H_{eff}}{\delta h(\mathbf{r})} + \xi(\mathbf{r}, t) \tag{1.100}$$

where the operator L is defined via its Fourier transform

$$\tilde{L}(\mathbf{k}) = \frac{D k}{2\phi_c^2} \tag{1.101}$$

Now if we look at Eq. (1.99) we see that solving the equation without noise will give a function of $k^3 t$, which in real space corresponds to x^3 / t. From this we see that the coarsening length scale grows as $\ell(t) \sim t^{\frac{1}{3}}$ and consequently the coarsening exponent is $z = \frac{1}{3}$. Coarsening for conserved model B or diffusive dynamics is slower than that of model A [33]. One of the reasons for this slowing down with respect to nonconserved dynamics is that material must be physically transported by diffusion (by exchanging spins in the language of lattice spin models), where as for model A dynamics the composition can change at any given point by *spin flipping*. As a cautionary note, if we had taken the Hamiltonian in Eq. (1.47) and applied model B conserved dynamics, as in Eq. (1.31), for the height field we would not have obtained this equation.

We can actually do better than the above sharp interface approximation as Eq. (1.87) can be written as

$$Q(k)\frac{\partial \tilde{h}(\mathbf{k}, t)}{\partial t} = -Dk^2 \sigma \tilde{h}(\mathbf{k}, t) - \tilde{\chi}(\mathbf{k}, t) \tag{1.102}$$

where

$$Q(k) = \int dz dz' \, f'(z) \, \tilde{G}(z - z', \mathbf{k}) f'(z') \tag{1.103}$$

Notice that from Eq. (1.102) that

$$\langle \chi(\mathbf{k}, t)\chi(\mathbf{k}', t')\rangle = 2DT(2\pi)^d \delta(t - t')\delta(\mathbf{k} + \mathbf{k}')Q(k) \tag{1.104}$$

and so

$$\frac{\partial \tilde{h}(\mathbf{k}, t)}{\partial t} = -\tilde{L}(k)\tilde{\mu}(\mathbf{k}) + \eta(\mathbf{k}) \tag{1.105}$$

where $\mu(\mathbf{x}) = \delta H_{eff}/\delta h(\mathbf{x})$, $\tilde{L}(k) = D/Q(k)$ and

$$\langle \eta(\mathbf{k}, t)\eta(\mathbf{k}', t')\rangle = 2T(2\pi)^d \delta(t - t')\delta(\mathbf{k} + \mathbf{k}')\tilde{L}(k) \tag{1.106}$$

1.3 Lattice models

1.3.1 The Ising model

We take a system of size $L' \times L' \times L$, composed of N sites i. At each site corresponds a value $\sigma_i = \pm 1$. The Hamiltonian of the Ising model is

$$H = -\sum_{\langle ij\rangle} J\sigma_i\sigma_j + B\frac{V(\sigma_i) + V(\sigma_j)}{2} \tag{1.107}$$

where $\sum_{\langle ij\rangle}$ is a sum over all pairs of nearest neighbours, and the external parameter B having the energy dimension is applied to the funcion of the internal variables $V(\sigma_i)$ which has been symmetrized. The Ising model[4, 34] is therefore a lattice model with short interactions between particles. Since all particles σ_i in the system are equal to $\pm!$, this system is called a lattice based spin model. When σ_i is continuous, it is called the XY model [35]. J is called the coupling parameter of the system, and can be non-uniform, with the nearest neighbours interaction being $J = J_{ij}$. If $J_{ij} = 0$, the system favorises homogeneous phases and is called ferromagnetic. Otherwise, the system favorises configurations where each spin has an opposite sign with respect to all of their neighbours, which modelises antiferromagnetic materials. We will pose $J = 1$.

The mean-field theory with a ϕ^4 potential has been developed from this model [36]. Exact relationship between both of them has been found in 4 dimensions and above [37]. A fast way to convince ourselves is to take the finite difference derivative at first order of Eq (1.18). If we suppose the sole role of the potential is to set the field to $\pm\phi_C$ on each site, then we have

$$\begin{aligned}[\boldsymbol{\nabla}\phi(i)]^2 &= \left(\frac{\partial\phi(i)}{\partial x}\right)^2 + \left(\frac{\partial\phi(i)}{\partial y}\right)^2 + \left(\frac{\partial\phi(\mathbf{i})}{\partial z}\right)^2 \\ &= (\phi(x, y, z) - \phi(x + 1, y, z))^2 + (\phi(x, y, z) - \phi(x, y + 1, z))^2 + (\phi(x, y, z) - \phi(x, y, z + 1))^2 \\ &= 2(1 - \phi(x, y, z)\phi(x + 1, y, z) + 2(1 - \phi(x, y, z)\phi(x, y + 1, z) + 2(1 - \phi(x, y, z)\phi(x, y, z + 1)\end{aligned} \tag{1.108}$$

where we've set the distance between two sites to 1. From this we easily see some bulk energy to which we add the sites' nearest neighbours interactions in an Ising-like fashion.
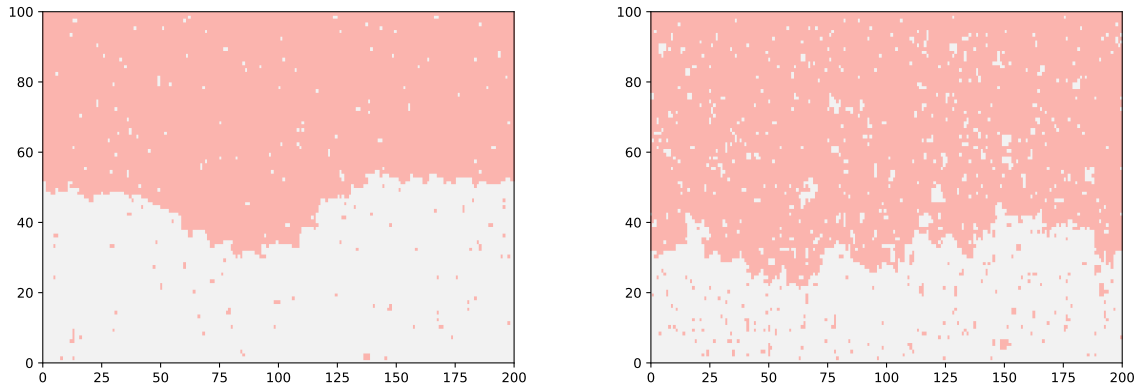
Figure 1.4: Snapshot of Monte Carlo simulations of the Ising model for two different temperatures in two dimensions($T = 0.7T_C$ (left) and $T = 0.95T_C$ (right)) with periodic boundary conditions in x and fixed ones in y.

This model precisely describes phase transitions in uniaxial magnetic systems[38, 39, 40]. It is also the simplest model of its eponymous universality class, which also contains liquid/gas transitions and binary fluids. In these mappings, $n_i = \frac{1}{2}(1 - \sigma_i) = 0, 1$ represents occupation of a cell of a lattice fluid or σ_i gives the label of a binary species A or B. This model does not have a phase transition in 1D, but a phase transition in 2D was foumd in 1944[23] at the critical temperature

$$T_{2D,C} = \frac{2J}{k_B \ln(1 + \sqrt{2})} \simeq 2.27 \frac{J}{k_B} \tag{1.109}$$

The renormalization group approaches have a deep connexion with the Ising model [41, 2]. Even though results have been found for $d = 4$ (which is the upper critical dimension), no analytical solution has been found in 3 dimensions. Numerous numerical simulations [42, 43] have shown that the 3-dimensional phase transition occurs at

$$T_{3D,C} \simeq 4.51 \frac{J}{k_B} \tag{1.110}$$

By making the transformation[2]

$$n_i = \frac{\sigma_i + 1}{2} \tag{1.111}$$

so that $n_i(\sigma_i = 1) = 1$ and $n_i(\sigma_i = -1) = 0$, we obtain

$$H = -\sum_{\langle ij \rangle} J_{ij} \left(4n_i n_j - 2(n_i + n_j) + 1 \right) + B \sum_{\langle ij \rangle} \frac{V(\sigma_i) + V(\sigma_j)}{2} \tag{1.112}$$

where the constant term $\sum_{\langle ij \rangle} J_{ij}$ does not change the partition function behaviour. We have then

$$\begin{aligned} H_{LG} &= -4 \sum_{\langle ij \rangle} J_{ij} n_i n_j + 2 \sum_{\langle ij \rangle} J_{ij}(n_i + n_j) + B \sum_{\langle ij \rangle} \frac{V(\sigma_i) + V(\sigma_j)}{2} \\ &= -4J \sum_{\langle ij \rangle} J n_i n_j + \mu_c \sum_i n_i + B \sum_{\langle ij \rangle} \frac{V(\sigma_i) + V(\sigma_j)}{2} \end{aligned} \tag{1.113}$$

where we have set $J_{ij} = J$ constant and defined the intrinsic chemical potential for a liquid-gas system as $\mu_c = 4Jc$, with c the number of nearest neighbours. A positive magnetic phase is thus analogous

to a high density state such a liquid, while the negative magnetic phase is equal to a low density state such as a gas. An onsite potential $V(\sigma_i)$ further modifies the chemical potential, $\mu = \mu_c + \delta\mu[V(\sigma_i)]$. The chemical potential μ is the conjugate variable to the total number of particles $\sum_i n_i$, while the magnetic field B is the conjugate variable to the total magnetisation $\sum_i \sigma_i$. The two are connected through the mapping such that $B \sim \mu - \mu_c$, so that liquid-gas and Ising model systems share common thermodynamic features such as the universality class for critical fluctuations. For the fluid the grand canonical ensemble corresponds to the Gibbs ensemble with fixed T and μ and canonical ensemble with fixed T and N . In the magnetic system these ensembles correspond to fixed T, B and T, M respectively. The model also describes adsorption of a gas in a lattice or binary fluids between particles of different species A and B.

By imposing $+-$ boundary conditions in the z direction, we force the existence of an interface Those BC can be fixed, imposing $\sigma(z = 0) = -1$ and $\sigma(z = L) = +1$, or free but with a local external field $V(z) = h(\delta_{0,z} - \delta_{z,L})$. An interface is characterized by its mean and its width. The easiest way to do so is to fit the magnetization profile

$$m(z) = \frac{1}{L'^2}\langle\sum_{xy}\sigma(x,y,z)\rangle \tag{1.114}$$

to mean field results from Eq (1.43) . The mean position of the interface is

$$m = \langle h\rangle = \frac{1}{L'^2}\langle\sum_i\sigma_i\rangle \tag{1.115}$$

The width of the interface is then defined as

$$w^2 = \langle h^2\rangle - \langle h\rangle^2 \tag{1.116}$$

This can be rewrtiten [44] as

$$w^2 = 2\frac{\int_0^L dz\, z\frac{dm(z)}{dz}}{\int_0^L dz\frac{dm(z)}{dz}} \tag{1.117}$$

We now defined the surface tension of the interface as the free energy difference between the bulk and interface [45]. Is Z^{++} si the partition function of a system with $(++)$ BC, and Z^{+-} with $(+-)$ BC, then the surface tension [46] is given by

$$\sigma = \lim_{L',L\to\infty}\frac{1}{L'^2}\ln\left(\frac{Z^{+-}}{Z^{++}}\right) \tag{1.118}$$

By diagonalization of the transfer matrix (which we will define later), we find that the surface tension of a the interface between two pure phases $+$ and $-$ is given in a two-dimensional Ising model [5] by

$$\sigma = 2\beta J + \log(\tanh(\beta J)) \tag{1.119}$$

1.3.2 The Solid-On-Solid Model

In order to get the Edwards-Wilkinson equation of an interface from statistical field theory, we have used the approximation

$$\phi(\mathbf{x}, t) = f(z - h(\mathbf{r}, t)) \tag{1.120}$$

We translate the same approximation in order to study interfaces in lattice models by

$$\sigma_{i,j} = \mathrm{sgn}(h_i - j) \tag{1.121}$$

where $\mathrm{sgn}(x < 0) = -1$ and $\mathrm{sgn}(x > 0) = 1$, and h_i is the height of the interface at site i. This is the low temperature approximation of the Ising model, where there are no overhangs from the $+$ phase into the $-$ phase and vice versa. If we note $J_\perp$ the vertical bond energy between two Ising spins and $J_\parallel$ the horizontal bond energy, this approximation becomes equivalent to a highly anisotropic Ising model where $J_\perp \gg J_\parallel$ [47].

In a slab or semi-infinite geometry as seen in Fig 1.5, the height of the interface corresponds to the number of spins $-$ in the column i, while for an infinite geometry, we define h_i as the number of excess spins $-$ with respect to the mean height, set in the figure at $z = 0$ [48]. In this representation, height profiles represent an interface height and not a number of particles, since there is no entropy term associated with the number of ways that the h_i particles on each site can be chosen from the N particles available. In chapter 4, we will address a model with those characteristics. Using the identities

$$\min(a, b) = \frac{|a + b| - |a - b|}{2} \tag{1.122}$$

$$\max(a, b) = \frac{|a + b| + |a - b|}{2} \tag{1.123}$$

we have

$$\sum_{j=0}^{L} \mathrm{sgn}(h - j)\,\mathrm{sgn}(h' - j) = L - 2|h - h'| \tag{1.124}$$

For a 2-D Ising model of size $L' \times L$, the Ising Hamiltonian (1.107) is rewrtiten as

$$H = 2JL'(1 - L) + 2J \sum_{i=0}^{L'} |h_i - h_{i+1}| + B \sum_{i=0}^{L'} V(h_i) \tag{1.125}$$

with external potential

$$BV(h_i) = B \sum_{j=0}^{L} V(\mathrm{sgn}(h_i - j)) \tag{1.126}$$

For periodic boundary conditions, we set $h_{L'} = h_0$.

Another way to compute this energy for a SOS configuration is to directly count the number of energy bonds for a $L' \times L$ Ising model under the approximation (1.121). There are $L - 1$ vertical bonds per column, where all have an energy of $-J$, while the link that goes though the interface has an energy of $+J$. The total contribution to energy from vertical bonds is thus

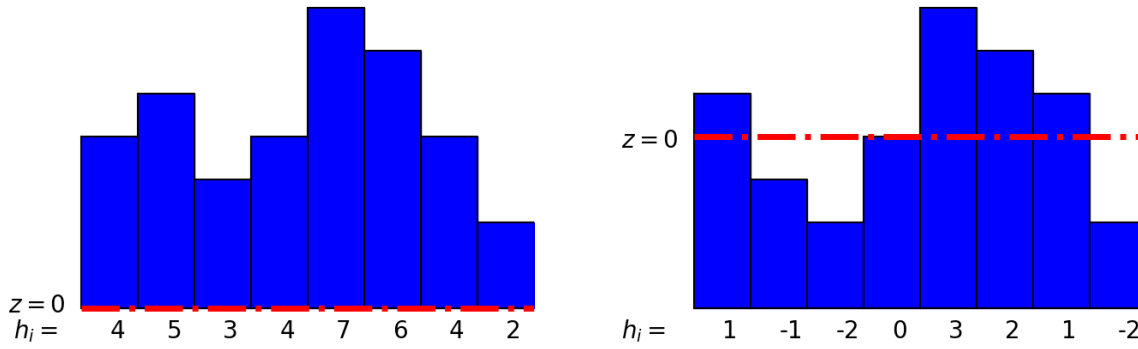$$E_\perp = -JL'(L - 2) \tag{1.127}$$

Figure 1.5: Possible configuration of the SOS model for a semi-infinite geometry (left) and infinite geometry (right). The red line shows the origin $z = 0$. In the i-th column the interface is at height h_i. Particles under the interface are from the Ising $-$ phase, while particles over it are from the $+$ phase.

There are L$'$ $\times$ L horizontal bonds. In a pure phase system, the horizontal energy would be $-$JL$'$L. Nevertheless, there are $\sum_i |h_i - h_{i+1}|$ bonds which have an energy of +J, which gives the horizontal energy contribution

$$E_\parallel = -JL'L + 2J\sum_i |h_i - h_{i+1}| \tag{1.128}$$

By adding both, we find back Eq (1.125).

By setting 2J = J and getting rid of the bulk energy, we obtain the **Solid-On-Solid Hamiltonian**

$$H = J\sum_{i=0}^{L'} |h_i - h_{i+1}| + B\frac{V(h_i) + V(h_{i+1})}{2} \tag{1.129}$$

The first system where the SOS model has been applied was crystals' growth in 1972 [6]. Since then, the model has been used with some success in naphthalene cristals[49], experimental expitaxial growth[50], polymer membranes [51, 52], or interfacial wetting [53].

In the SOS model, the sites i of height h_i can take any value in [0, L]. The Restrictied Solid-On-Solid model (RSOS) is a variation where sites can only take the value $h_{i+1} \in [h_i - 1, h_i, h_i + 1]$[54]. This approximation works for very low temperatures or very smooth interfaces [55, 56].

Another model, closer to the continuous model of Hamiltonian (1.47) is the Discrete Gaussian model which has the following gaussian interaction

$$H = J\sum_{i=0}^{L'} (h_i - h_{i+1})^2 + B\frac{V(h_i) + V(h_{i+1})}{2} \tag{1.130}$$

and also has a restricted version. The SOS model has an exact relation with the XY model [57], no matter the power law used for the interaction. With a generalization of this model to continuous heights, it has been shown that extreme deviations statistics of the interface is described by a scaling function [58]. Since the energy costs of height differences $0, \pm 1$ are the same in every SOS model no matter the exponent in the energy costs of height differences, one expects the qualitative freatures of all those models to be the same at low temperature, since height differences are typically small [59].

Since the dimensionality of the system has been reduced in only taking into account the height interface h_i at site i instead of the position of all particles, we can think of an interface as a partially self-avoiding walk. This idea, which will be developed in section 3.2, has proven quiet powerfull in finding exact solutions of the generating function [60] or the extreme deviations statistics of the interface [61, 58].
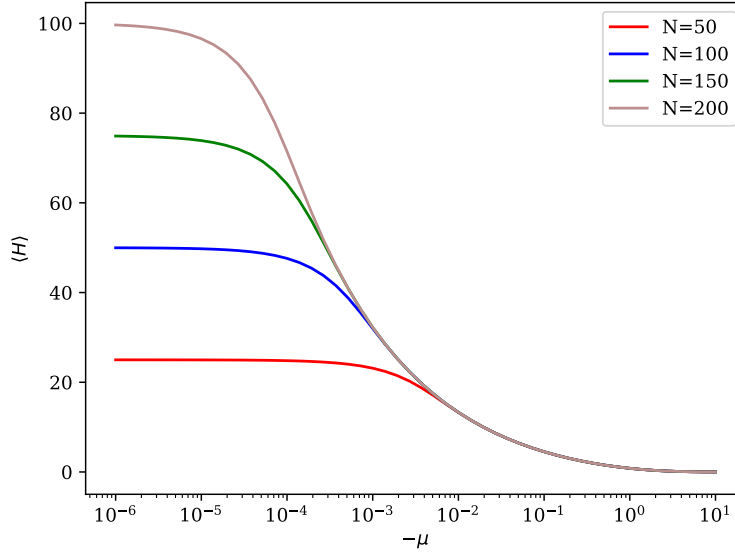
Figure 1.6: Mean height of the SOS interface (1.132) with respect to $-\mu$ through diagonalization of the transfer matrix for $\beta = 1$, in the limit $L' \to \infty$.

In the canonical ensemble, the height interface is fixed to N, which is translated in the partition function as

$$Z(N) = \sum_{h_0 h_1 \dots h_{L'}} \exp(-\beta \sum_i H(h_i, h_{i+1})) \delta_{\sum_i h_i, N} \tag{1.131}$$

In the grand-canonical ensemble, the conjugate variable to the height interface is the chemical potential μ, and the grand partition function Ξ is related to the canonical partition function by

$$\begin{aligned} \Xi(\mu) &= \sum_N Z(N) \exp((\beta \mu N) \\ &= \sum_{h_0 h_1 \dots h_{L'}} \exp(-\beta H_{eff}(h_0, h_1, \dots, h_{L'}) \end{aligned} \tag{1.132}$$

where

$$H_{eff} = J \sum_{i=0}^{L'} |h_i - h_{i+1}| + \sum_{i=0}^{L'} BV(h_i) - \mu h_i \tag{1.133}$$

In Fig 1.6, we plot the mean number of particles per site with respect to the chemical potential, for different size of the system, in the thermodynamic limit $L' \to \infty$. When the chemical potential is too small, the Lagrange's multiplier of the mean height is negligible, allowing the interface to fluctuate freely. Since the height of the interface is then evenly spread over all possible configurations, the mean value for $\mu = 0$ becomes $\frac{L}{2}$.

1.3.3 Transfer matrix

In a more general fashion, we can rewrite the Hamiltonian as

$$H = \sum_{i=0}^{L'} f(h_i, h_{i+1}) + BV(h_i, h_{i+1})$$

$$
T = \begin{bmatrix}
\ddots & \vdots & \iddots \\
e^{-\beta H(-1,-1)} & e^{-\beta H(-1,0)} & e^{-\beta H(1,-1)} \\
\dots & e^{-\beta H(0,0)} & \dots \\
e^{-\beta H(1,-1)} & e^{-\beta H(1,0)} & e^{-\beta H(1,1)} \\
\iddots & \vdots & \ddots
\end{bmatrix}
\tag{1.139}
$$

Figure 1.7: Infinite and symmetrical transfer matrix 1.135.

where $f(h_i, h_j)$ is the energy interaction between two nearest neighbours and $BV(h_i, h_j) = B\frac{V(h_i)+V(h_j)}{2}$ is the external potential. We can rewrite the partition function as

$$
Z = \sum_{h_1=0}^{L} \sum_{h_2=0}^{L} \dots \sum_{h_{L'}=0}^{L} \exp(-\beta \sum_{i=0}^{L'} H(h_i, h_{i+1})) = \sum_{h_1 h_2 \dots h_{L'}} \prod_{i=0}^{L'} \exp(-\beta H(h_i, h_{i+1}))
\tag{1.134}
$$

We define the transfer matrix

$$
T(h_i, h_j) = e^{-\beta H(h_i, h_j)}
\tag{1.135}
$$

In Fig 1.7, we have represented an infinite matrix corresponding the limit $L \to \infty$, where each site can take any value in $[-\infty, \infty]$. To diagonalize numerically such matrices, we translate the whole system with $h_i \to h_i - \frac{L}{2}$, where L is the matrix's size, which me make tend to ∞. The constraint (1.131) cannot be expressed in the transfer matrix formalism, which induces a change in properties from this ensemble with respect to the transfer matric results [62].

Since the system has periodic boundary conditions $h_{L+1} = h_1$, we have $T(h_L, h_{L+1}) = T(h_L, h_1)$ [63]. The matrix is thus symmetric, which means it can be diagonalized with eigenvectors and eigenvalues

$$
T|\lambda\rangle = \lambda|\lambda\rangle
\tag{1.136}
$$

Those eigenvectors are orthonormal

$$
\langle\lambda|\lambda'\rangle = \delta_{\lambda\lambda'}
\tag{1.137}
$$

We set λ_0 as the biggest eigenvalue of T, by λ_1 the second biggest eigenvalue, and so on. The partition function can then be rewritten, in terms of the transfer matrix [5] by

$$
Z = \sum_{h_1 h_2 \dots h_{L'}} \prod_i T(h_i, h_{i+i}) = Tr(T^{L'}) = \sum_\lambda \langle\lambda|T^{L'}|\lambda\rangle = \sum_\lambda \lambda^{L'}
\tag{1.138}
$$

In the thermodynamic limit $L' \to \infty$, only the biggest eigenvector is relevant since the partition function becomes

$$
Z(L \to \infty) \simeq \lambda_0^{L'}
\tag{1.140}
$$

We find that the free energy per site is

$$
f = -\frac{1}{L'\beta} \ln(Z) \simeq -\frac{1}{\beta} \ln(\lambda_0)
\tag{1.141}
$$

In Fig 1.8 we plot the evolution of the free energy per site $\Omega(L')$ without external field, compared to the thermodynamic limit. We determine that the thermodynamic limit becomes valid for $L' > 150$.
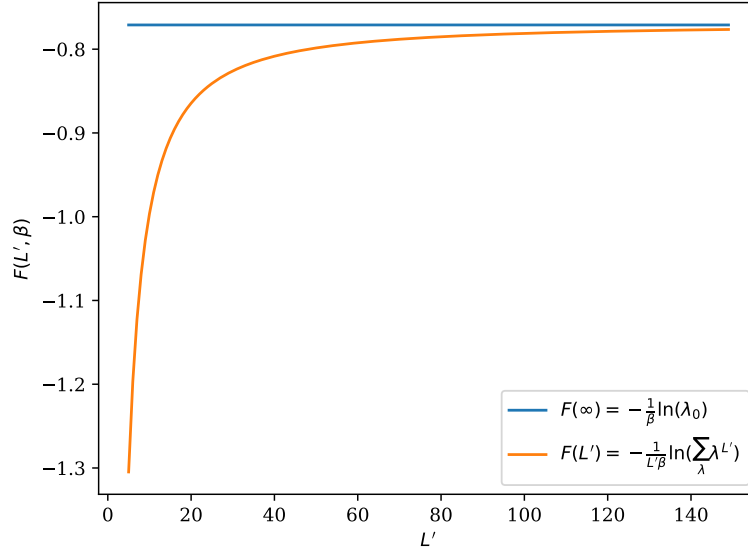
Figure 1.8: Free energy per site $\Omega(L')$ with respect to the number of sites L' compared to the thermodynamic value $\Omega(\infty)$, for a system of maximum height $L = 100$, $\beta = 1$, $J = 1$ and $V(h_i) = 0$.

To compute the mean height value per site M, we introduce the height matrix $\hat{M}$ defined by its action over the vectors $|h\rangle$ in the matrix transfer's base by

$$= \delta_{h,h'} h \tag{1.142}$$

We thus find that the density is

$$M = \langle h \rangle = \frac{1}{L'} \sum_i h_i = \frac{1}{Z} \sum_\lambda \lambda^{L'} \langle \lambda | \hat{M} | \lambda \rangle \simeq \langle \lambda_0 | \hat{M} | \lambda_0 \rangle \tag{1.143}$$

We deduce the mean displacement per site

$$w^2 = \langle (h - M)^2 \rangle = \frac{1}{Z} \sum_\lambda \lambda^{L'} \langle \lambda | \hat{M}^2 | \lambda \rangle - \langle \lambda | \hat{M} | \lambda \rangle^2 \simeq \langle \lambda_0 | \hat{M}^2 | \lambda_0 \rangle - M^2 \tag{1.144}$$

We can find thos two obersables by computing the first and second moment of the probability distribution that a site i is at height h_i

$$p(h) = \frac{1}{Z} \sum_\lambda \lambda^{L'} \langle \lambda | h \rangle^2 \simeq \langle \lambda_0 | h \rangle^2 \tag{1.145}$$

The two-point correlation function of the system is computed by

$$C(r) = \langle h_i h_{i+r} \rangle - M^2 = \frac{1}{Z} \sum_{\lambda \neq \lambda_0} \langle \lambda_0 | M | \lambda \rangle \langle \lambda | M | \lambda_0 \rangle \left(\frac{\lambda}{\lambda_0} \right)^r \tag{1.146}$$

which becomes, in the long distance r limit,

$$C(r) \simeq \langle \lambda_0 | M | \lambda_1 \rangle \langle \lambda_1 | M | \lambda_0 \rangle \left(\frac{\lambda_1}{\lambda_0} \right)^r \tag{1.147}$$

The correlation function has an exponential decay at large distances, which allows us to define the correlation length at large distance ξ

$$\xi = - \frac{1}{\ln(\frac{\lambda_1}{\lambda_0})} \tag{1.148}$$

1.4 Systems driven by imposed hydrodynamic flows

Here we consider what happens when a system is driven out of equilibrium. By driven we mean that energy is injected into the system by a laser [64], by inducing a hydrodynamics flow, for instance a shear flow induced in a Couette cell in liquids [65, 19] or in glassy materials [66, 67]. In principle we should analyse this system with model H dynamics which couples diffusive model B dynamics to hydrodynamics in the low Reynolds number Stokes flow regime. In these dynamics the order parameter field will itself induce a hydrodynamics flow which will modify the imposed one. However this full situation is very difficult to analyse and to a first approximation we can assume that the back reaction of the order parameter field on the hydrodynamic flow is small with respect to the imposed hydrodynamic flow and so we can simply write

$$\frac{\partial \phi(\mathbf{x}, t)}{\partial t} + \nabla \cdot (\mathbf{v}(\mathbf{x})\phi(\mathbf{x}, t)) = -\mathrm{L}\frac{\delta \mathrm{H}}{\delta \phi(\mathbf{x})} + \eta(\mathbf{x}, t), \tag{1.149}$$

where L is given by the underlying model A or B dynamical operator and the noise has the correlation function as given by Eq. (1.26), and $\mathbf{v}(\mathbf{x})$ is the imposed (time independent) hydrodynamic flow or can equally well be an external drive imposed on the colloidal particles, due to the gravitational or electric field for example.

The simplest case one can consider is where the driving field $\mathbf{v}(\mathbf{x}) = \mathbf{v}_0$ is uniform [68, 69]. Unfortunately this simple driving does not lead to a new steady state. Basically all of the colloidal particles acquire an average velocity $\mathbf{v_0}$ and so move along at the same speed relative to each other. Mathematically this can be seen by making the Galilean transformation

$$\phi(\mathbf{x}, t) = \phi(\mathbf{x} - \mathbf{v}_0 t, t) = \phi(\mathbf{y}, t) \tag{1.150}$$

This transformation eliminates the driving from the evolution equation (1.149) and so we find an equilibrium system.

The most studied example is where the driving is a shear flow [19, 70]. The effective dynamics of the surface term in the presence of a shear flow, parallel to the interface [9, 29], is written as

$$\mathbf{v}(\mathbf{x}) = \gamma z \mathbf{e}_x \tag{1.151}$$

The addition of a shear flow leads to the appearance of a nonlinear term in h and the interface statistics thus become non-Gaussian. In Fig 1.10 we show the influence of such a shear flow in numerical simulations, which is exactly the behaviour to be seen in capillary waves in polymer melts [65, 19], see Fig 1.9 . The shear has a confining effect on the interface [71, 72, 73], thus increasing the effective surface tension of the system. In Chap 5 we study the effect of a uniform driving $\nu(\mathbf{x}) = \gamma \mathbf{e}_c$.
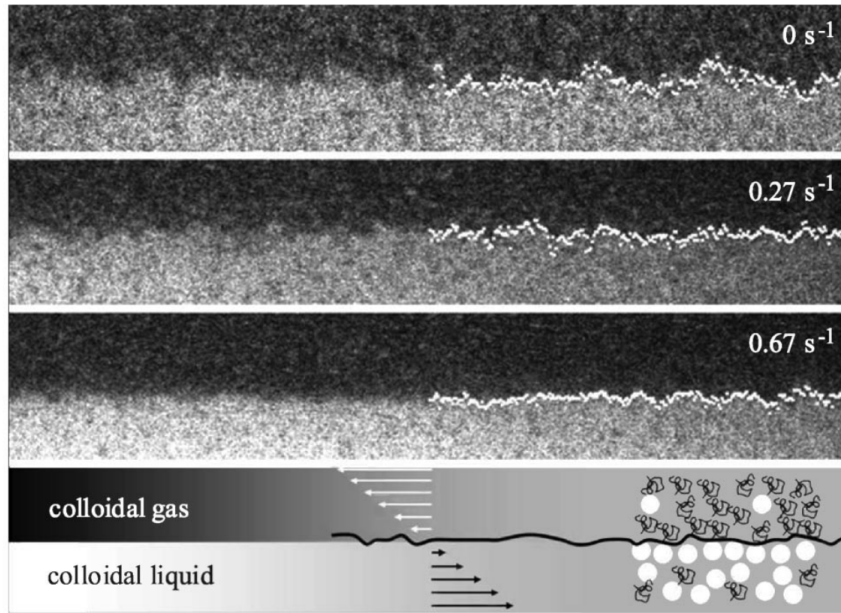
Figure 1.9: Snapshot of the interface a sample of fluorescently labeled poly(methyl methacry-late) (PMMA) colloidal spheres in polystyrene close to the critical point, for different shear rates. The bottom panel schematically shows the flow geometry with the plane of zero velocity located at the interface. From [19].
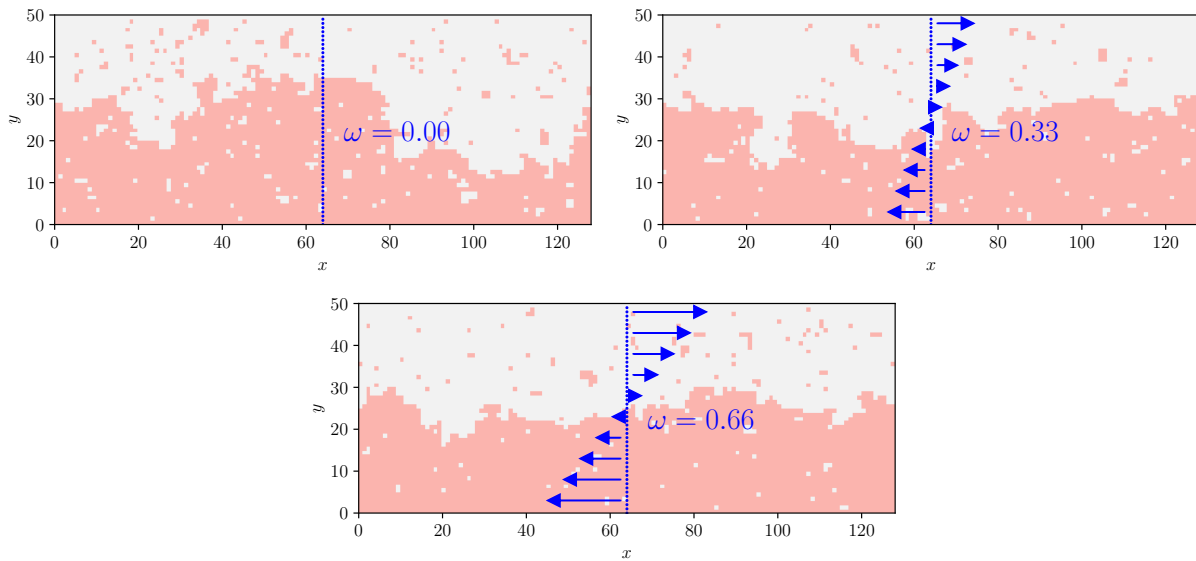

Figure 1.10: Snapshot of a 2D Ising model with respect to the shear (1.151) with Kawasaki dynamics at T = $0.9\mathrm{T}_{\mathrm{2D,C}}$.

1.5 Conclusion

Statistical field theory [22] gives us a method to study the dynamics of equilibrium fields [36]. The surface tension of such a system is then defined as the difference of free energy between the bulk and the interface [25, 5]. The two main models are model A and model B [18], which decribe the dynamics of a field respectively in grand-canonical and the canonical ensemble. From those equations, we have defined what is an interface and have derived the Edwards-Wilkinson equation [30] for both ensembles. The Ising model [4, 34] provides a good way to study the bahviour of the field by discretization, which is easier to compute in numerical simulations [10]. The same kind of dimensional reduction can be done in order to get an interface lattice model which is called the Solid-On-Solid model [6]. This model allows the use of the transfer method in an easier way than the Ising model[74]. Also, the presence of out-of-equilibrum hydrodynamic flows tend to present interesting features. One such example is thee Couette shear [19], which has been found to smoothen the interface [72].

Chapter 2

Numerical methods

In 1949, Metropolis *et.al* [75] presented a method to compute, through Monte Carlo simulations, the expectation value of statistical quantities. If Q is an observable quantity of a statistical system, such as the total energy or density of particles per site, then the expectation value is computed by weighting its value over all configurations C with respect to their statistical weight. If we consider the system to be at thermodynamic equilibrium, then every configuration C follows the Gibbs-Boltzmann distribution, and the mean value $\langle Q \rangle$ is

$$\langle Q \rangle = \frac{\sum_C Q(C) \exp(-\beta E(C))}{\sum_C \exp(-\beta E(C))} \tag{2.1}$$

For example, in a SOS system of size 100×100 - which is small compared to the thermodynamic limit as discussed in figure 1.8 - there exist 100^{100} different possible configurations. In comparison, numerical simulations can explore up to 10^9 configurations in a reasonable amount of CPU time.

Nevertheless, lattice models are well fitted for Monte Carlo simulations, where the goal is to compute such quantities. In the SOS model, all observables (and even quantities not observable such as the free energy) can be directly computed thanks to the matrix transfer in the grand-canonical ensemble. Nevertheless, as stated prior, the canonical ensemble stays out of reach of that method.

In this chapter, we start by explaining how Monte Carlo Metropolis algorithm works based upon the statistical ensemble we're interested in, at or out of equilibrium. At last, I will give some technical considerations about optimizing numerical simulations.

This work has been made possible thanks to the Mésocentre de Calcul Intensif Aquitain (MCIA) [20], where I've made the vast majority of the numerical simulations. All the code I've produced can be found on Github [21] under Creative Commons BY 3.0 licence[1]. Numerical simulations where made with C++, parallelization with MPI, data treatment with Python, and some minor scripts in Bash.

2.1   Estimator

Monte Carlo simulations explore the configurations' space in a random fashion [10] with a probability $p(C)$ which we will define later. By choosing M states $C_0, ..., C_M$, the estimator Q_M of Q is given by

$$Q_M = \frac{\sum_{i=0}^{M} Q(C_i) p(C_i)^{-1} \exp(-\beta E(C_i))}{\sum_{i=0}^{M} p(C_i)^{-1} \exp(-\beta E(C_i))} \tag{2.2}$$

The bigger the M, the better estimate the estimator provides for $\langle Q \rangle$, up to the limit $Q_{M \to \infty} = \langle Q \rangle$. If we select the configurations over which we sample the system according to the Gibbs-Boltzmann

---

[1]https://creativecommons.org/licenses/by/3.0/fr/deed.en

distribution $p(v) = Z^{-1} e^{-\beta E(C)}$, the estimator of $\langle Q \rangle$ is

$$Q_M = \frac{1}{M} \sum_{i=0}^{M} Q(C_i) \tag{2.3}$$

The error over this estimate is

$$E(Q) = \sqrt{\frac{2\tau}{M}(\langle Q^2 \rangle - \langle Q \rangle^2)} \tag{2.4}$$

This error does depend from the correlation time τ since if two states are really close in time, they would be strongly correlated, adding little information to the estimator. In practice, we just need $\frac{\tau}{M} < 10^{-4}$ to obtain an error under 1%. This correlation time τ is computed through the autocorrelation function

$$\mathscr{C}(t) = \langle Q(t')Q(t+t') \rangle - \langle Q \rangle^2 = \frac{1}{t} \int_0^t Q(t')Q(t+t') - \langle Q \rangle^2 dt' \tag{2.5}$$

which behaves as an exponential at long time[76]. A first order estimate of τ is thus given for

$$\tau = \int_0^\infty \mathscr{C}(t)/\mathscr{C}(0) dt \tag{2.6}$$

Similarly, the measurement of the correlation length ξ is given at first order by integration the two-point correlation function

$$\mathscr{C}(j) = \frac{1}{L'} \sum_{i=0}^{L'} \langle h_i h_{i+j} \rangle - \langle h \rangle^2 \tag{2.7}$$

2.2 Monte Carlo Metropolis algorithm

We now want to know how to choose configurations with the correct equilibrium probability.

A dynamic for systems with a discrete configuration state can be built using Markov chains. Let the dynamic evolve in a discrete time n, and $p_n(C)$ the probability that the system is in configuration C at time n. On the time step, if the system is in state C, it can jump to another state C$'$ with a transition probability $\rho(C \to C')$. The system at time $n+1$ thus only depends of the state at time n : that's a Markovian process. The probability $p_{n+1}(C)$ to be in state C at time $n+1$ is equal to the probability that the system was already in state C at time n and stays put with a transition probability $\rho(C \to C)$, plus the probability that it was in state C$'$ and jumps towards C with a transition probability $\rho(C' \to C)$. The master equation of such a dynamic is

$$p_{n+1}(C) = \rho(C \to C) p_n(C) + \sum_{C' \neq C} \rho(C' \to C) p_n(C') \tag{2.8}$$

Since $\rho(C' \to C)$ is a probability, it meets the requirements

$$\sum_{C'} \rho(C' \to C) = 1 \tag{2.9}$$

Now, if the dynamics describes a system in interaction with a heat bath, the equilibrium distribution is given by

$$p_{eq}(C) = \frac{\exp(-\beta E(C))}{Z} \tag{2.10}$$

with Z the partition function. Since the equilibrium distribution is also stationary, we have

$$p_{eq}(C) = \rho(C \rightarrow C) p_{eq}(C) + \sum_{C' \neq C} \rho(C' \rightarrow C) p_{eq}(C') \qquad (2.11)$$

The emergence of equilibrium probability densities ensures that the transition rate from a state to another one is equal to the rate from the reciprocal transition

$$\sum_{C'} p(C) \rho(C \rightarrow C') = \sum_{C'} p(C') \rho(C' \rightarrow C), \qquad (2.12)$$

which leads to the detailed balance condition [10]

$$\frac{\rho(C' \rightarrow C)}{\rho(C \rightarrow C')} = \frac{p(C)}{p(C')} = \frac{\exp(-\beta E(C))}{\exp(-\beta E(C'))} \qquad (2.13)$$

Hence by adopting the detailed balance condition for the transition probabilities, the steady state distribution computed by Eq (2.11) corresponds to the equilibrium Gibbs-Boltzmann distribution. During a Metropolis step, the transition probability of $C \rightarrow C'$ depends of the probability $g(C \rightarrow C')$ that this transition would be chosen amongst all the other possible transitions, and the acceptance rate $A(C \rightarrow C')$, which gives

$$\rho(C \rightarrow C') = g(C \rightarrow C') A(C \rightarrow C') \qquad (2.14)$$

For a lattice model site L' sites, we say that a Monte Carlo time step is done when we have proceeded to L' transition tries.

2.2.1 Glauber dynamics

In the SOS model with L' sites of height comprised in $[0, L]$, the Glauber algorithm [77] makes us chose a site i at random with a uniform probability $\frac{1}{L'}$ and an integer $\alpha = \pm 1$ with probability $\frac{1}{2}$. If the configuration C has the Hamiltonian $H(h_0, h_1..., h_i, ...h_{L'})$, then the new generated configuration will have the Hamiltonian $H(h_0, h_1..., h_i + \alpha, ...h_{L'})$. If $\alpha = +1$, then we add a particle at site i, otherwise we remove one. In the case that $h_i + \alpha \notin [0, L]$, the generated configuration is not valid and discarded. If the generated configuration is valid, the probability of selecting this transition is

$$g(C \rightarrow C') = \frac{1}{2L'} \qquad (2.15)$$

We thus have

$$\frac{\rho(C \rightarrow C')}{\rho(C' \rightarrow C)} = \frac{A(C \rightarrow C')}{A(C' \rightarrow C)} = \exp(-\beta(E(C') - E(C))) \qquad (2.16)$$

Is it possible to choose any acceptance rate $A(C \rightarrow C')$ which satisfies detailed balance. A Metropolis algorithm is an algorithm which has the following acceptance rate

$$A(C \rightarrow C') = \begin{cases} \exp(-\beta(E(C') - E(C))) & \text{if } E(C') - E(C) > 0 \\ 1 & \text{otherwise} \end{cases} \qquad (2.17)$$

In practice, if $\Delta E > 0$, we randomly choose an integer uniformly in $r \in [0, 1]$. If $r < A(C \rightarrow C')$ then the transition is accepted. Otherwise, the transition is rejected and the system stays in the configuration C.

Since $\sum_i h_i$ is not conserved over time, Glauber dynamics corresponds to model A.

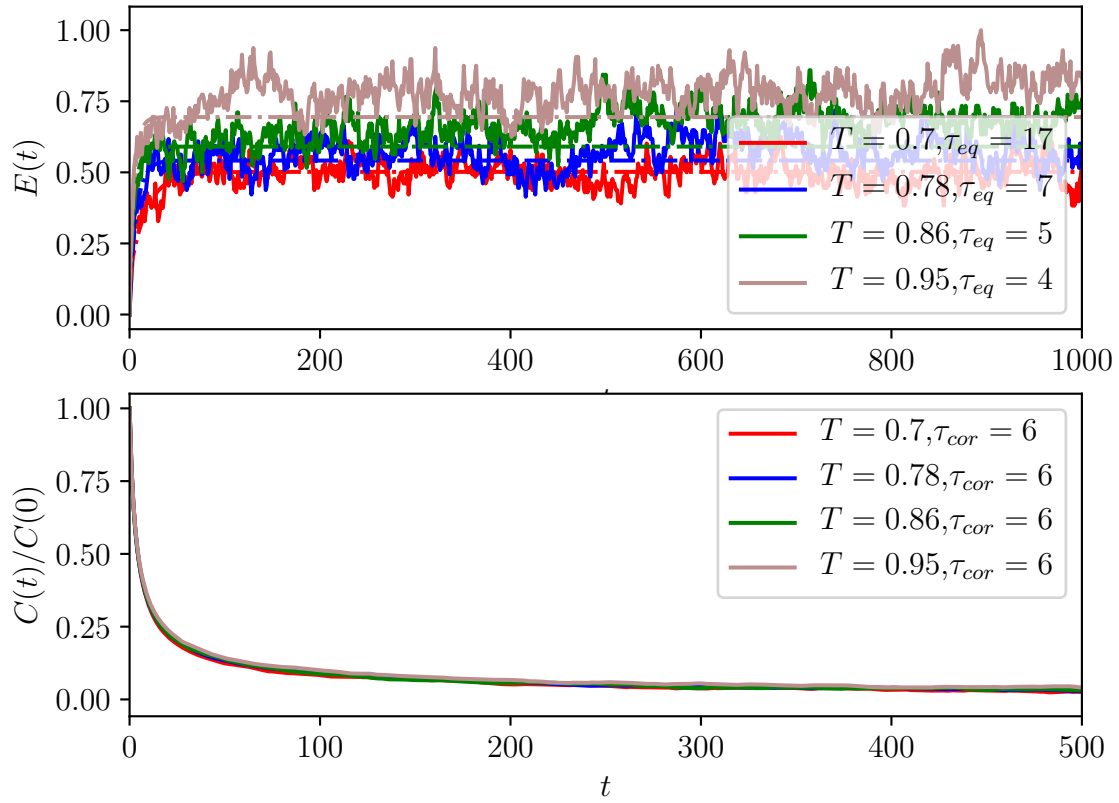Figure 2.1: Plot of the energy per site (top) and the autocorrelation function (bottom) with Glauber dynamics from an initial state where $h_i = 0$, for different temperatures.
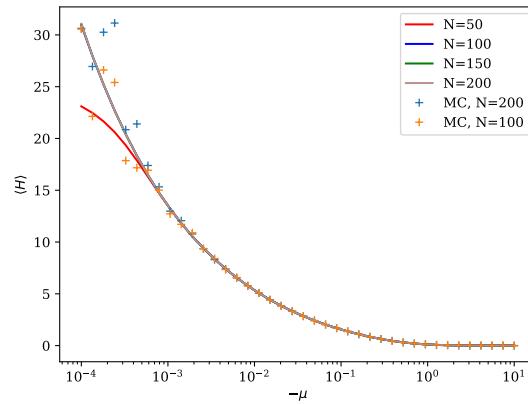

Figure 2.2: Mean height value per site with respect to μ different system size L both by Glauber dynamics and diagonalization of the transfer matrix (which has already been shown in Fig 1.6) for $\beta = 1$ and $L' = 256$.

The energy difference between two configurations is

$$\Delta E = |h_{i-1} - (h_i + \alpha)| + |h_{i+1} - (h_i + \alpha)| - |h_{i-1} - h_i| - |h_{i+1} - h_i| \tag{2.18}$$

It is not needed to compute the total height at each time step. We can stock $\sum_i h_i$ in a variable that is updated each time a transition is accepted by

$$\langle h \rangle_{M+1} = \langle h \rangle_M + \alpha \tag{2.19}$$

We can do the same for $\sum_i h_i^2$, which gives us the interface's width, or the total energy of the system with $\sum_i |h_i - h_{i+1}|$.

In order to accelerate the equilibration process, we can directly start from the total height computed by the transfer matrix. We then get the equilibrium correlation time by looking at $E(t)$. It is better practice to study the equilibration time by taking the total energy rather than the number density, or magnetization, since without an external potential, the interface is delocalised and total number of particles is only bounded by the boundary conditions. In Fig 2.1, we show the energy with respect to time and the autocorrelation function of the system in absence of chemical potential from a ground state $h_i = 0$ for all i. The very small correlation and equilibration times means that numerical simulations reach the equilibrium distribution after 10^3 MC steps, so that 10^7 MC steps will give accurate results.

In the SOS model, we expect to have the results from the Glauber dynamics to be exactly the same as the transfer matrix method, as shown in Fig 2.2. Since the interface is not localised for small μ, even though we reach thermal equilibrium fast, the mean height fluctuates a lot, making its measurement irrelevant in the delocalised limit. Since we can get exact results from the transfer matrix, the Glauber dynamics presents little interest for SOS models in the grand-canonical ensemble. Nevertheless, because there does not exist a transfer matrix formulation of the canonical ensemble, Monte Carlo simulations become interesting.

2.2.2 Kawasaki dynamics

Now we would like to have an algorithm for the canonical ensemble, where the total height stays constant. In the Kawasaki's algorithm [78], we randomly choose a site i with probability $\frac{1}{L'}$, and one of its two neares neighboors $i-1$ or $i+1$ with probability $\frac{1}{2}$. For example, if we take the neighboor site $i-1$ (it holds the same for the site $i+1$), we generate a new configuration with Hamiltonian $H(h_0, ..., h_{i-1} + 1, h_i - 1, ...h_{L'})$, where we have taken a particle from site i to diffuse it to the other site. The selection probability is

$$g(C \rightarrow C') = \frac{1}{2L'} \tag{2.20}$$

We also chose the same acceptance rate as in Glauber's dynamics (2.17).

Here, the total height is obviously conserved. In the case that we transfer a particle to site i to site $i+1$, the energy difference is

$$\Delta E = |h_{i-1} - (h_i - 1)| + |h_{i+1} + 1 - (h_i - 1)| + |h_{i+1} + 1 - (h_{i+2})|$$
$$- (|h_{i-1} - h_i| + |h_{i+1} - h_i| + |h_{i+1} - h_{i+2}|) \tag{2.21}$$

In Fig 2.3, we remark that both the equilibration and the correlation times are larger than for non-conserved dynamics, which is normal since the correlation length during coarsening goas as $t^{\frac{1}{2}}$ in model A and as $t^{\frac{1}{3}}$ in model B. Nevertheless they are of the same order of magnitude, which means that numerical simulations will take up CPU times on the same scale.
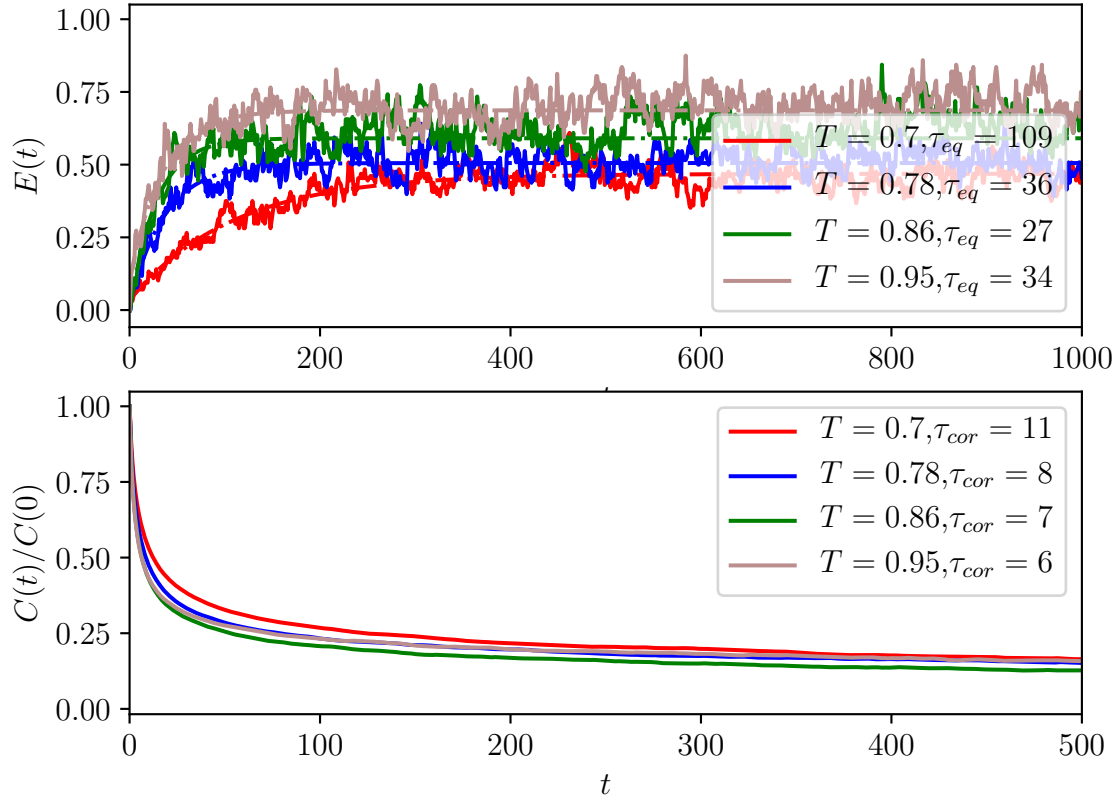
Figure 2.3: Plot of the energy per site (top) and the autocorrelation function (bottom) with Kawasaki dynamics from an initial state where $h_i = 0$, for different temperatures.

This dynamics describes the diffusion of particles at the interface. It is thus possible to add some hydrodynamic flow which breaks equilibrium. Since we have supposed that our configurations obeys the Gibbs-Boltzmann distribution, the Metropolis method stays pertinent if we assume that the dynamic is slow compared to the heat exchange with the reservoir.

2.3 Computing size dependent free energy

2.3.1 The Layer method

It is not possible to compute from Monte Carlo simulations the free energy of a system, since it is not a derivative of the partition function. However, we can compute its derivative with respect to the system size. This is useful to compute. As detailed later in Sec 3.1, the total free energy of the confined system has a bulk and a singular part

$$F(t, h, L) = L'^2 \left(L f_{bulk} + \beta^{-1} f_{ex} \right) \tag{2.22}$$

where f_{bulk} is a bulk term, and f_{ex} the excess free energy due to boundary conditions and to system spanning correlations. The thermodynamic force per unit area is defined as

$$p(t, h, L) = -\frac{1}{L'^2} \frac{\partial F}{\partial L} = -f_{bulk} - \beta^{-1} \frac{\partial f_{ex}}{\partial L} \tag{2.23}$$

We see that this force is composed of a bulk term and an excess term, which is the Casimir force, defined as The related to the Casimir force per unit area by

$$f_{casimir} = -\beta^{-1} \frac{\partial f_{ex}}{\partial L} \tag{2.24}$$

In the limit $L \to \infty$, the excess free energy due to the confinement is zero, so we can can substract the bulk free energy from Eq (2.22) with respect to the inifinite system. For two systems of size L_1 and L_2, where $\left(\frac{L_1}{L_2}\right)^d \ll 1$, at first order the Casimir force is thus

$$f_{ex}(L_1) \simeq -\frac{1}{L'^2} \frac{\partial F(L_1)}{\partial L} + \frac{1}{L'^2} \frac{\partial F(L_2)}{\partial L} \tag{2.25}$$

To achieve that, Vasilyev [11] developed a method to compute this derivative thanks to a dummy coupling parameter. Even though the system's size is discrete, it is possible to obtain a continuous-like size of the system thanks to the progressive decoupling the k-th layer of the system. If H_0 is the Hamiltonian of size L and H_1 the Hamiltonian of size $L-1$ (see Fig 2.4), then we define the crossover Hamiltonian as

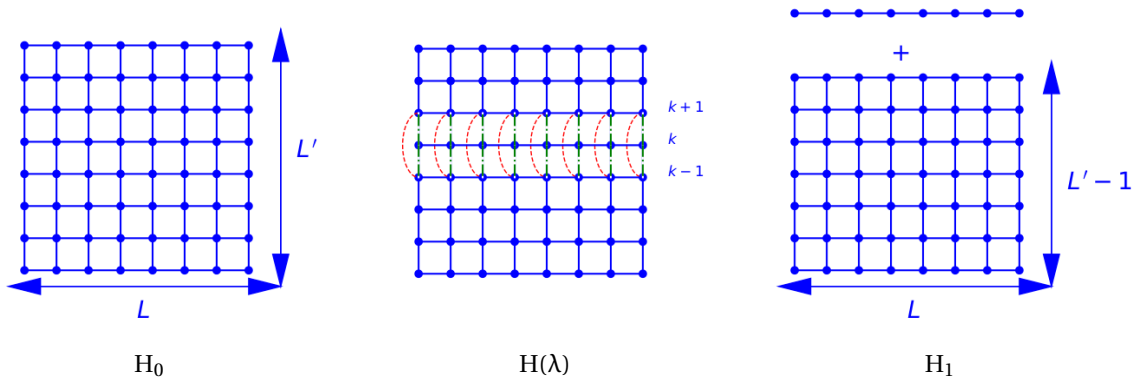$$H_{cr}(\lambda) = (1 - \lambda)H_0 + \lambda H_1 \tag{2.26}$$

Figure 2.4: Progessive decoupling of the k-th layer of the system in order to compute the freen energy through the Crossover Hamiltonian. Blue bonds have an energy of βJ, red ones an energy of $\lambda \beta J$ and the green ones an energy of$(1 - \lambda)\beta J$. Reproduction 2D of [11].

with $\lambda \in [0,1]$, which interpolates from H_0 to H_1 when λ goes from 0 to 1. As λ goes on, we gradually decouple the k-th layer of the system, which means that the interaction energy of all vertical bonds between layer k and layers $k-1$ and $k+1$ are now equal to $(1-\lambda)\beta J$, while we gradually couple the layers $k+1$ and $k-1$ with an energy $\lambda\beta J$. The crossover Hamiltonian $H_{tr}(\lambda)$ also depends on the position of the decoupled layer $k \in 1,2,...,L$. The free energy associated with this system is

$$F_{cr}(\lambda) = -k_B T \ln\left(\sum_{h_1...h_L} \exp(-\beta H_{tr}(\lambda))\right) \tag{2.27}$$

From the derivative of the free energy with respect to λ, we find

$$\frac{\partial F_{cr}(\lambda)}{\partial\lambda} = \langle H_1 - H_0\rangle_{H_{cr}(\lambda)} \tag{2.28}$$

where $\langle\cdot\rangle_{H_{cr}(\lambda)}$ represents the statistical mean value in the crossover system, easily computable in numerical simulations. By integrating over the coupling constant, we have

$$F_1 - F_0 = \int_0^1 d\lambda\langle H_1 - H_0\rangle_{H_{cr}(\lambda)} \tag{2.29}$$

Finally, in the thick limit where $L \gg 1$, we find

$$-\frac{\partial F(t,h,L)}{\partial L} \simeq \int_0^1 d\lambda\langle H_1 - H_0\rangle_{H_{cr}(\lambda)} \tag{2.30}$$

Even though $H_{cr}(\lambda)$ depends of which layer we decided to decouple, and by transition $H_1 - H_0$ and $\langle H_1 - H_0\rangle_{H_{cr}(\lambda)}$, the integrand $\int_0^1 d\lambda\langle H_1 - H_0\rangle_{H_{tr}(\lambda)}$ should be independent of this choice, as long as boundary conditions are not affect by the k-th layer.

For the SOS model, it is possible to exactly compute the energy variation produced by the decoupling. We find that

$$H_{cr,\text{SOS}}(\lambda) = H_{0,\text{SOS}} -$$
$$\frac{\lambda J}{2}\sum_x \left[\text{sgn}(k-1-h(x))\,\text{sgn}(k+1-h(x)) - \text{sgn}(k-h(x))\big(\text{sgn}(k-1-h(x)) + \text{sgn}(k+1-h(x))\big)\right] \tag{2.31}$$

where the prefactor $\frac{1}{2}$ take into account the prefactor between Ising and SOS models in Hamiltonian (1.125). By doing the table of values , we notice that every term in the sum is equal to -1 independently of k, since contrary to Ising models, SOS models do not possess any bulk energy. We thus have to find another method to compute the thermodynamic force in the SOS model.

2.3.2 The Lopes-Jacquin-Holdsworth method

Since the Layer method does not work for our models, we have to look to other ways. In the case of a chemical potential conjugated with the total height, we see that [12]

$$\langle\sum_i h_i\rangle(\mu,L) = -\frac{\delta F(\mu,L)}{\delta\mu} \tag{2.32}$$

If we integrate over the chemical potential, we have

$$\Delta F(\mu_1,\mu_2) = F(\mu_1,L) - F(\mu_2,L) = -\int_{\mu_1}^{\mu_2} d\mu'\langle\sum_i h_i\rangle_{\mu'} \tag{2.33}$$

In the case where we know the analytical forme of the free energy in the limits $\mu_2 \to \infty$ or $\mu_1 \to 0$, this method provides a way to directly measure the free energy of the system for any temperature or size by integrating over the chemical potential.

In the limit $\mu_2 \to \infty$, the correlation length at the reference state will be small so that the reference free energy will be essentially that of the bulk. As a consequence, it should contain all the information of the Casimir force (2.23). That derivative force can then be computed by

$$\delta L \frac{\partial F(\mu_1, L)}{\partial L} = \Delta F(\mu_1, \mu_2, L) - \Delta F(\mu_1, \mu_2, L - \delta L) \tag{2.34}$$

where δL is the difference thickness between two systems, and which is then independent of μ_2 in the large chemical potential limit as the free energy $F(\mu_2, L)$ converges to the bulk energy. Since in Kawasaki dynamics the total height is constant, this method does work only for model A.

The computation of the difference of free energy depends largely of the chemical potential μ_2. However, since we are interested in the Casimir force (2.25), it is sufficient to chose a suitable chemical potential μ_2 for which the excess free energy can be safely considered negligible [12] . We define the function

$$D(\mu, L_1, L_2) = \langle M(L_1) - M(L_1 - 1) - (M(L_2) - M(L_2 - 1) \rangle \tag{2.35}$$

where $M = \sum_i h_i$ are taken at the same temperature and chemical potential, omitted in the notation for the sake of lightness. The contribution of high μ becomes negligible to the Casimir force when the function D becomes null.

The method only makes sense in the Glauber dynamics. In the Kawasaki dynamics, since $\sum_i h_i$ is set to a constant, the integration is done over a constant. We will see in Sec 3.3 a generalized method to bypass this problem.

2.4   Tips and tricks

The simulation's speed of SOS models is so great compared to Ising ones that it is possible to study systems over a wider range of parameters. A SOS simulation of 10^7 MC steps takes roughly 20 minutes to complete once fully optimized. We see that if we want to launch hundreds of those simulations, it can easily take days, which forces us to optimize the code. In C++, if compiling with g++, the first thing to do is to compile the programme with the $-O3$ flag, which makes you gain an order of magnitude in CPU time.

The most important part of Monte Carlo simulations are the pseudo Random Number Generator (pRNG), which are called at least twice for each transition attempt. The C++ standard library proposes the function *default_random_engine* as the default pRNG. A lot of CPU time can be saved by switching to *sfc64* or *xoroshiro* pRNGs. Furthemore, the generation of ± 1 numbers only require one bit, while the pRNG always generates a 64-bits number, thus wasting 63-bits at each boolean generation. A wasteless method which speeds considerably the simulation's speed can be found in [79].

Lastly, the easiest way to gain real time is to make the code parallel. We can do that either by domain decomposition - which would allow us to simulate larger systems - or parallelise directly over the simulation's parameters (as the temperature or the chemical potential). While the first one is useless in SOS model because of the short correlation length of such systems, the latter can be done via two libraries : OpenMP and MPI. It took me some time to understand that the memory-shared OpenMP protocol has a lot of problems with pRNGs, making this library not suited for Monte Carlo simulations. On the contrary, the MPI library provides impermeability between threads, which makes it the better choice.

2.5 Conclusion

In this chapter, we have explained how to compute expectation values of observables in our system [10], thanks to the Monte Carlo Metropolis algorithm [75]. For that, we need to suppose that the system is in thermal equilibrium with a heat bath, and that it respects detailed balance. We have two different possible algorithms : the Glauber dynamics [77] allows to study the systems in the grand-canonical ensemble, while the Kawasaki dynamics [78] is for canonical ones. Nevertheless, since the transfer matrix method gives exact results for the grand-canonical ensemble, only the Kawasaki dynamics is relevant for SOS models.

In addition to that, measuring the free energy of the system is not an easy task, as we can only compute its derivative. The first method we have presented is about progressively decoupling a layer of the system [11], even though for SOS models, which do not possess a bulk energy, the method does not work. Another method is to integrate over the conjugate variable coupled to the total height [12], which is the chemical potential. This method does not work for Kawasaki algorithms. Since as we have discussed Glauber simulations are not relevant for our models, we find that we have no way to compute the free energy in Monte Carlo methods for the only relevant ensemble which is the canonical one. In a latter chapter, we will see how to fix this issue.c

Chapter 3

Equilibrium Interface models and their finite size effects

Models for interfaces arise naturally in phase separated systems, as explained in 1. Finite size corrections are manifested when the correlation length becomes of the order of magnitude of the system's size. When undergoing a continuous phase separation, the system exhibits finite size corrections which are manifested by a long range critical Casimir interaction, which we describe in the first section. In the second section we examine finite size effects in continuous interface models in one dimension, and show that while they have similar long-range interactions, the forces induced by interface confinement are quite different, and will be compared to the GSOS model. In the last section, we compute the size-dependent eigenvalues of the transfer matrix for the free SOS model, and compare the results with previous works.

3.1 The Casimir effect

Here we explain the critical Casimir effect. For completeness we start by explaining the quantum Casimir effect as it was in the quantum context that the effect was first observed [14]. We also describe the basis of the Lifshitz theory that generalises Casimir's contribution to general dielectric materials beyond the perfectly conducting plate paradigm.

3.1.1 Quantum Casimir effect

In an ideal conductor, the free charges can move arbitrarily quickly to cancel out any electric in the plane [80]. Thus, a perfectly conducting plate in the (x, y) plane imposes boundary conditions on the electromagnetic field

$$\mathbf{E} \times \mathbf{n} = \mathbf{0}; \ \mathbf{B} \cdot \mathbf{n} = 0 \tag{3.1}$$

The quantum Hamiltonian for the electromagnetic field is given by

$$H = \sum_{\mathbf{k}, \lambda} \hbar \omega(\mathbf{k}, \lambda) \left[a^\dagger(\mathbf{k}, \lambda) a(\mathbf{k}, \lambda) + \frac{1}{2} \right] \tag{3.2}$$

Here λ denotes the polarisation (there are two polarisation states) and $\mathbf{k}$ the wave vector. The dispersion relation for photons is

$$\omega(\mathbf{k}, \lambda) = |\mathbf{k}| c. \tag{3.3}$$

The ground state energy of the electromagnetic field [14] is given by

$$E_0 = \langle 0|H|0 \rangle = H = \sum_{\mathbf{k}, \lambda} \frac{1}{2} \hbar \omega(\mathbf{k}, \lambda) = \sum_{\mathbf{k}} \hbar |\mathbf{k}| c \tag{3.4}$$

The presence of conduction plates at $z = 0$ and $z = L$ means that the wave vectors k_z must be quantised according to $k_z = n\pi/L$ where $n \in \{0, 1, 2, \cdots\}$ while if the (x, y) plane has a large area A we can write

$$\sum_{k_x, k_y} \cdot = \frac{A}{(2\pi)^2} \int d^2\mathbf{k} \cdot \tag{3.5}$$

This then gives

$$E_0(L) = \frac{\hbar cA}{(2\pi)^2} \sum_{n=0}^{\infty} \int d^2\mathbf{k} \left(\mathbf{k}^2 + \frac{n^2\pi^2}{L^2}\right)^{\frac{1}{2}} \tag{3.6}$$

$$= \frac{\hbar cA}{(2\pi)} \sum_{n=0}^{\infty} \int_0^{\infty} k dk \left(\mathbf{k}^2 + \frac{n^2\pi^2}{L^2}\right)^{\frac{1}{2}} \tag{3.7}$$

The problem with the above expression is that it is clearly divergent. However it can be rendered finite by cutting off the high momentum degrees of freedom by writing

$$E_0(L) = \frac{\hbar cA}{(2\pi)} \sum_{n=0}^{\infty} \int_0^{\infty} k dk \left(\mathbf{k}^2 + \frac{n^2\pi^2}{L^2}\right)^{\frac{1}{2}} f\left((\mathbf{k}^2 + \frac{n^2\pi^2}{L^2})^{\frac{1}{2}}\right) \tag{3.8}$$

where f is a smooth function such that $f(p) = 1$ for $p \ll \Lambda$ and $f(p) = 0$ for $p \gg \Lambda$. Here, Λ is an ultraviolet cut-off and f thus only counts the contribution of photons with a momentum less than $\hbar\Lambda$. For this sort of calculation to make physical sense the physical result we get at the end should be independent of both the choice of f and Λ.

In the limit $L \to \infty$ we can replace the sum over discrete modes by an integral, as usual in statistical physics,

$$E_0(L) = \frac{\hbar cA}{(2\pi)} \int_0^{\infty} \frac{L}{\pi} d\nu \int_0^{\infty} k dk \left(\mathbf{k}^2 + \nu^2\right)^{\frac{1}{2}} f\left((\mathbf{k}^2 + \nu^2)^{\frac{1}{2}}\right) \tag{3.9}$$

where we have used $d\nu = \pi/L$. We thus see that for large L we have

$$E_0(L) = AL\epsilon_{bulk} \tag{3.10}$$

where ϵ_{bulk} is a bulk energy density per unit of volume, that is to say the total energy is extensive. The computation above only calculates the energy of the EM field between the plates. If the physical system extends up to $L' \gg L$, then the total energy of both the interior and the exterior of the plates is given by

$$E_{total}(L) = E_0(L) + A(L' - L)\epsilon_{bulk} \tag{3.11}$$

We see that the part of the energy that depends on L is given by

$$U(L) = E_0(L) - AL\epsilon_{bulk} \tag{3.12}$$

It is the derivative of U which gives the physical interaction between the two plates, the pressure associated with this interaction in the colloid science literature is called the disjoining pressure [81] where to compute the effective interaction the bulk pressure has to be subtracted. Now we simply write

$$AL\epsilon_{bulk} = \frac{\hbar cA}{(2\pi)} \int_0^{\infty} dn \int_0^{\infty} k dk \left(\mathbf{k}^2 + \frac{n^2\pi^2}{L^2}\right)^{\frac{1}{2}} f\left((\mathbf{k}^2 + \frac{n^2\pi^2}{L^2})^{\frac{1}{2}}\right) \tag{3.13}$$

where we have put the L dependence in the integral. This then gives

$$U(L) = \frac{\hbar cA}{(2\pi)} \left[\sum_{n=0}^{\infty} g(n) - \int_0^{\infty} dn\, g(n)\right] \tag{3.14}$$

where

$$g(n) = \int_0^\infty k \, dk \left(\mathbf{k}^2 + \frac{n^2\pi^2}{L^2} \right)^{\frac{1}{2}} f\left((\mathbf{k}^2 + \frac{n^2\pi^2}{L^2})^{\frac{1}{2}} \right) = \frac{1}{2} \int_{\frac{n^2\pi^2}{L^2}}^\infty du \, u^{\frac{1}{2}} f(u^{\frac{1}{2}})$$

(3.15)

We now use the Euler-Mauclarin formula

$$\sum_{n=0}^\infty g(n) - \int_0^\infty dn \, g(n) = -B_1 g(0) - \frac{1}{2} B_2 g'(0) - \frac{1}{24} B_4 g'''(0) - \cdots$$

(3.16)

where B_n are the Bernoulli numbers[1]. We find that

$$g'(n) = -\frac{\pi^3}{L^3} n^2 f\left(\frac{n\pi}{L} \right)$$

(3.17)

and noticing than in the region around $n = 0$, $f = 1$ is a constant, we show that

$$g'(0) \quad = \quad 0$$ (3.18)

$$g''(0) \quad = \quad 0$$ (3.19)

$$g'''(0) \quad = \quad -\frac{2\pi^3}{L^3}$$ (3.20)

Higher order derivatives are zero so the full result is given by the first three terms of the Euler-Maclaurin formula. We thus find

$$U(L) = \frac{\hbar c A}{(2\pi)} \left[-g(0) - \frac{\pi^3}{360 L^3} \right]$$

(3.21)

The first term independent of L can be interpreted as a surface energy. The effective L dependent interaction is given by

$$U_{int}(L) = -\frac{\hbar \pi^2 c A}{720 L^3}$$

(3.22)

We see that the effective interaction is attractive. Interestingly Casimir thought that his calculation could explain the stability of the electron [14, 82] The model of the electron is one of a perfectly conducting shell carrying an electric charge e. If the radius of the shell is a then the electrostatic energy of due to the charge is given by

$$E_{Charge} = \frac{e^2}{8\pi a \epsilon_0}$$

(3.23)

There is thus a repulsive force on the shell which should make it expand. Casimir thought that the Casimir force on a spherical geometry, if is an attractive force as is the case for the parallel plate geometry, could stabilise the electron. Clearly by dimensional analysis

$$E_{Cas} = -\frac{Z\hbar c}{a}$$

(3.24)

The balance of the Casimir and electric forces would then require

$$Z = \frac{e^2}{8\pi \hbar c}.$$

(3.25)

However, in the case of conducting spherical shell, the constant $Z \simeq -0.046175$ is negative [83, 84, 85], while the same calculation for a cylindrical geometry predicts an attractive force [84].

---

[1]The first Bernoulli numbers are explicitly given by $B_1 = 1$, $B_2 = \frac{1}{2}$, $B_4 = -\frac{1}{30}$

3.1.2 Lifshitz Theory

The Casimir calculation is based on the boundary conditions imposed on the EM field due to a conductor. However, this is an ideal mathematical limit, conductors being conductors because free charges can move to cancel out the electric field in the conducting surface. The Casimir force can also be seen as due to correlations induced in the charge fluctuations in each plate, which allows for an alternative method based on sources which recovers the Casimir force [86, 87]. In a sense therefore the effect can be interpreted without reference to the zero point energy of the vacuum and the Casimir calculation works due to the fact that the mathematical limit in going to a perfect conductor works. Using a stochastic formulation of electrodynamics by Rytov [88], the Casimir calculation was generalized by Lifshitz for interactions between arbitrary electrical bodies, characterized by their local electric and magnetic response[15]. Even though this theory is very general, the microscopic justification is not completely rigorous, source terms (random currents and dipole fluctuations) are introduced to Maxwell's equations to give a Langevin formulation of Maxwell's equations in the presence of dielectric bodies. The correlation functions of the white noise terms depend on the temperature of the system and are determined via the quantum fluctuation dissipation theorem. The Lifshitz theory is computationally difficult to work with and it was reformulated in a way more useful for practical calculations and that can be applied to experimental setups [89, 90]. Rytov's formulation has the advantage that it can be used to treat out of equilibrium situations where different bodies are held at different temperatures. This allows both the computation of out of equilibrium forces and radiative heat transfer.

The theory in the presence of electromagnetic media is written in terms of the electric and magnetic fields **E** and **B** and the displacement and magnetizing fields **D** and **H** which are assumed to obey local relations in real space and Fourier space

$$\tilde{\mathbf{D}}(\omega) = \epsilon(\omega)\tilde{\mathbf{E}}(\omega); \ \tilde{\mathbf{B}}(\omega) = \mu(\omega)\tilde{\mathbf{H}}(\omega) \tag{3.26}$$

where $\tilde{\epsilon}(\omega)$ and $\tilde{\mu}(\omega)$ are the frequency dependent permittivity and permeability. The boundary conditions at the interface between two materials 1 and 2 are given by

$$B_{1n} = B_{2n} \qquad D_{1n} = D_{2n} \tag{3.27}$$

$$E_{1t} = E_{2t} \qquad H_{1t} = H_{2t} \tag{3.28}$$

where n denotes the normal component and t the tangential component to the interface.

Forces can be computed using the vacuum (assuming that the surface where the force is computed is next to the vacuum) Maxwell stress tensor.

$$T_{ij} = \epsilon\left(E_i E_j - \frac{1}{2}\delta_{ij}E^2\right) + \frac{1}{\mu}\left(B_i B_j - \frac{1}{2}\delta_{ij}B^2\right) \tag{3.29}$$

Notice that the stress tensor is quadratic in the fields **E** and **B**, this means that even if the fields are on average zero, both thermal and quantum fluctuations give rise to forces.

In media Maxwells equations are

$$\nabla \times \mathbf{E} \ = \ -\frac{\partial \mathbf{B}}{\partial t} \tag{3.30}$$

$$\nabla \times \mathbf{H} \ = \ \mathbf{J} - \frac{\partial \mathbf{D}}{\partial t} \tag{3.31}$$

$$\nabla \cdot \mathbf{D} \ = \ \rho \tag{3.32}$$

$$\nabla \cdot \mathbf{B} \ = \ 0 \tag{3.33}$$

In a dielectric medium or conductor where there are no applied external fields there is no free charge or current . As such, the average values of **E** and **B** are zero. Rytov's idea was to add a random

current to induce both thermal and quantum fluctuations into the problem. If we assume that the only contribution to the current comes from a fluctuating polarization density **P** we can write

$$\frac{\partial \rho}{\partial t} + \nabla \cdot \mathbf{J} = 0 \implies \nabla \cdot \left[-\frac{\partial \mathbf{P}}{\partial t} + \mathbf{J} \right] = 0 \tag{3.34}$$

where we have used

$$\rho = -\nabla \cdot \mathbf{P} \tag{3.35}$$

This means that the current is given by

$$\mathbf{J} = \frac{\partial \mathbf{P}}{\partial t} \tag{3.36}$$

or in Fourier space

$$\tilde{\mathbf{J}}(\omega) = i\omega \tilde{\mathbf{P}}(\omega) \tag{3.37}$$

Now if we assume that the fluctuations in the polarization density are uncorrelated in space, the fluctuation dissipation theorem tells us that the correlation function of the polarization density in Fourier space is given by

$$\langle P_\alpha(\omega;\mathbf{x})P_\beta^\dagger(\omega;\mathbf{x}')\rangle_{sym} = \frac{\hbar\epsilon''(\omega)}{2}\coth\left(\frac{\hbar\omega}{2k_BT}\right)\delta(\omega-\omega')\delta(\mathbf{x}-\mathbf{x}')\delta_{\alpha\beta} \tag{3.38}$$

$$\epsilon(\omega) = \epsilon'(\omega) + i\epsilon''(\omega) \tag{3.39}$$

The Lifshitz calculation for slab geometries gives a force per unit area between two slabs of media separated by a distance L

$$
\begin{aligned}
\frac{F}{A} &= -\frac{k_BT}{\pi c^3}\sum_{n=0}^{\infty}\omega_n^3\int_1^{\infty}dp\,p^2\left[1-\frac{(s_1+p)(s_2+p)}{(s_1-p)(s_2-p)}\exp(-\frac{2p\omega_nL}{c})\right] \\
&+ \left[1-\frac{(s_1+p\epsilon_1)(s_2+p\epsilon_2)}{(s_1-p\epsilon_1)(s_2-p\epsilon_2)}\exp(-\frac{2p\omega_nL}{c})\right]
\end{aligned}
\tag{3.40}
$$

where $\epsilon = \epsilon_0\epsilon$, $s_i = \sqrt{\epsilon_i - 1 + p^2}$, $\omega = \frac{2\pi nk_BT}{\hbar}$ are the Mastubara frequencies [8] and $\epsilon_i = \epsilon_i(i\omega_n)$. Note that the integral over real frequencies has become a sum over discrete Matsubara frequencies, they come from the poles in the hyperbolic cotangent.

One needs to know the dielectric response at imaginary frequency, this is done using the Kramers-Kronig relation

$$\epsilon(i\omega) = 1 + \frac{2}{\pi}\int_0^{\infty}d\zeta\frac{\zeta\epsilon''(\zeta)}{\omega^2+\zeta^2} \tag{3.41}$$

3.1.3 Critical Casimir effect

In systems having a continuous phase transition the correlation length diverges as the critical point is approached. This means that the correlation length has a size comparable to that of the system size, this leads to strong finite-size effects in the free energy. Following the arguments of Fisher and de Gennes [3], we describe how a version of the Casimir effect is manifested in critical systems.

3.1.3.1 Bulk scaling for near critical systems

The free energy for a system consisting of N spins has a singular part at a critical temperature T_c which can be written as

$$F(t,h) = Nf(t,h) \tag{3.42}$$

where $t = (T - T_c)/T_c$ measures the distance from the critical point and h is the external applied magnetic field. We assume that we are in a system where the only relevant parameters are T and h (equivalently the concentration or chemical potential of a binary mixture), which is true for $d < 4$ [7]. Now if we carry out a renormalisation group transformation blocking spins in blocks of linear size b into new effective spins, the RG transformation gives

$$N f(t, h) = N' f(t', h')$$
(3.43)

Clearly the number of spins in the blocked system is given by $b^d N' = N$ and the RG transformation for t and h are given by $t' = b^{y_1} t$ and $h' = b^{y_2} h$, where y_1 and y_2 are positive and are the RG exponents for the fields t and h (from which all critical exponents can be deduced). This then means that

$$f(t, h) = \frac{1}{b^d} f(b^{y_1} t, b^{y_2} h)$$
(3.44)

We begin by working with $t > 0$ but the arguments here are trivially generalisable to the case $t < 0$. In Eq. (3.44) is we choose b such that $b^{y_1} t = 1$, then, at the critical field $h = 0$, we find

$$f(t, 0) = t^{\frac{d}{y_1}} f(1, 0)$$
(3.45)

The singularity in the specific heat is defined via

$$c \sim \frac{\partial^2}{\partial t^2} f(t, 0)$$
(3.46)

and so we find

$$c \sim t^{\frac{d}{y_1} - 2} \sim t^{-\alpha}$$
(3.47)

where α is the exponent associated with the divergence of the specific heat. This means that

$$\alpha = 2 - \frac{d}{y_1}$$
(3.48)

The RG transformation for the correlation function has the form

$$C(r, t, h) = \lambda^2(b) C(r/b, b^{y_1} t, b^{y_2} h)$$
(3.49)

Clearly length scales transform as $r' = r/b$. Again setting $h = 0$ and choosing $b^{y_1} t = 1$ gives

$$C(r, t, h) = \lambda^2(t^{-\frac{1}{y_1}}) C(r/t^{-\frac{1}{y_1}}, 1, 0).$$
(3.50)

The correlation function, by definition is given by

$$C(r, t) \sim f(r/\xi),$$
(3.51)

where ξ is the correlation length. This immediately tells us that $\xi = t^{-\frac{1}{y_1}}$ and from the usual definition

$$\xi \sim t^{-\nu}$$
(3.52)

we have $\nu = 1/y_1$. These two formula for y_1 then give the hyper scaling relation

$$\alpha = 2 - d\nu.$$
(3.53)

The exponents α and ν are the ones that are important in the critical Casimir effect.

3.1.3.2 Finite size scaling

Consider a system which is finite in one direction with either periodic boundaries or two surfaces. While the critical system has $h = 0$ there can be local surface fields at each surface a and b. This represents a preference of the surfaces for one phase or the other. The finite scaling hypothesis for a slab system of large area A but with finite width L can be stated as

$$f(t, h_a, h_b, L^{-1}) = \frac{1}{b^d} f(b^{y_1} t, b^{y_a} h_a, b^{y_b} h_b, bL^{-1})$$ (3.54)

We thus see that the field L^{-1} is a relevant field with RG exponent $y_L = 1$. The surface fields are not necessarily relevant so we can have y_a and y_b positive or negative. The important point about finite size scaling is that when L is finite the singularity due to the thermodynamic phase transition is smoothed out by the system's finite size (note that we assume that the system has no two-dimensional phase transition in the region we are looking at). First we see that when L is large there should be a bulk contribution to the free energy plus a surface term (so we are considering the limit $L \to \infty$ before $\xi \to \infty$)

$$f(t, h_a, h_b, L^{-1}) = f(t, h_a, h_b, 0) + L^{-1} \frac{\partial f(t, h_a, h_b, 0)}{\partial x_4}$$
$$= \frac{1}{b^d} f(b^{y_1} t, b^{y_a} h_a, b^{y_b} h_b, 0) + \frac{1}{b^{d-1}} L^{-1} \frac{\partial f(b^{y_1} t, b^{y_a} h_a, b^{y_b} h_b, 0)}{\partial x_4}$$ (3.55)

where we have carried out the Taylor expansion for L^{-1} small using both versions of Eq. (3.58) and $\frac{\partial}{\partial x_n}$ indicates the partial derivative with respect to the nth argument. The second term gives a total contribution to the singular part of the free energy of the order $AL \times L^{-1}$ and is thus a surface tension γ and so we have

$$\gamma = \frac{1}{b^{d-1}} \frac{\partial f(b^{y_1} t, b^{y_a} h_a, b^{y_b} h_b, 0)}{\partial x_4}$$ (3.56)

Setting $bt^{y_1} = 1$ then gives close to the critical point

$$\gamma \sim t^{\frac{d-1}{y_1}} \frac{\partial f(1, \lim_{t \to 0} t^{-\frac{y_a}{y_1}} h_a, \lim_{t \to 0} t^{-\frac{y_a}{y_1}} h_b, 0)}{\partial x_4} = t^{(d-1)\nu} C' = \xi^{-(d-1)} C'$$ (3.57)

The formula relating the surface tension and the correlation length, in the above C' is a constant depending on the universality class.

Now if we keep L finite and set $b^{y_1} t = 1$ in Eq. (3.58) we find

$$f(t, h_a, h_b, L^{-1}) = t^{\frac{d}{y_1}} f(1, t^{-\frac{y_a}{y_1}} h_a, t^{-\frac{y_b}{y_1}} h_b, t^{-\frac{1}{y_1}} L^{-1})$$ (3.58)

which can be written as

$$f(t, h_a, h_b, L^{-1}) = \frac{1}{\xi^d} f(1, \xi^{y_a} h_a, \xi^{y_b} h_b, \xi/L)$$ (3.59)

This can then be written as

$$f(t, h_a, h_b, L^{-1}) = \frac{1}{L^d} \theta(\frac{L}{\xi}, \xi^{y_a} h_a, \xi^{y_b} h_b)$$ (3.60)

Now crucially as $\xi \to \infty$ the function θ is analytic so we can take the limit $\xi \to \infty$ without any problems to find

$$f(0, h_a, h_b, L^{-1}) = \frac{1}{L^d} \theta(0, \lim_{\xi \to \infty} \xi^{y_a} h_a, \lim_{\xi \to \infty} \xi^{y_b} h_b)$$ (3.61)

Clearly for each surface we have 3 possibilities: $\lim_{\xi \to \infty} \xi^{y_a} h_a = \pm\infty$, if the surface fields are relevant, as well as $\lim_{\xi \to \infty} \xi^{y_a} h_a = 0$ if the surface fields are irrelevant. There is clearly also a similar argument

when the system has periodic boundary conditions and there are no surface fields. Near the critical point depending on the boundary conditions there should be scaling functions when the surface fields attract the same phase $\theta_{++}(x)$, where they attract different phases and $\theta_{+-}(x)$, and $\theta_{pbc}(x)$ when the boundary conditions are periodic. There should also be a zero surface field case θ_{00} when the surfaces fields are irrelevant or zero (this is however unlikely). Fisher and de Gennes argued, without proof, that the force for $(++)$ boundary conditions should be attractive where as the $(+-)$ case should produce repulsive forces [3, 91] .

The total singular part of the free energy is thus given by

$$
F = AL f(t, h_a, h_b, L^{-1}) = \frac{A}{L^{d-1}} \theta(\frac{L}{\xi}, \xi^{y_a} h_a, \xi^{y_b} h_b).
\tag{3.62}
$$

The scale of the energy is set by the energy of thermal fluctuations $k_B T$ we thus find that

$$
F(t = 0) = \frac{k_B TAC}{L^{d-1}}
\tag{3.63}
$$

where C is a constant depending on the surface universality class.

3.2   Finite size scaling in one dimensional interface models

We have seen that confinement generated Casimir forces appear when the correlation length of the fluctuations in a system becomes of the order of the minimum size of the system, be it for perfect conductor plates in vacuum or in confined critical systems. We have also seen that interfaces between two phases can described by surface models. If we consider just a surface model, it is physically obvious that finite size effects will also arise in these systems. In what follows we will study the size dependence of a number of continuous and discrete interface models (corresponding to the interfaces of two dimensional systems). While long range forces are generated by confinement we find that these models have quantitatively different behaviours to the critical Casimir effect. However if one assumes a phenomenological proposal by Privman [16] to introduce a finite size correction to the surface tension, the critical Casimir effect can be quantitatively recovered.

3.2.1   Continuous models in one dimension

In one dimension the partition function for a surface model of the type discussed in Sec 1.2 can be written as a path integral

$$
Z(t) = \int d[h] \exp\left(-\frac{\beta\sigma}{2} \int_0^t h'^2(x) dx - \beta \int_0^t V(h(x)) dx\right)
\tag{3.64}
$$

where t is the length of the system and the notation is so chosen as the variable x con be thought of as a time in path integral language. It is convenient to fix both the starting point $h(0) = x$ and the end point $h(t) = x$ and define what is known as the propagator [8]

$$
K(h, h', t) = \int_{h(0)=h} d[h]\delta(h' - h(t)) \exp\left(-\frac{\beta}{2} \int_0^t \sigma h'^2(x) dx - \beta \int_0^t V(h(x)) dx\right)
\tag{3.65}
$$

The propagator is an example of a path integral and is the sum over all paths going between h and h' in what can be taken to be the time t. It can be shown [92] that the path integral obeys an imaginary time Schrödinger equation

$$
\frac{\partial K(h, h', t)}{\partial t} = -\hat{H} K(h, h', t)
\tag{3.66}
$$

where $\hat{H}$ is the Hamiltonian operator

$$\hat{H} = -\frac{1}{2\sigma\beta}\frac{\partial^2}{\partial h^2} + \beta V(h) \tag{3.67}$$

and, with a suitable normalisation, the initial condition

$$K(h, h', t) = \delta(h - h') \tag{3.68}$$

If the Hamiltonian operator $\hat{H}$ has eigenfunctions ψ_n, normalised so that

$$\int dh\, \psi_n^2(h) = 1 \tag{3.69}$$

and with eigenvalues ϵ_n, it is easy to see that the propagator can be written as

$$K(h, h', t) = \sum_n \exp(-t\epsilon_n)\psi_n(h)\psi_n(h') \tag{3.70}$$

If we take a system with periodic boundary conditions but otherwise leave the initial value $h(0)$ of the height to be free, then using the normalisation of the eigenfunctions, we find

$$Z(t) = \int dh K(h, h, t) = \sum_n \exp(-t\epsilon_n) \tag{3.71}$$

Now in the thermodynamic limit $t \to \infty$ if there is a gap between the ground state energy ϵ_0 and the first excited state, $g = \epsilon_1 - \epsilon_0$ which is non-zero, we can apply ground state dominance

$$Z(t) = \exp(-t\epsilon_0) \tag{3.72}$$

which gives the free energy per unit length as

$$f = \frac{1}{\beta}\epsilon_0 \tag{3.73}$$

As well as the free energy we are interested in the probability distribution of the height at a single point (which is independent of the point chooses due to invariance by translation of the system). For instance the probability distribution of $h(0)$ is given by

$$\begin{aligned}
p_1(h) &= \frac{\int d[h]\delta(h(0) - h)\exp\left(-\frac{\beta}{2}\int_0^t h'^2(x)dx - \beta\int_0^t V(h(x))dx\right)}{Z(t)} \\
&= \frac{K(h, h, t)}{Z(t)} \\
&= \frac{\sum_n \exp(-t\epsilon_n)\psi_n^2(h)}{\sum_n \exp(-t\epsilon_n)}
\end{aligned} \tag{3.74}$$

and so as $t \to \infty$, ground state dominance gives

$$p_1(h) = \psi_0^2(h) \tag{3.75}$$

We see that the normalisation of the probability density function for h follows from the normalisation of the wave functions.

The joint probability density function for two heights separated by a time or distance x is given by

$$p_2(h, h', x) = \frac{\int d[h]\delta(h(0) - h)\delta(h(x) - h')\exp\left(-\frac{\beta}{2}\int_0^t h'^2(x)dx - \beta\int_0^t V(h(x))dx\right)}{Z(t)}$$

$$= \frac{K(h, h', x)K(h', h, t - x)}{Z(t)}$$

$$= \frac{\sum_{nm}\exp(-x\epsilon_n)\psi_n(h)\psi_n(h')\exp(-[L - x]\epsilon_m)\psi_m(h')\psi_m(h)}{\sum_n\exp(-t\epsilon_n)} \tag{3.76}$$

Due to ground state dominance only the term with $m = 0$ survives in the sum above (as as x is taken such that $x \ll t$) as we find

$$
\begin{aligned}
p_2(h, h', x) &= \sum_n \psi_0(h')\psi_0(h)\psi_n(h')\psi_n(h)\exp(-x[\epsilon_n - \epsilon_0])) &\tag{3.77}\\
&= p_1(h)p_1(h') + \sum_{n>0} \psi_0(h')\psi_0(h)\psi_n(h')\psi_n(h)\exp(-x[\epsilon_n - \epsilon_0])) &\tag{3.78}
\end{aligned}
$$

From this we see that when $x[\epsilon_n - \epsilon_0] \gg 1$ for all n and so in particular $x[\epsilon_1 - \epsilon_0] \gg 1$ we have

$$p_2(h, h', x) \sim p_1(h)p_2(h') \tag{3.79}$$

so that the height at large distances are uncorrelated or equivalently are independent random variables. This gives a correlation length

$$\xi = \frac{1}{\epsilon_1 - \epsilon_0}. \tag{3.80}$$

3.2.2 The confined elastic line

Here we consider the case where $V(h) = 0$ for $0 < h < L$ and $V(h) = 0$ otherwise. This corresponds to a one dimensional elastic line confined between two impenetrable walls separated by a distance L. The Hamiltonian $\hat{H}$ is that for a quantum well of width L and with eigenfunctions [93]

$$\psi(h) = \sqrt{\frac{2}{L}}\sin(\frac{\pi(n + 1)h}{L}) \tag{3.81}$$

where $n \geq 0$ are integers. From this we see that the ground state energy is

$$\epsilon_0 = \frac{1}{2\sigma\beta}\frac{\pi^2}{L^2} \tag{3.82}$$

and so, in the thermodynamic limit, the free energy per unit length is

$$f = \frac{1}{2\sigma\beta^2}\frac{\pi^2}{L^2} = \frac{T^2\pi^2}{2\sigma L^2} \tag{3.83}$$

Here the pressure (in this case pressure in a force per unit length) is given by

$$P = -\frac{\partial f}{\partial L} = \frac{\pi^2 T^2}{\sigma L^3}, \tag{3.84}$$

and we see that it is repulsive. Physically, the fluctuations of the surface repel the walls. The pressure has the Casimir like characteristic that it behaves as a long range power law type interaction, however a two dimensional critical Casimir system (see (3.63)) would have a free energy per unit length $f = CT/L$. We also see that the free energy scales a T^2 rather than T (as is the case for the Casimir interaction).

Having said this, a critical system has zero surface tension and so using a model with a finite surface tension for the critical interface is clearly not appropriate. However it has been conjectured by Privman [16] that the term σ, which Privman refers to the stiffness, should be modified by finite size effects (although he considers a case where the height L of the system and the length t are of the same order). The simplest conjecture proposed by Privman[16] is that

$$\sigma(L) \approx \sigma_b + \frac{Ta}{L} \tag{3.85}$$

so that a has no dimensions. This amounts to assuming that the corrections are analytic in the variable $1/L$. It seems difficult to justify this from a more microscopic view, however if we use this we find that

$$f = \frac{1}{2\sigma(L)\beta^2} \frac{\pi^2}{L^2} = \frac{T^2\pi^2}{2[\sigma_b + \frac{Ta}{L}]L^2} \tag{3.86}$$

Now if we associate the critical point where $\sigma_b = 0$ we find

$$f_c = \frac{T\pi^2}{2aL} \tag{3.87}$$

and this does have exactly the form predicted for a critical system in Eq. (3.63).

Using Eq. (3.80) we find that the correlation length is given by

$$\xi = \frac{2}{3} \frac{\sigma L^2}{T\pi^2} \tag{3.88}$$

thus it increases as the surface tension is increased or the temperature is lower. This makes physical sense as the surface should become *flatter* under these conditions. Also, as the system becomes more confined, the correlation length increases, again as confinement kills fluctuations. The correlation length tells us that if we wanted to simulate this system then we need to take

$$t \gg \xi \tag{3.89}$$

in order to be in the thermodynamics limit and so $t \gg \frac{\sigma L^2}{T\pi^2}$, thus for L large, in general we would need to simulate rather large systems. The probability distribution function of the height at a single point is given by

$$p_1(h) = \frac{2}{L} \sin^2(\frac{\pi h}{L}) \tag{3.90}$$

and from this we find

$$\langle h \rangle = \frac{L}{2} \tag{3.91}$$

which is rather obvious. The width of the interface is given by

$$w = \sqrt{\langle h^2 \rangle - \langle h \rangle^2} \tag{3.92}$$

and here it is given by

$$w = L\sqrt{\frac{1}{12} - \frac{1}{2\pi^2}} = 0.180756\,L \tag{3.93}$$

During this thesis we have considered models of surfaces where the overall surface integral is fixed. In magnetic systems this corresponds to systems with conserved magnetisation. It is surprisingly difficult to deal with this constraint in a hard way both for continuous surfaces, treated via the Schrödinger equation, and for discrete systems with the transfer matrix. In principle one can always introduce a

magnetic field to fix the average total magnetisation to zero. Howeve,r there will always be fluctuations around the average value. Normally in thermodynamics one can fix the magnetisation per site to zero by applying an external magnetic field (which is zero in systems having an up down symmetry). If there are N sites, the fluctuations of the magnetisation by site scale as $1/\sqrt{N}$. However, the total magnetisation has fluctuations of the order of $\sqrt{N}$ and so the condition of fixed total magnetisation is only imposed approximately by an applied magnetic field.

In the confined Edwards Wilkinson model we consider the magnetisation M defined by

$$\text{M} = \int_0^t dx\, h(x) \tag{3.94}$$

We know, from symmetry arguments, that without an external applied field we have

$$\langle \text{M} \rangle = \frac{t\text{L}}{2} \tag{3.95}$$

which can be shown explicitly from the formula

$$\langle \text{M} \rangle = t \int_0^\text{L} dh\, h \psi_0^2(h) \tag{3.96}$$

Interestingly, if we write things in terms of the traditional bra and ket notation of quantum mechanics, we see that

$$\langle \text{M} \rangle = t \langle 0|h|0 \rangle \tag{3.97}$$

and we note that

$$\langle 0|h|0 \rangle = \Delta \epsilon_{0,1}(h) \tag{3.98}$$

where $\Delta \epsilon_{0,1}(h)$ is the shift in the ground state energy to first order in perturbation theory induced by a perturbation of the potential $\Delta\text{V}(h) = h$. However this is just the obvious thermodynamic expression

$$\langle \text{M} \rangle = -t \frac{\partial}{\partial \lambda} f(\lambda)|_{\lambda=0}, \tag{3.99}$$

for a potential $\text{U}(h) = \text{V}(h) + \lambda h$. The variance of M can be computed by using Eq. (3.78), which gives

$$\langle \text{M}^2 \rangle_c = \int_0^t dx dx' [h(x)h(x') - \langle h^2 \rangle]$$
$$= \sum_{n \rangle 0}^\infty \left(\int_0^\text{L} dh\, h \psi_0(h) \psi_n(h) \right)^2 \int_0^t dx dx' \exp(-[\epsilon_n - \epsilon_0]|x - x'|) \tag{3.100}$$

and for large t carrying out the integration over x and x' gives

$$\langle \text{M}^2 \rangle_c = 2t \sum_{n>0} \frac{1}{\epsilon_n - \epsilon_0} \left(\int_0^\text{L} dh\, h \psi_0(h) \psi_n(h) \right)^2 \tag{3.101}$$

From second order perturbation theory we see that this is just equivalent to the thermodynamic identity

$$\langle \text{M}^2 \rangle_c = -\text{T} t \frac{\partial^2}{\partial \lambda^2} f(\lambda)|_{\lambda=0} \tag{3.102}$$

Using the explicit form of the eigenfunctions we find

$$\langle \text{M}^2 \rangle_c = \frac{16\text{L}^4 t \sigma \beta}{\pi^2} \sum_{n=1}^\infty \frac{1}{(n+1)^2 - 1} \left[\int_0^1 du\, u \sin(\pi u) \sin(\pi(n+1)u) \right]^2 \tag{3.103}$$

It can then be shown that

$$\int_0^1 du \, u \sin(\pi u) \sin(\pi(n+1)u) = -\frac{2(n+1)(1+\cos((n+1)\pi))}{\pi^2[(n+1)^2-1]^2} \tag{3.104}$$

From this we see that only the modes where n is odd contribute to the fluctuations of the magnetisation. Consequently we find

$$\langle \mathrm{M}^2 \rangle_c = \frac{256\mathrm{L}^4 t\sigma\beta}{\pi^6} \sum_{n, \text{ odd},=1}^{\infty} \frac{(n+1)^2}{[(n+1)^2-1]^5} \tag{3.105}$$

$$= \frac{1024\mathrm{L}^4 t\sigma\beta}{\pi^6} \sum_{k=0}^{\infty} \frac{(k+1)^2}{[(2k+2)^2-1]^5} \tag{3.106}$$

$$= \frac{\mathrm{L}^4 t\sigma\beta(15-\pi^2)}{\pi^4}. \tag{3.107}$$

This formula deserves some comment. A first trivial comment is that that $\langle \mathrm{M}^2 \rangle_c \sim t$ in accordance with the thermodynamic arguments given above. Secondly the variance diverges as $\sigma\beta \to \infty$, which is normal as the low energy configuration zero mode - a straight line - is unaffected by the confining walls and so in principal this line can lie anywhere on $[0, \mathrm{L}]$, explaining the scaling with L^4.

3.2.3 The Airy line

In the above well known example we confine the surface and then compute the pressure. This is an example of the constant volume ensemble. Physically we could also consider the case of a system which is confined softly by an externally imposed pressure P_0 (which can also be treated as a chemical potential depending on the context) in the constant pressure ensemble. In this case the potential is given by

$$\mathrm{V}(h) = \begin{cases} \mathrm{P}_0 h & \text{for } h > 0 \\ \infty & \text{for } h \le 0 \end{cases}$$

The time independent Schrödinger equation for the eigenfunctions here is

$$-\frac{1}{2\sigma\beta}\frac{d^2\psi_n(h)}{dh^2} + \mathrm{P}_0\beta h\psi_n(h) = \epsilon_n\psi_n(h) \tag{3.108}$$

The corresponding eigenfunctions have boundary conditions $\psi_n(0) = 0$ due to the hard wall potential at $h = 0$ and they must also decay to zero as $h \to \infty$ so as to be normalisable.

The key to finding the eigenfunctions is to transform the Schrödinger into the Airy equation which is

$$\frac{d^2 y(x)}{dx^2} - xy(x) = 0. \tag{3.109}$$

This equation has solutions $\mathrm{Ai}(x)$ which decay as

$$\mathrm{Ai}(x) \sim \frac{\exp(-\frac{2}{3}x^{\frac{3}{2}})\Gamma(\frac{5}{6})\Gamma(\frac{1}{6})}{4\pi^{\frac{3}{2}}x^{\frac{1}{4}}}, \tag{3.110}$$

as $x \to \infty$ and so are normalizable as eigenfunctions. For $x \langle 0$ the Airy function oscillates and has an infinite number of negative zeros $-\alpha_n$ such that $\mathrm{Ai}(-\alpha_n) = 0$.

We make the change of variable $h = \ell z'$ to find

$$\frac{1}{2\sigma\beta\ell^2}\frac{d^2\psi_n(z')}{dz'^2} - \mathrm{P}_0\beta\ell(z' - \epsilon_n)\psi_n(z') = 0, \tag{3.111}$$

where $\varepsilon_n = \epsilon_n/(P_0\beta\ell)$. Now we chose ℓ so that

$$2\sigma\beta^2 P_0 \ell^3 = 1, \tag{3.112}$$

and we see that

$$\ell = \left(\frac{1}{2\beta^2\sigma P_0}\right)^{\frac{1}{3}}, \tag{3.113}$$

is an intrinsic length scale.

$$\frac{d^2\psi_n(z')}{dz'^2} - (z' - \varepsilon_n)\psi_n(z') = 0. \tag{3.114}$$

Finally if we use $z = z' - \varepsilon_n$ we obtain Airy's equation [94]

$$\frac{d^2\psi_n(z)}{dz^2} - z\psi_n(z) = 0 \tag{3.115}$$

and so

$$\psi_n(z) = c_n \text{Ai}(z), \tag{3.116}$$

where c_n is a normalisation constant. This means that in terms of the original height variable h,

$$\psi_n(h) = c_n \text{Ai}(\frac{h}{\ell} - \varepsilon_n). \tag{3.117}$$

The boundary condition $\psi_n(h)$ then show that we must choose $\varepsilon_n = \alpha_{n+1}$. This means that the ground state energy is

$$\epsilon_0 = \alpha_1 P_0 \beta \ell = \frac{\alpha_1 P_0 \beta}{(2\sigma\beta^2 P_0)^{\frac{1}{3}}} = \frac{\alpha_1 P_0^{\frac{2}{3}}\beta^{\frac{1}{3}}}{2^{\frac{1}{3}}\sigma^{\frac{1}{3}}}, \tag{3.118}$$

and where we note that $\alpha_1 = 2.33811$.

$$f = \frac{\alpha_1 P_0^{\frac{2}{3}}}{2^{\frac{1}{3}}\sigma^{\frac{1}{3}}\beta^{\frac{2}{3}}}. \tag{3.119}$$

From the original partition function we see that h is conjugate to P_0 and so we find the average height is given by

$$\bar{h} = \langle h \rangle = \frac{\partial f}{\partial P_0} = \frac{2}{3}\frac{\alpha_1}{2^{\frac{1}{3}}\sigma^{\frac{1}{3}}\beta^{\frac{2}{3}}P_0^{\frac{1}{3}}} = \frac{2}{3}\alpha_1\ell, \tag{3.120}$$

and solving for P_0 in terms of $\overline{h}$ gives

$$P_0 = \frac{4}{27}\frac{\alpha_1^3 T^2}{\sigma\overline{h}^3}, \tag{3.121}$$

we see that P_0 behaves exactly in the same way as the pressure of a confined elastic line in term of the temperature and surface tension. Only the overall numerical prefactor is different.

The correlation length is given by

$$\xi = \frac{2^{\frac{1}{3}}(\sigma T)^{\frac{1}{3}}}{(\alpha_2 - \alpha_1)P_0^{\frac{2}{3}}}. \tag{3.122}$$

When written in terms of $\overline{h}$ the above correlation length behaves in the same way as for the free elastic line, however when P_0 is fixed we see that the behavior as a function of T and σ is quite different. The correlation length still increases with σ but now decreases as the temperature is decreases.
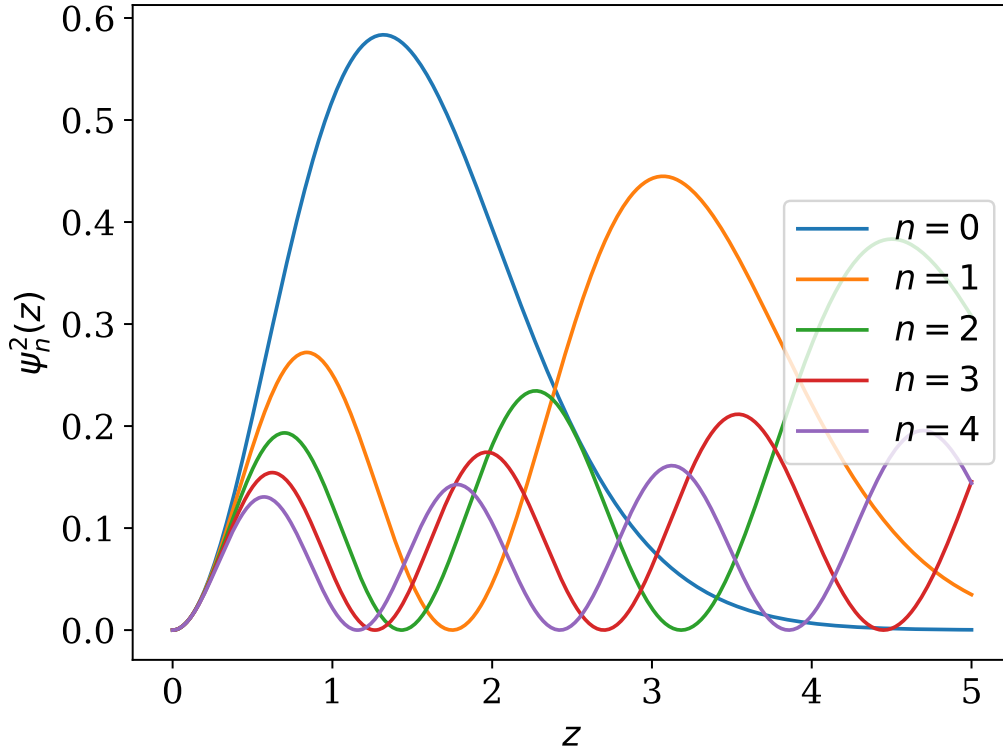
Figure 3.1: The scaled probability density function $p(z)$ for the distribution of the height at a single point for the Airy line given in Eq. (3.124)

The probability density function for the height of the interface at a single point is given by

$$p_1(h) = \frac{\text{Ai}^2(\frac{h}{\ell} - \alpha_1)}{\int_0^\infty dh' \text{Ai}^2(\frac{h'}{\ell} - \alpha_1)} \tag{3.123}$$

However if we write the height variable in terms of the length scale ℓ, $h(x) = \ell z(x)$ we find that z has the single point probability density function

$$p(z) = \frac{\text{Ai}^2(z - \alpha_1)}{\int_0^\infty dz' \text{Ai}^2(z' - \alpha_1)} = \frac{\text{Ai}^2(z - \alpha_1)}{\text{Ai}'^2(-\alpha_1)}. \tag{3.124}$$

Using this we find the average height is given by

$$\langle h \rangle = \overline{h} = \ell z_0, \tag{3.125}$$

where

$$z_0 = \frac{\int_0^\infty dz z \text{Ai}^2(z - \alpha_1)}{\int_0^\infty dz \text{Ai}^2(z - \alpha_1)}. \tag{3.126}$$

Interestingly comparison with the thermodynamic calculation giving Eq. (3.120) shows that the identity

$$z_0 = \frac{2}{3}\alpha_1, \tag{3.127}$$

must hold- this surprising identity can be verified numerically. Here we find that the average height given by

$$\langle h \rangle = 0.697089 \, \ell. \tag{3.128}$$

The variance of the magnetisation is then given by

$$\langle M^2 \rangle_c \quad = \quad -TL\frac{\partial^2}{\partial \lambda^2} f(\lambda)|_{\lambda=0} = -TL\frac{\partial^2}{\partial P^2} f(P)|_{P=P_0} \tag{3.129}$$

$$= \quad L\frac{\alpha_1}{2^{\frac{1}{3}}\sigma^{\frac{1}{3}}\beta^{\frac{5}{3}}}\frac{2}{9}P_0^{-\frac{4}{3}}. \tag{3.130}$$

In terms of the average height this then gives

$$\langle M^2 \rangle_c = \frac{9}{4\alpha_1^3}L\sigma\beta\overline{h}^{-4} \tag{3.131}$$

3.3 The generalized Lopes-Jacquin-Holdsworth Method

In Sec 2.3.2, we have shown a way to numerically compute the free energy of a system at a chemical potential μ in absence of another potential. Here we generalise the method for any kind of external potential. We will explain the method for the Ising model, but the derivation for the SOS model is straightforward.

For any external field which can be written as $BV(\sigma)$, where $V(\sigma)$ is a function of the internal microscopic variables σ_i, the Hamiltonian of the Ising model is

$$H = -J\sum \sigma_i \sigma_j - B\sum_i V(\sigma_i) \tag{3.132}$$

The mean value of the external potential is

$$\langle \sum_i V(\sigma_i) \rangle = \sum_{\mathbf{h}} \sum_i V(\sigma_i) \exp(-\beta H)$$

$$= -\frac{\partial F(\mu)}{\partial B} \tag{3.133}$$

where F is the free energy of the system. We see that for any potential of the form (3.135), we can integrate the previous equation to find

$$F(B_1) - F(B_2) = -\int_{B_1}^{B_2} dB' \langle \sum_i V(\sigma_i) \rangle_{B'} \tag{3.134}$$

In the case where we know the analytical form of the free energy in the limits $B_2 \to \infty$ or $B_1 \to 0$, this method provides a way to directly measure it for any temperature or size by integrating over the chemical potential. From the total free energy, we recover the Casimir form through Eq (2.34). The limit $B_1 \to 0$ is the free system limit, and the free energy can not be computed analytically. However, when $B_2 \to \infty$, for the majority of external fields $BV(\sigma)$ in which we are interested, there is often a configuration limit whose free energy can be computed analytically. For example, if $V(\sigma) = \sigma$, the configuration limit is the one where all spins point towards the same direction, leading to a free energy of 0. Thus, we have

$$F(B_1) - F_{analytic}(\infty) = -\int_{B_1}^{\infty} dB' \langle \sum_i V(\sigma_i) \rangle_{B'} \tag{3.135}$$

In numerical simulations, it is not possible to range over infinity, and a criterion has to be defined to know the error made between the analytic case $\mu_2 = \infty$ and the maximal μ_2 achieved in simulations. As in Eq (2.35), we define the function

$$D(B, L_1, L_2) = \langle M^*(L_1) - M^*(L_1 - 1) - (M^*(L_2) - M^*(L_2 - 1)) \rangle \tag{3.136}$$

with the generalized magnetization $M^* = \sum_i V(\sigma_i)$. A suitable upper limit of integration if we want to get the Casimir force is when the function D reaches 0 within the precision of the simulation.

For the SOS Hamiltonian

$$H = J \sum_i |h_i - h_{i+1}| + B \sum_i V(h_i) \tag{3.137}$$

we define the generalised mean height as

$$h^* = \langle \sum_i V(h_i) \rangle \tag{3.138}$$

Eqquation (3.135) writes as

$$F(B_1) - F(B_2) = - \int_{B_1}^{B_2} d\mu' h^*(B') \tag{3.139}$$

which can be directly be verified with the transfer matrix. In the limit $B \to \infty$, the generalised height is zero, while the free energy $F(\infty)$ can often be computed analytically. To minimize the error between the analytical limit and the numerical simulations, a suitable choice of the upper integration's limit B_2 is given by

$$\int_{B_2}^{\infty} dB' h^*(B')) \ll \int_{B_1}^{B_2} dB' h^*(B') \tag{3.140}$$

An heuristic argument to find a suitable upper limit for integration is when $h^*(B_2) \ll h^*(B_1)$. In Fig 3.2, we see the free energy computed from the matrix transfer, compared to the integration procedure (3.135) for the SOS model for the chemical potential $V(h_i) = h_i$ in Monte Carlo simulations, where we see the agreement for B_2 large enough.

Since the order parameter is conserved in model B, the generalized Lopes-Jacquin-Holdswroth method can be used to compute the free energy for Kawasaki dynamics for potentials different from the chemical potential. As a proof of concept, we take a potential of the form

$$V(h_i) = -|h_i - \frac{L}{2}| \tag{3.141}$$

Such potential will press the interface along $h = 0$ and $h = L$ compared to the classical chemical potential which presses the interface at $h = 0$, as seen in Fig 3.3. Far away from $\frac{L}{2}$, both potentials are equivalent in symmetric fashion, and shall behave similarly for large B, because the free energy only depends on the interface fluctuations and not the mean height.

In the $B \to \infty$ limit, the system has two equilibrium positions $h = 0$ et $h = L$, which gives the transfer matrix

$$T = e^{\beta B \frac{L}{2}} \begin{pmatrix} 1 & e^{-\beta JL} \\ e^{-\beta JL} & 1 \end{pmatrix} \tag{3.142}$$

The eigenvalues are $\lambda_{\pm} = e^{\beta B \frac{L}{2}}(1 \pm e^{-\beta JL})$, which gives us the free energy

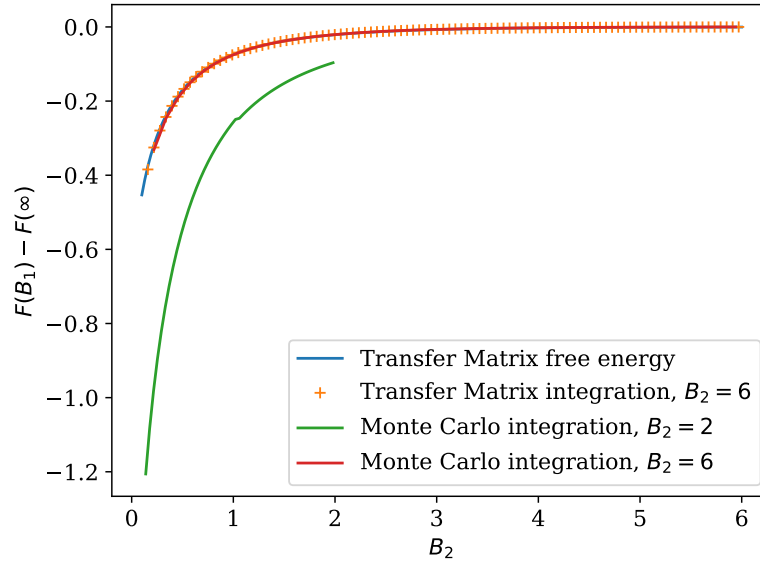$$F(B \to \infty) = -B \frac{L}{2} \tag{3.143}$$

Figure 3.2: Difference in free energy directly computed from transfer matrix, compared to numerical integration over the generalized height, for different upper limit B_2. The parameters are $L' = 256$, $L = 200$ and $\beta = 1$ for $5e7$ Monte Carlo steps.

We plotted in Fig 3.4 the difference of free energy computed from the transfer matrix between B_1 finite and $B_2 = 1$, and the integration procedure (3.139) with the generalized height with the matrix transfer and Monte Carlo simulations, both for Glauber and Kawasaki dynamics. The disagreement between the expected value and the simulation results are from a B_2 too small, which we also see in the integration of the generalized height from the transfer matrix. We can convince ourselves by doing the integration from the transfer matrix for a larger B_2. Also, it is worth noting that for this system, there is no significant difference in results for the two different dynamics.

This method opens a new way to compute the free energy for any kind of external potential of the form $BV(h)$, or $BV(\sigma)$ in the case of the Ising or SOS models for conserved and non-conserved dynamics, such as non-uniform external fields [95].

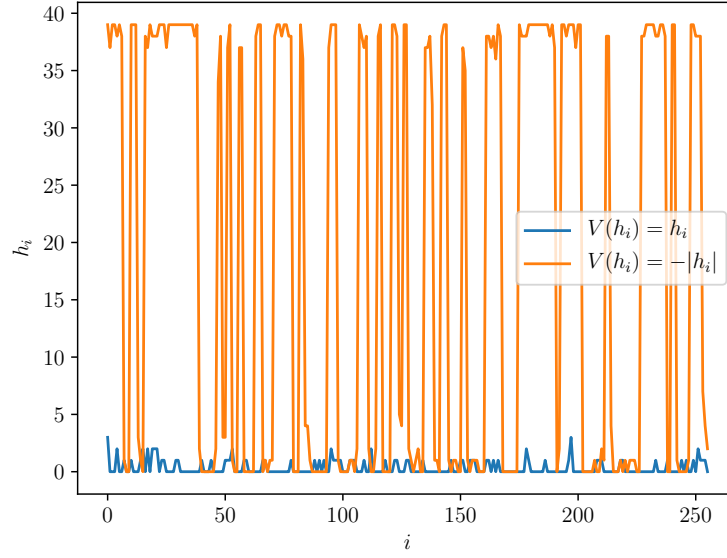Figure 3.3: Snapshots of systems for the potential (3.141) and the chemical potential for $\beta = 1$ and B = 2 with L = 40 and L$'$ = 256
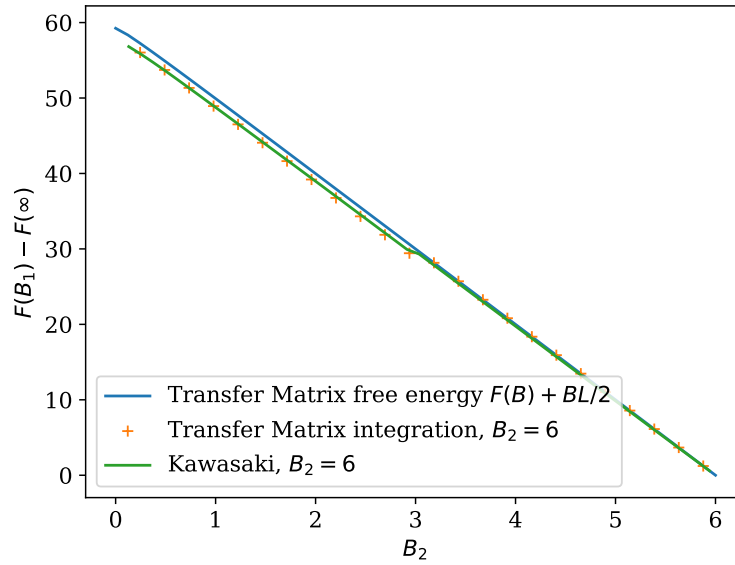

Figure 3.4: Difference in free energy directly computed from transfer matrix with the potential (3.141), compared to numerical integration over the generalized height. The parameters are L$'$ = 256, L = 20 and $\beta = 1$, $B_2 = 1$ for 10^7 Monte Carlo steps.

3.4   The confined solid on solid model

From exact diagonalization of the SOS transfer matrix in the infinite case [96], finite-size effects were studied both for the SOS and RSOS model [97, 98]. Nevertheless the derivation of eigenvectors and eigenvalues were not explicit in the latter case. Those eigenvalues are a multiple of an integer, and the study of the eigenvalues issued from an odd integer where also not discussed. We also add an analysis to the correlation length and the limits of high and low temperatures for the free energy.

   We consider here the free interface confined between 0 and L, with no external field. The SOS transfer matrix is thus given by

$$T(h_i, h_j) = \exp(-\beta J |h_i - h_j|) \tag{3.144}$$

Since positions are comprised from 0 to L, we can write the transfer matrix as

$$T_{ij} = \exp(-\beta J |i - j|). \tag{3.145}$$

We introduce

$$r = \exp(-\beta J) \tag{3.146}$$

To find the eigenvectors of T, we consider the vector denoted by $[a]$ which has components

$$[a]_i = a^i, \tag{3.147}$$

where i is an index ranging from 0 to L. The action of the SOS transfer matrix on this vector is given by

$$[T[a]]_i = \sum_{j=0}^{L} r^{|i-j|} a^j \tag{3.148}$$

and we find

$$
\begin{aligned}
[T[a]]_i &= r^i \sum_{j=0}^{i} r^{-j} a^j + r^{-i} \sum_{j=i+1}^{L} r^j a^j \\
&= r^i \sum_{j=0}^{i} r^{-j} a^j + r^{-i} \sum_{k=0}^{L-i-1} r^{i+1+k} a^{i+1+k} \\
&= r^i \frac{1 - r^{-(i+1)} a^{i+1}}{1 - r^{-1})a} + r a^{i+1} \frac{1 - r^{L-i} a^{L-i}}{1 - ra} \\
&= \left[\frac{ra}{1 - ra} - \frac{\frac{a}{r}}{1 - \frac{a}{r}} \right] a^i + \frac{r^i}{1 - \frac{a}{r}} - \frac{r^{L+1-i} a^{L+1}}{1 - ra}
\end{aligned}
\tag{3.149}
$$

We now define

$$\lambda(a) = \frac{ra}{1 - ra} - \frac{\frac{a}{r}}{1 - \frac{a}{r}} = \frac{\frac{1}{r} - r}{\frac{1}{r} + r - a - \frac{1}{a}} \tag{3.150}$$

and notice that

$$\lambda(a) = \lambda(a^{-1}) \tag{3.151}$$

We can thus write

$$[T[a]]_i = \lambda(a) a^i + \frac{r^i}{1 - \frac{a}{r}} - \frac{r^{L+1-i} a^{L+1}}{1 - ra} \tag{3.152}$$

Now, considering the action of the transfer matrix on the vector $[a^{-1}]$, we find

$$[T[a^{-1}]]_i = \lambda(a) a^{-i} + \frac{r^i}{1 - \frac{1}{ra}} - \frac{r^{L+1-i} a^{-(L+1)}}{1 - \frac{r}{a}} \tag{3.153}$$

We now look for an eigenvector of the form

$$\mathbf{v} = [a] + c[a^{-1}] \tag{3.154}$$

The action of T on $\mathbf{v}$ is

$$\left[T\left([a] + c[a^{-1}] \right) \right]_i = \lambda(a)[a^i + ca^{-i}] + r^i \left(\frac{1}{1 - \frac{a}{r}} + \frac{c}{1 - \frac{1}{ra}} \right) - r^{L+1-i} \left(\frac{a^{L+1}}{1 - ra} + c\frac{a^{-(L+1)}}{1 - \frac{r}{a}} \right) \tag{3.155}$$

and we see that $\mathbf{v}$ is an eigenvector, with eigenvalue $\lambda(a)$, if

$$\frac{1}{1 - \frac{a}{r}} + \frac{c}{1 - \frac{1}{ra}} = 0 \tag{3.156}$$

$$\frac{a^{L+1}}{1 - ra} + c\frac{a^{-(L+1)}}{1 - \frac{r}{a}} = 0 \tag{3.157}$$

The above equations imply that

$$c = -\frac{ra - 1}{a(r - a)} \tag{3.158}$$

and

$$c^2 = a^{2L} \tag{3.159}$$

Therefore we find

$$v_i = a^i \pm a^{L-i} \tag{3.160}$$

Ground state eigenvector

We expect the ground state eigenvector (corresponding to the largest eigenvalue) to be symmetric with respect to the middle of the system and so

$$v_i = v_{L-i} \tag{3.161}$$

which implied that we should have $c = a^L$.

This then gives the equation determining the values of a for the largest eigenvalue, and in general for the eigenvalues which are symmetric ($c = 1$),

$$a^{L+1} = \frac{1 - ra}{r - a}. \tag{3.162}$$

As a check on the above derivation we can consider the case L = 1 so we have two sites. Here we see that the transfer matrix is given explicitly by

$$T = \begin{pmatrix} 1 & r \\ r & 1 \end{pmatrix} \tag{3.163}$$

and the largest eigenvector is easily seen to be given by

$$\lambda_0 = 1 + r \tag{3.164}$$

In this case, we seethat Eq. (3.162) gives

$$a^2 = \frac{1 - ra}{r - a} \tag{3.165}$$

which has three solutions

$$a_1 = -1 \tag{3.166}$$

$$a_2 = \frac{1}{2}\left(-\sqrt{r^2 + 2r - 3} + r + 1\right) \tag{3.167}$$

$$a_3 = \frac{1}{2}\left(\sqrt{r^2 + 2r - 3} + r + 1\right) \tag{3.168}$$

We see that $a_2 = 1/a_3$, and $|a_2| = |a_3| = 1$, and that

$$\lambda(-1) = \frac{1 - r}{1 + r} \tag{3.169}$$

while

$$\lambda(a_2) = \lambda(a_3) = 1 + r \tag{3.170}$$

corresponds to the maximal eigenvalue. Note that $\lambda(-1)$ is not the other eigenvalue of the transfer matrix, this has to be found by considering solutions with $c = -1$, as we will see later.

The equation (3.162) determining a can also be written as

$$a^L = -\frac{r - \frac{1}{a}}{r - a} \tag{3.171}$$

From this we see that if a is a solution then $1/a$, and that $a = -1$ is always a solution.

We now introduce θ and

$$a = \exp(i\theta) \tag{3.172}$$

Then the parameter of the eigenvector is

$$\exp(iL\theta) = -\frac{r - \exp(-i\theta)}{r - \exp(i\theta)} \tag{3.173}$$

From Eq (3.150), we have

$$\lambda(\theta) = \frac{\sinh(\beta J)}{\cosh(\beta J) - \cos(\theta)}. \tag{3.174}$$

Notice that in order to construct a real eigenvector corresponding to λ_0 we can use the fact that both $v_i(a) = a^i + a^{L-i}$ and $v_i(a^{-1}) = a^{-i} + a^{-L+i}$ are both eigenvectors with the same eigenvalue. This means that $u_i(a) = v_i(a) + v_i(-a)$ is also an eigenvector and all its components are real.

Clearly the largest eigenvalue corresponds to the value of θ closest to 0, so we look for an eigenvalue such that $L\theta \sim 1$. We write

$$\phi = L\theta \tag{3.175}$$

For L large, this gives

$$\exp(i\phi) \approx -\frac{r - 1 + i\frac{\phi}{L}}{r - 1 - i\frac{\phi}{L}} \approx -1 + 2i\frac{\phi}{L(1 - r)} \tag{3.176}$$

and so we find to leading order in $1/L$

$$\theta = \frac{(2n + 1)\pi}{L} \tag{3.177}$$

However we notice that this approximation is only valid if $L(1 - r) \gg 1$. For large β this approximation is simply equivalent to $L \gg 1$, however when β is small it requires that $H\beta \gg 1$.

The closest eigenvector to the real axis has $n = 0$ and so we have

$$\lambda_0 \approx \frac{\sinh(\beta J)}{\cosh(\beta J) - \cos(\frac{\pi}{L})} \approx \frac{\sinh(\beta J)}{\cosh(\beta J) - 1 + \frac{\pi^2}{2L^2}} \approx \coth(\frac{\beta J}{2})(1 - \frac{\pi^2}{4\sinh^2(\frac{\beta J}{2})L^2}) \tag{3.178}$$

In the limit $L \to \infty$, the ground-state eigenvalue is the same as the Sine-Gordon chain of length $L' \to \infty$ fixed at $h(0) = h(L') = 0$ and using a SOS interaction between nearest neighbors [96], which is normal since boundary conditions on the x-axis are negligible in the thermodynamic limit.
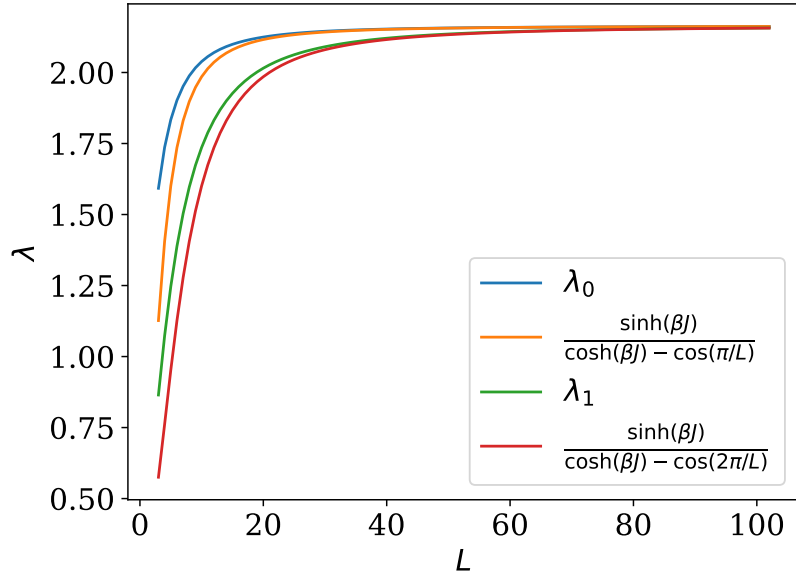
Figure 3.5: λ_0 and λ_1 as a function of L computed by numerical diagonalisation of the transfer matrix, compared to the analytical approximations for large L: Eq. (3.178) and Eq. (3.181). Here we have chosen for J = 1 and β = 1.

First excited state eigenvector

In order to compute the second eigenvalue λ_1 we look for an odd or antisymmetric solution with $c = -1$. We thus find

$$\exp(iL\theta) = \frac{r - \exp(-i\theta)}{r - \exp(i\theta)} \tag{3.179}$$

For large L we look for a solution of the form $\theta = \phi/L$ and this gives

$$\exp(i\phi) \approx 1 \tag{3.180}$$

and so we chose solutions $\phi = 2n\pi$ for integer n. However the solution $n = 0$ which corresponds to $a = 1$ has $v(i) = a^i - a^{L-i} = 0$ and so does not correspond to an eigenvector. We thus take the next solution $\phi = 2\pi$ which gives

$$\lambda_1 \approx \frac{\sinh(\beta J)}{\cosh(\beta J) - \cos(\frac{2\pi}{L})} \approx \frac{\sinh(\beta J)}{\cosh(\beta J) - 1 + \frac{2\pi^2}{L^2}} \approx \coth(\frac{\beta J}{2})(1 - \frac{\pi^2}{\sinh^2(\frac{\beta J}{2})L^2}) \tag{3.181}$$

In Fig 3.5, we show the agreement between the computation of the first two eigenvalues !!!! computed by numerical diagonalisation and compared with the analytical approximations Eq. (3.178) and Eq. (3.181) which are valid for the large L limit

The correlation length is then given by

$$\xi = \frac{1}{\ln(\frac{\lambda_0}{\lambda_1})} = \frac{1}{\ln(\frac{\cosh(\beta J) - \cos(\frac{\pi}{L})}{\cosh(\beta J) - \cos(\frac{2\pi}{L})})} \approx \frac{4}{3}\frac{\sinh^2(\frac{\beta J}{2})L^2}{\pi^2} \tag{3.182}$$

and we see that this has the same form as that for the free elastic line in Eq. (3.88). Furthermore, the free energy per site is given in the thermodynamic limit and for large L by

$$f = -\frac{1}{\beta}\ln(\lambda_0) \approx -\frac{1}{\beta}\left[\ln(\coth(\frac{\beta J}{2})) - \frac{\pi^2}{4\sinh^2(\frac{\beta J}{2})L^2}\right] \tag{3.183}$$

and this gives a pressure

$$P = -\frac{\partial f}{\partial L} = \frac{T\pi^2}{2\sinh^2(\frac{\beta}{2})L^3} \tag{3.184}$$

This has the same form as the pressure for the elastic line in Eq. (3.84) if we make the identification of the effective surface tension to be used in the elastic line model

$$\sigma_{eff} = \frac{2}{\beta}\sinh^2(\frac{\beta J}{2}) \tag{3.185}$$

We should note that this is also consistent with the equality deduced by comparing the correlation length of the two models.

We see that in the limit of large L and for appropriately low temperatures, the finite size SOS model reproduced the phenomenology of the elastic line (confined Edwards-Wilkinson surface). This is not surprising as a low temperatures jumps of more that two lattice spacings in the height are suppressed by a factor or $\exp(-\beta J)$ with respect to staying at the same height moving up or down by one site. The low temperature SOS model thus becomes effectively equivalent to the RSOS model and thus is equivalent to a local random walk model.

High temperature limit

To explore the high temperature limit we can note that if we write

$$z = r - \exp(-i\theta) \tag{3.186}$$

we can write Eq. (3.173) as

$$\exp(iL\theta) = -\frac{z}{\bar{z}} = \exp(2i\psi + i\pi) \tag{3.187}$$

where

$$\tan(\psi) = \frac{\sin(\theta)}{r - \cos(\theta)} \tag{3.188}$$

This then gives

$$L\theta = 2\psi + \pi \tag{3.189}$$

and so

$$\tan(\psi) = \frac{\sin(\theta)}{r - \cos(\theta)} = \tan(\frac{L\theta}{2} + \frac{\pi}{2}) = -\cot(\frac{L\theta}{2}) \tag{3.190}$$

which finally gives

$$\tan(\frac{L\theta}{2}) = \frac{\cos(\theta) - r}{\sin(\theta)} \tag{3.191}$$

In this form we see that our calculations agree with those of Svravick et al [97]. Futhermore when $\beta \to 0$ we know that the elements of the transfer matrix all tend to one and that the largest eigenvalue has all components equal. This means that in the infinite temperature limit, $\theta = 0$. Therefore in Eq. (3.191) we look for solutions where θ is small. Taylor expanding gives to leading order

$$\frac{L\theta^2}{2} \approx 1 - r - \frac{\theta^2}{2} \tag{3.192}$$

which gives

$$\theta \approx \sqrt{\frac{2(1-r)}{L+1}} \tag{3.193}$$

However the above expansion assumes that $\theta L \ll 1$ and so

$$\sqrt{2L(1-r)} \ll 1 \tag{3.194}$$

This means that the height can fluctuate by of order L from site to site. The high temperature approximation is thus equivalent to

$$\theta \approx \sqrt{\frac{2\beta J}{L+1}}. \tag{3.195}$$

Therefore at high temperature this means that $L\beta J \ll 1$. This gives a maximal eigenvalue

$$\lambda_0 = L + 1 \tag{3.196}$$

and the free energy

$$f = -\frac{1}{\beta} \ln(L+1) \tag{3.197}$$

which is the obvious result coming from the infinite temperature entropy. This result suggests that the solution for θ at small β can be written as a perturbation series of the form

$$\theta = \sqrt{\beta J} \sum_{n=0}^{\infty} b_n (\beta J)^n \tag{3.198}$$

The first two terms give

$$\theta = \sqrt{\beta J} \left[\sqrt{\frac{2\beta J}{L+1}} - \beta J \frac{2+2L+L^2}{6\sqrt{2}(1+L)^{\frac{3}{2}}} \right] \tag{3.199}$$

and from this we find

$$f = -\frac{1}{\beta} \ln(L + 1 - \beta J \frac{L^2 + 2L}{3}) \tag{3.200}$$

and where we show in Fig 3.6 the agreement of the high-temperature approximation (3.200) with respect to the direct diagonalization of the transfer matrix. As pointed out above this result gives the high temperature entropy but it also exhibits the correct average energy ϵ per unit length at high temperature. To see this we note that all values of h are equiprobable at infinite temperature and so

$$\epsilon = \frac{1}{(L+1)^2} J \sum_{i,j=0}^{L} |i-j| = J \frac{L^2 + 2L}{3} \tag{3.201}$$
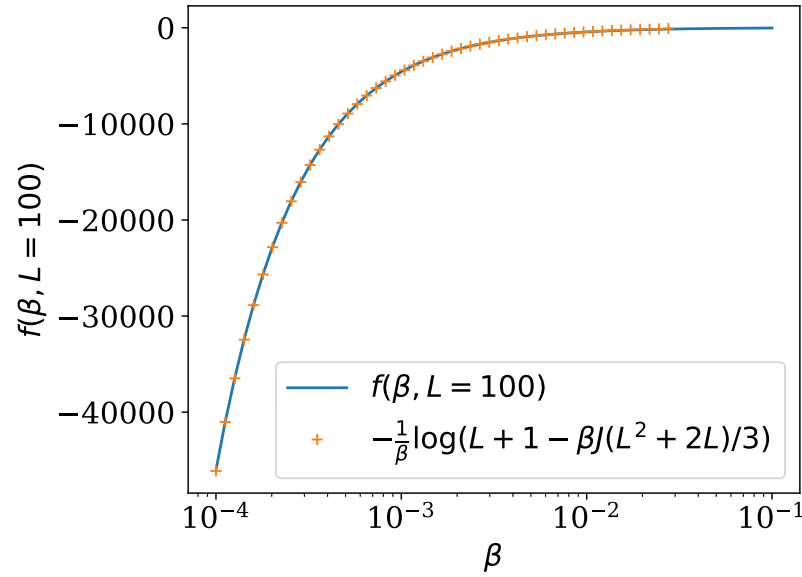
Figure 3.6: Free energy with respect to β for L = 100 and J = 1 in the high-temperature limit, by direct diagonalization of the transfer matrix and by Eq (3.200).

3.5 Conclusion

Finite-size effects corrections in the free energy are important when the correlation length becomes of the order of magnitude of the system's size. The derivative of the free energy with respect to the system size yields a confinement pressure, which can be seen for electromagnetic fields [14, 88, 15] and for critical systems [3], which has long-range interaction.

For continuous 1D interface systems, we use the path integral method [8] to compute the energy of all states, which gives us in the thermodynamic limit $f = \frac{1}{\beta}\epsilon_0$ and the correlation length $\xi = \frac{1}{\epsilon_1 - \epsilon_0}$. The computation of the free energy of a continuous 1D interface is thus mapped to a 1D quantum problem. This method can be used for all potentials $V(h)$, and so we apply it to two speficic cases. In the confined elastic line, which gives us the free energy per unit length $f = \frac{T^2 \pi^2}{2\sigma L^2}$, which gives a different power-law than the critical Casimir force. That is to be expected, since critical systems have no surface tension, but using a conjecture [16] about the finite-size corrections on the surface tension, we show the correspondence between both models in the case $\sigma = 0$. In the semi-infinite geometry though, we compute the average height when the interface is under pressure.

For discrete Solid-On-Solid models, the path integral cannot be directly applied, and methods adapted to discrete systems must be used.

The first method is to compute the free energy through numerical simulations. We generalize the LJH method [12] to any external potential both for Ising and SOS models, and compare it to the transfer matrix in the case of SOS for Kawsasaki dynamics in the SOS model - which was the special case where neither the Layer method nor the LJH method were pertinent.

For the confined SOS interface, we followed Švrakić [97] to obtain the exact eigenvalues and eigenvectors of the transfer matrix in the case $V(h) = 0$. This gives us a free energy which has a the same dependence to the system's size than the confined elastic line.

Chapter 4

Beyond Solid-On-Solid : the Particles-Over-Particles model

While Ising models describe bulk behaviour of magnetic systems [4, 34] but can also be used to describe interfaces between two coexisting phases [46], a direct interface lattice models exists, which is called Solid-On-Solid. This model was first studied by Gilmer and Bennema [99, 6] as a way to compute the crystal growth, whose dynamical equation will be later known as the Edwards-Wilkinson equation [30, 31] . In a second time, correspondance between SOS and the highly anisotropic Ising model at low temperature where found [47, 96], with the exact derivation of the SOS hamiltonian from the Ising one explained in Sec 1.3.2. When using an exponent of 2 in the interaction between nearest sites, the Gaussian SOS exhibits similar behavior to fluid interfaces [100, 101]. In Monte Carlo simulations for the Ising model, spins are taken with a uniform probability [75, 10], which allows the study of interface dynamics [102, 103, 72, 104]. On the contrary in the SOS aproximation it is the heights which are taken with a uniform probability [50, 62] thus discarding bulk information.

Driven by this lack of correspondence between both models, in this chapter we modernize Temperley's model [105] with a model that we call **Particles-Over-Particles** which takes into account combinatorial terms, giving rise to an entropic contribution. By noticing that the height h of the interface is the sum of all particles of size $a = 1$ which are put under it, we first develop the partition function and transfer matrix of our model and compare it to Ising and SOS (to our knowledge there has been no direct comparison between Ising and SOS in litterature), then we develop the M-particles system where we introduce multiple types of particles stacked vertically, where each type may obey to a different dynamic, kinetic coefficient or difusive constant.

4.1 The model

In a SOS system of size L' , the height of the interface at site i is noted $h_i \in [0, L]$ at site i, and fixing the total number of particles to be N the partition function is given by

$$Z_{SOS}(N) = \sum_{h_0 h_1 \dots h_{L'}} \delta_{\sum_i h_i, N} \exp\left(-\beta J \sum_{i=1}^{L'} |h_{i+1} - h_i| - \beta B \sum_{i=1}^{L'} V(h_i)\right) \tag{4.1}$$

where $V(h)$ is a function of the internal variables h_i and B the coupling parameter which has the dimension of energy. As we do in the case of a perfect gas, if the height profiles represent particle numbers which are all identical, the partition function is given by

$$Z_{POP}(N) = \frac{1}{N!} \sum_{h_1, h_2 \cdots h_{L'}} \delta_{\sum_{i=1}^{L'} h_i, N} \frac{N!}{\prod_{i=1}^{L'} h_i!} \exp\left(-\beta J \sum_{i=1}^{L'} |h_{i+1} - h_i| - \beta B \sum_{i=1}^{L'} V(h_i)\right) \tag{4.2}$$

Here the combinatorial term $\frac{N!}{\prod_{i=1}^{L} h_i!}$ represents the number of ways that the h_i particles on each site can be chosen from the N particles available. In the same fashion as the Solid-On-Molid, we call this model the **Particles-Over-Particles model**, since we stack particles in columns of height h_i. The constraint on the particle number makes the computation of the partition function at fixed N complicated both analytically and numerically. However, if we change to the grand canonical ensemble using the formula

$$\Xi = \sum_N \exp(\beta\mu N) Z_{POP}(N) \tag{4.3}$$

where Ξ is the grand partition function and μ the chemical potential, we find

$$\Xi_{POP} = \sum_{h_1, h_2 \cdots h_{L'}} \frac{1}{\prod_{i=1}^{L'} h_i!} \exp\left(-\beta J \sum_{i=1}^{L'} |h_{i+1} - h_i| - \beta B \sum_{i=1}^{L'} [V(h_i) - \mu h_i]\right) \tag{4.4}$$

The model differs from the usual solid on solid model in that a number of particle configurations give rise to the same height configurations. The grand partition function can then be written as

$$\Xi = \sum_{h_1, h_2 \cdots h_{L'}} \exp\left(-\beta H_{eff}(h_1, h_2 \cdots h_{L'})\right) \tag{4.5}$$

where

$$H_{eff} = J \sum_{i=1}^{L'} |h_{i+1} - h_i| + \sum_{i=1}^{L'} [BV(h_i) - \mu h_i + \frac{1}{\beta} \ln(h_i!)] \tag{4.6}$$

The transfer matrix is

$$T_{POP}(h, h') = T_{SOS}(h, h') \exp\left(-\frac{\ln(h) + \ln(h')}{2}\right) \tag{4.7}$$

Contrary to the SOS model where there needs to be a confining external field in order to localize the interface [106, 107], the entropic term gives a stable position for the interface. In absence of external field $B = 0$, the effective potential is given by

$$V_{eff}(h) = -\mu h + \frac{1}{\beta} \ln(h!) \tag{4.8}$$

If the chemical potential is large enough, the number of particles N is large enough, so we can use Striling's formula and approximate a continuous derivative with the finite-difference in h, so we have

$$V_{eff}(h)' = -\mu + \frac{1}{\beta} \ln(h) \tag{4.9}$$

which gives the mean height

$$\langle h \rangle = \exp(\beta\mu) \tag{4.10}$$

In Fig 4.1, we show the mean height (4.10) compared to the transfer matrix diagonalisation with different matrix size and the Monte Carlo simulations at $\beta = 1$. We see that when $\langle h \rangle \gg 1$, the Stirling's formula becomes valid and Eq (4.10) becomes accurate. Since $\langle h \rangle$ cannot exceed the maximum size of the system, saturation occurs at large μ. SOS mean height is also plotted as a reference, where we see that even in the limit $\mu = 0$, the mean height is equal to $\langle h \rangle (\mu = 0) = \frac{L}{2}$.

The Kawasaki implementation is straigthforward, we choose a particle n with probability $\frac{1}{N}$ at each Monte Carlo step, then we attempt to move the particle to the left or right using Metropolis acceptance rate.
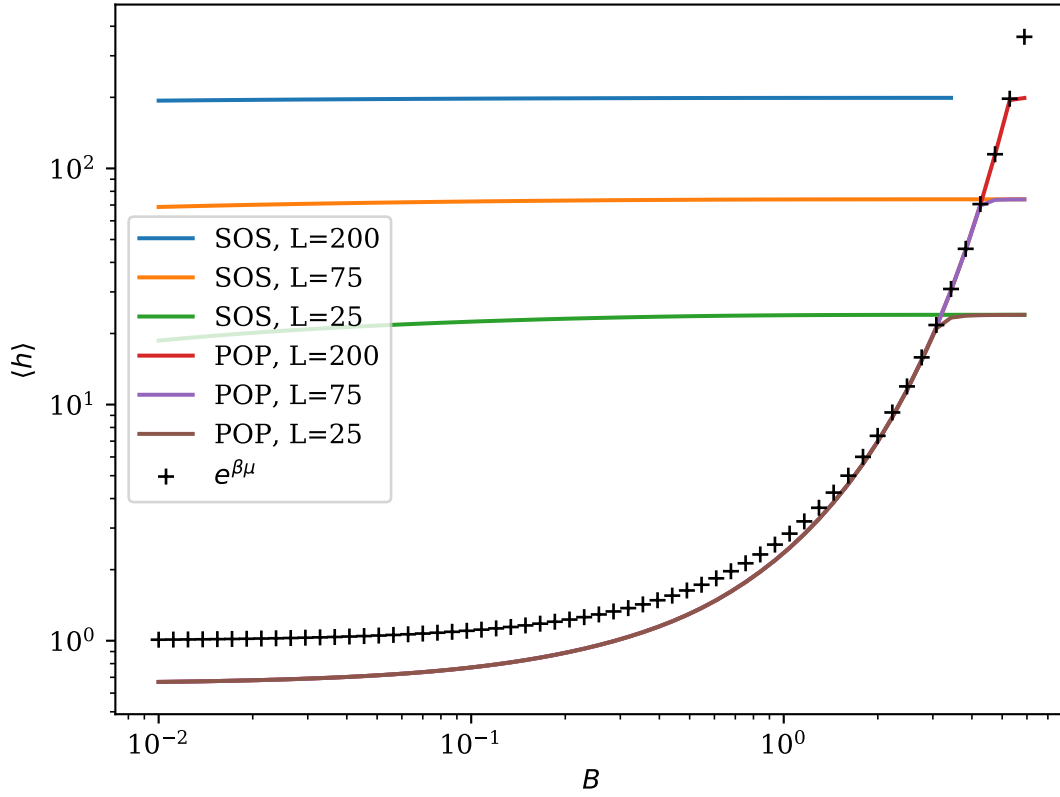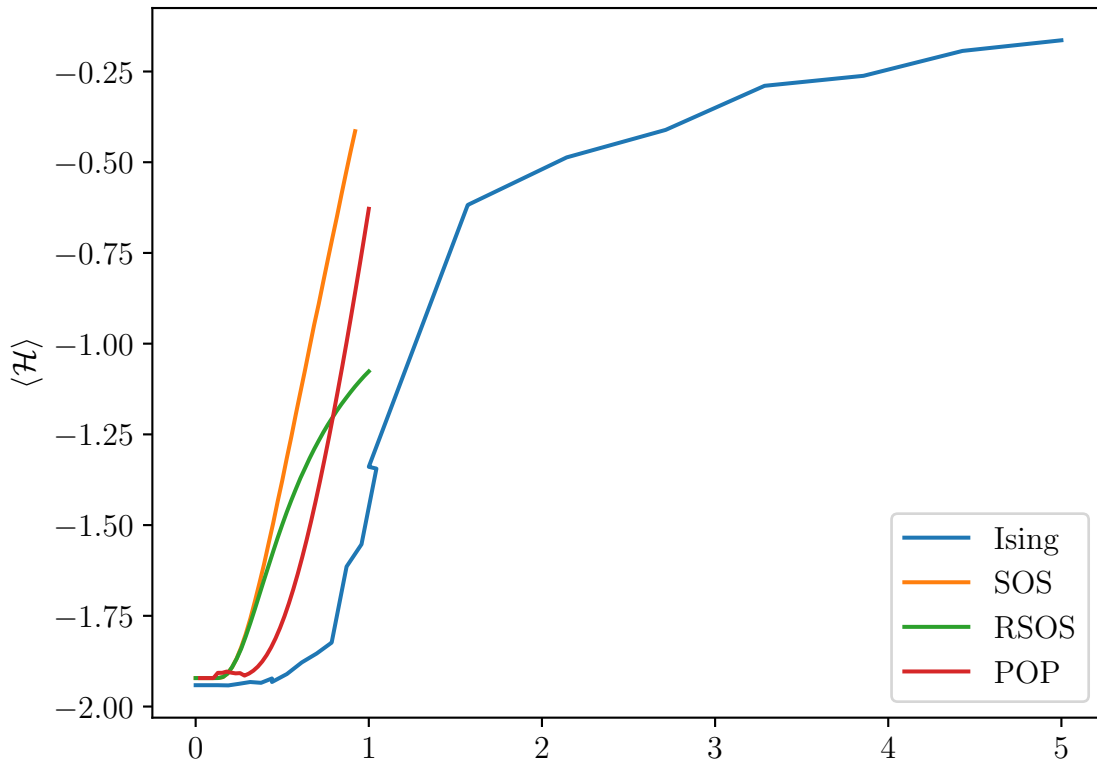
Figure 4.1: Mean height of the SOS (for reference) and POP model with respect the chemical potential µ through transfer matrix with different maximal heights in the thermodynamic limit $L' \to \infty$, compared to the Striling's approximation Eq (4.10),at $\beta = 1$.

The Glauber case is trickier. At equilibrium, we expect that as many particles are added as substracted, so we attempt with probability 0.5 to add a particle, and to remove one with the same probability. When adding a particle, we choose a site i with uniform probability $1/L'$, so the selection rate is

$$g(h_i \rightarrow h_i + 1) = \frac{1}{2L'} \tag{4.11}$$

To remove a particle [1], we choose a particle n with uniform probability $1/N$, meaning that the selection probability is

$$g(h_i \rightarrow h_i - 1) = \frac{h_i}{2N} \tag{4.12}$$

In the case that there is no particle in the system, we skip that phase and we immeidately proceed to attempt to add a new particle. In order to satisfy detailed balance, we thus need acceptance rates such that verify

$$\frac{g(h_i \rightarrow h_i + 1)}{g(h_i + 1 \rightarrow h_i)} \frac{A(h_i \rightarrow h_i + 1)}{A(h_i \rightarrow h_i + 1)} = \frac{N}{L'(h_i + 1)} \frac{A(h_i \rightarrow h_i + 1)}{A(h_i \rightarrow h_i + 1)}$$
$$= \exp(-\beta(E(h_i + 1) - E(h_i))) \tag{4.13}$$

Chosing an acceptance rate that satisfies this condition is not as easy as the Metropolis acceptance rate [75], and we provide no clear answer as to how solve this problem. Using the Metropolis acceptance rate ($A(\mu \rightarrow \nu) = 1$ if $\Delta_E \langle 0 \rangle$ does not to provide the correct equilibrium averages expected by the transfer matrix.

Here, the combinatoric term is directly taken into account in the selection probability, which is why it is difficult to find a good acceptance rate. Nevertheless, it is posible to use uniform selection probability as with SOS and introduce the combinatoric term in the energy.

In Fig 4.2, we plot the internal energy of the Ising, SOS, RSOS and POP models with respect to temperature in absence of external fields and $\mu = 0$ wtih non-conserved dynamics. discuss the graph once plots are better

4.2 M-**particles POP system**

The Ising model with spins $\sigma = \pm 1$ has a direct mapping with liquid/gas and binary mixtures systems [2], which are systems with two types of particles (for the liquid/gas model we can say that σ is a "density particle"). On the contrary, SOS models only need the existence of one type of particles, since everything that is over the interface is not taken into account. We can immagine multi-layering of non-miscible liquids having different densities [108, 109], forming many layers with $M - 1$ interfaces, M being the number of particles type. We can decide to study one specific interface between two particle types, and in such case the classic SOS model would be enough, with J being the surface tension between both liquids.

In this multi-layered system, we consider a model of a surface delimiting a bulk phase of L' sites which contains M different particle types $p_1...p_M$, N_m is the total number of particles of type m and

---

[1]In C++, we can use a $std :: vector$ in which we add or remove particles. After each success attempt, we rebuild the distribution $std :: uniform\_int\_distribution(0, N - 1)$, where N is the number of particles. This operation is lightweight and should not cause any slowing down. For the next section's algorithm with multiple particle types, we use $std :: discrete\_distribution\langle\rangle$.
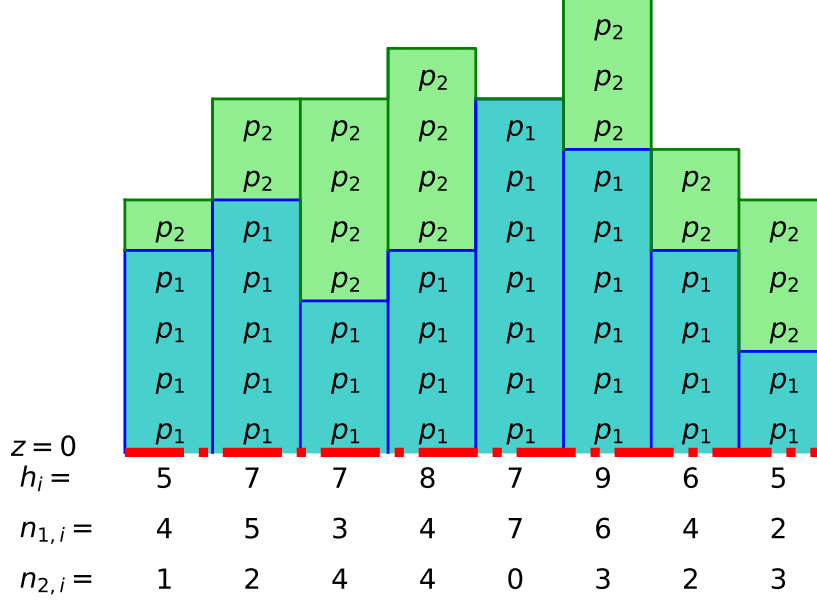
Figure 4.3: Possible POP configuration with two types of particles p_1 and p_2. The red line shows the origin $z = 0$. In the i-th column the interface is at height h_i, with $n_{1,i}$ particles of type p_1 at site i, and same for particles p_2. Over the interface, there are no particles.

$n_{m,i}$ denotes the number of particles of type m at site i. The interface height is $h_i = \sum_m n_{m,i}$. Taking into account the entropic contribution, the effective Hamiltonian for the model is

$$H[M] = J\sum_i |h_i - h_{i+1}| + B\sum_i V(h_i) - \sum_m \mu_m \sum_i n_{m,i} + \frac{1}{\beta}\sum_m \sum_i \ln(n_{m,i}) \qquad (4.14)$$

We assume that the particles in each column are demixed, i.e. the permitted particle configurations are taken to be stacked vertically such that the stack of p_{m+1} particles lies on top of the p_m particles, as seen in Fig 4.3 for M = 2. The first term in the Hamiltonian corresponds to the surface tension with a gas phase above the stacks of particles. As disccused with the SOS model, we can have a restricted or gaussian version of Eq 4.14.

The grand partition function is given by

$$\Xi = \sum_{\mathbf{n_1}...\mathbf{n_M}} \exp(-\beta H[M]) \qquad (4.15)$$

If M = 2, the the statics of the above can be reduced to the study of a single particle model by making the change of variable $n_{2,i} = h_i - n_{1,i}$. Using the binomial relation $(a + b)^{n_1} = \sum_{h'=0}^h \frac{h!}{h'!(h-h')!} a^{h'} b^{h'-h}$, the sum over the variables $n_{1,i}$ can be trivially carried out and we find

$$\Xi = \sum_{\mathbf{h}} \exp\left(-\beta J\sum_i |h_i - h_{i+1}| - \beta B\sum_i V(h_i) - \sum_i \ln(h_i!) + \beta\mu_e\sum_i h_i\right)$$
$$= \sum_{\mathbf{h}} \exp\left(-\beta H_{eff}(h_1, h_2...h_{L'})\right) \qquad (4.16)$$

where $\mu_e = \frac{1}{\beta}\ln(\exp(\beta\mu_1) + \exp(\beta\mu_2))$ is the effective chemical potential for the variables h_i. If we add a third type of particle, we see clearly see that the same reduction can be carried out. Thus, by recursivity, we can show that for any number of particle type M, we have the same effective Hamiltonian as

the single particle system (4.6), with an effective chemical potential

$$\mu_e = \frac{1}{\beta} \ln \left(\sum_m \exp(\beta \mu_m) \right) \tag{4.17}$$

An interesting thing to remark is that even if the chemical potential of a particle type $\mu_m = 0$, its contribution to the effective chemical potential is nonzero. This reduced theory can be numerically solved in equilibrium by transfer matrix methods.

Now let the subset $\bar{\text{M}}$ of particle types from the M particle types be in the canonical ensemble, while all the other ones are in the grand-canonical one. This is the so-called model C [18], which describes the coupling between conserved and non-conserved fields, such as impurities in liquids [110] or ionic conductors moving through a lattice set up by different types of ions [111, 112]. The total partition function is then

$$\Xi = \sum_h \exp \left(-\beta \text{H}_{eff}(h_1, h_2 ... h_{\text{L}'}) \right) \prod_{m \in \bar{\text{M}}} \delta_{\sum_{i=1}^{\text{L}'} h_i, \text{N}_m} \tag{4.18}$$

with the average number of particles $\langle n_{m,i} \rangle$ per site being

$$\begin{aligned} \langle n_m \rangle &= \frac{1}{\beta \text{L}'} \frac{\partial}{\partial \mu_m} \ln(\Xi) \\ &= \frac{1}{\beta \text{L}'} \frac{\partial \mu_e}{\partial \mu_m} \frac{\partial}{\partial \mu_e} \ln(\Xi) \\ &= \frac{\exp(\beta \mu_m)}{\sum_m \exp(\beta \mu_m)} \langle h \rangle \end{aligned} \tag{4.19}$$

where $\langle h \rangle = \langle \sum_m n_m \rangle$.

Mixing Glauber and Kawasaki dynamics for different particle types could be implemented using the following algorithm. Each non-conserved particle type possess a kinetic coefficient α_m, while each conserved particle type has a diffusive coefficient D_m. We set $p_m = \alpha_m$ if the particle is non-conserved, and $p_m = D_m$ otherwise, and we normalize it in order to have $\sum_m p_m = 1$. At each Monte Carlo step, a particle of type m is chosen with probability p_m, and then we proceed with Glauber or Kawasaki dynamics for a single-type particle system, as described in the previous section. To satisfy detailed balance, we have to understand how this coefficient p_m changes the selection probability g, and we get the same difficulties as in the single-particle type Glauber case.

Nevertheless, when all particles are under Kawasaki dynamics and $p_m = 1/\text{M}$ is a constant, then the ratio between selection rates is equal, which solves all the issues.

This algorithm could prove usefull for studying multi-particle systems where each particle type is under different potentials (think of an ion in a neutral solvent under magnetic field) or different temperature [113], some of them which are under non-equilibrium forces like shearing.

4.3 Continuum Theory

In order to understand the statics of the model we write a continuum version of the theory with M field $n_m(x)$ and we take the a Gaussian form for the surface energy

$$\text{H} = \int dx \frac{\sigma}{2} [\frac{d}{dx} (\sum_m n_m)]^2 + \text{V}(n_1(x), ..., n_{\text{M}}(x)) \tag{4.20}$$

where σ is the surface tension and

$$\text{V}(n_1(x), ... n_{\text{M}}(x)) = \sum_m -\mu_m n_m(x) + \text{T} n_m(x) [\ln(n_m(x)) - 1] \tag{4.21}$$

We have used Stirlings formula and thus assumed that the typical value of $n_m(x)$ aree large. We now expand $V(n_1(x),...n_M(x))$ by writing $n_m(x) = \overline{n}_m + \phi_m(x)$ where $(\overline{n}_1,..\overline{n}_M)$ is the minimum of $V(n_1,..n_M)$. Here we find

$$\overline{n}_m = \exp(\beta\mu_m) \tag{4.22}$$

This gives an effective Hamiltonian for the fluctuations of the fiels ϕ_m

$$H_f = \frac{\sigma}{2} \int dx [\frac{d}{dx}(\sum_m \phi_m]^2 + \sum_m r_m \phi_m^2(x) \tag{4.23}$$

where

$$r_m = \frac{T}{\sigma\overline{n}_m} \tag{4.24}$$

A straight forward calculation then shows that the Fourier transform of the connected height-height fluctuation correlation function is

$$\tilde{C}_{hh}(k) = \frac{T}{\sigma} \frac{1}{k^2 + r_e} \tag{4.25}$$

where $r_e = \prod_m r_m / \sum_m r_m$. We thus find

$$\langle h^2 \rangle = \frac{T}{2\sigma m_e} = \frac{1}{2}\sqrt{\frac{T\overline{h}}{\sigma}}, \tag{4.26}$$

where $\overline{h} = \sum_m \overline{n}_m$.

4.4 Conclusion

There are two ways of interpreting the interface's descritpion throught its height $\{h_i\}$. The first one is to only see the height as the interface's degrees of freedom [99, 6], while the second one is to interpret that height as a number of particles of type A which are below the interface with particles of type B, which is the physical phenomenon happening in crystal growth. This interpretation requires the addition of an etropic term [105], which localises the free interface in a semi-infinite geometry, contrary to SOS models [107]. The system can also be composed of multiple layers of different particles [multilayer], and this new model can take that into account for numerical simulations. The problem lies in the numerical algorithm. Taking a height with non-uniform probability is tricky, as it changes the selection probability $g(C \to C')$, so the acceptance probability $A(C \to C')$ is not as simple as the Metropolis one [75, 10]. We let the resolution of this problem - and as such the study of new physics through numerical simulations of this model - to the community.

Chapter 5

Driven interfaces

One of the most natural ways of creating a non-equilibrium steady state is by applying external driving forces, as shown in Fig 5.1. Driving arises naturally in sedimenting systems due to gravity, in systems with free charges under the action of an electric field, and also due to the radiation pressure exerted by a laser. Experiments where a phase separated colloidal system is sheared parallel to the interface show that driving due to shear tends to suppress surface fluctuations [19], and similar results are found where Ising models are numerically sheared [73, 104]. These results are somewhat surprising, for instance they are contrary to the observation that wind generates waves on the ocean. One may think that the precise nature of the driving plays a role, for instance uniformly driving a system may be intrinsically diferent to applying a shear field which is manifestly nonuniform.

In this capter we investigate driving using three different methos. In the first section - which is almost a verbatim of a paper we have published [17] - we develop model C interfaces (model B interface is invariant under galilian transformation under driving) and find that the height fluctuations are suppressed and the correlation length of the fluctuations is increased. In the second section, we discuss driving in the SOS model, where the galilean invariance is broken by the discrete-time nature of numerical simulations. In the last section, we use a similar approach than in the paper (which is the approach that gaves us the idea of the paper) for the Particles-Over-Particles model in the case of two different particles type.

5.1   The effect of driving on model C interfaces

Constructing a continuum model which is analytically tractable and is also affected by uniform driving is straightforward but contains some subtleties. In a continuum system it is clear that uniform driving can only move a system away from equilibrium when the driving acts differently on different particle types. For instance, consider a system of identical interacting Brownian particles driven by a uniform force. The force will induce the same average velocity on all the particles, consequently, in the frame moving with this average velocity, we will recover the unmodified equilibrium state. However, when multiple particle types are present, the mean velocity induced on different species are different and no Galilean transformation is possible. Perhaps the first such study of this phenomenon was due to Onsager [114], who studied the conductivity of electrolytes and in doing so showed how the correlation functions in the steady state were modified by the electric field. Recently there have been many studies of driven multi-particle Brownian systems [115, 116, 117, 118, 119, 120], including the electrolyte problem, and rich new physics has been found, even in the case of purely Gaussian theories [121, 122] based on stochastic density functional theory [123].

The dynamics of discrete particle systems is however affected by uniform driving of identical particles. The study of driven lattice gases has revealed a wide range of intriguing physical phenomena

and indeed shown how driving can even lead to phase separation [112, 124, 125, 102]. The discrete nature of the dynamics of these systems, both in space and time, means that no Galilean transformation to an equilibrium state exists. Analytical studies of these systems require a phase ordering kinetics description in terms of a continuum order parameter. In order to break Galilean invariance the local mobility of the particles can be taken to be dependent on the local order parameter, this is then sufficient to induce non-trivial steady states under driving [112, 125, 73, 104]. Interfaces between the separated phases in uniformly driven systems have non capillary behaviors which are, even today, not fully understood [125]. Taking random driving in a given direction also leads to non-equilibrium steady states, if the noise is Gaussian and white, the fluctuation dissipation theorem is violated and novel interface fluctuations are induced which, again, are not of the capillary type [124].

Driving can also be deterministic but space dependent, for instance if one considers applied shear flows, the spatial dependence of the flow means no Galilean transformation to an equilibrium steady state is possible and this therefore leads to non-equilibrium steady states. The effect of shear on interfaces in these type of systems yields interface equations of the stochastic Burgers type and the statistics are no thus longer Gaussian due to the presence of nonlinearities [9, 29, 73, 104, 70, 126]

In this chapter we analyse what is known, in the classification of Hohenberg and Halperin [18], as model C type dynamics for two fields, one with conserved model B type dynamics, which is in addition convected at a uniform velocity to mimic driving. We refer to this first field as the colloid field. This colloid field is coupled to an additional field which undergoes model A non-conserved dynamics and which is not subjected to the driving. The model A field can be thought of a passive solvent and its coupling to the model B field is chosen in such a way that it has no influence on the non-driven equilibrium steady state. We then derive the effective dynamics between two separated low temperature phases by using a method introduced in [9, 29] for the study of interfaces under shear flow. This method yields a Gaussian theory for the interface statistics and driving introduces interesting new physics, notably we find that the effective surface tension of the system is increased but also the correlation length of interface fluctuations (due to an effective gravitational term) are increased. These observations are in qualitative agreement with experimental results on sheared low tension interfaces in phase separated colloidal systems [19]. In this experimental system the interface fluctuations were also found to be well described by Gaussian statistics and this is our principal motivation for studying theories which remain Gaussian but are modified by driving. While the long wavelength theory we find is of a capillary type, we also find new, higher derivative terms, which are generated in the spectrum of the height fluctuations.

As an aside, we also show how the model introduced here can be used to analyse the effect of activity on the dynamics of the surface between two phases of active colloids. The activity is implemented by taking a different temperature for the colloid and solvent fields, this difference in temperatures leads to significantly modified surface statistics which again develop dependencies on static and dynamical variables of the model which otherwise remain hidden for the equilibrium version of the problem.

5.1.1 The underling two field model

We consider a coarse grained model for two scalar fields ψ and ϕ with Hamiltonian

$$H[\psi, \phi] = H_1[\psi] + H_2[\psi, \phi] \tag{5.1}$$

The Hamiltonian H_1 is of the classic Landau-Ginzburg form

$$H_1[\psi] = \int d\mathbf{x} \left[\frac{\kappa}{2} [\nabla \psi(\mathbf{x})]^2 + V(\psi(\mathbf{x})) - gz\psi(\mathbf{x}) \right] \tag{5.2}$$

The last term represents the energy due to a gravitational field and will introduce a finite correlation length in the fluctuations between the two phases. We assume that the above Hamiltonian has two
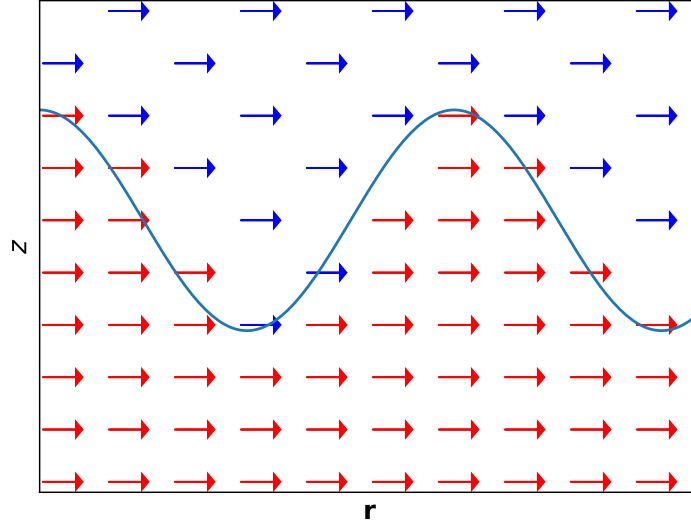
Figure 5.1: Schematics of the advection term $\mathbf{v} \cdot \nabla \psi(\mathbf{x}, t)$ for a field under the interface approximation (5.18). The red and blue phase respectively correspond to ϕ_2 and ψ_1, with $\phi_2 > \psi_1$, and the solid line the interface between phases.

stable phases with average concentrations of the field $\phi(\mathbf{x})$ given by the constant values ψ_1 and ψ_2, the difference between the order parameter in the two different phases is denoted by by $\Delta\psi = \psi_2 - \psi_1 > 0$. This means that we find the phase 1 as $z \to \infty$ and the phase 2 as $z \to -\infty$. The term H_2 is taken to be a simple quadratic coupling between the fields

$$H_2 = \int d\mathbf{x} \frac{\lambda}{2} (1 - \psi(\mathbf{x}) - \phi(\mathbf{x}))^2 \tag{5.3}$$

which is an approximative conservation law of total volume fraction of the phases. The field ϕ can be though of as the local volume fraction of the solvent in a colloidal system. However the presence of this solvent field does not change the effective equilibrium statistical mechanics of the colloid field ψ as the partition function can be written as

$$Z = \int d[\phi] d[\psi] \exp(-\beta H_1[\psi] - \beta H_2[\psi, \phi]) = C Z_{eff} \tag{5.4}$$

where Z_{eff} is the effective partition function for the field ψ, after we have integrated out the degrees of freedom corresponding to the field ϕ, and C is a constant term resulting from this integration. The effective partition function is thus simply given by

$$Z_{eff} = \int d[\psi] \exp(-\beta H_1[\psi]) \tag{5.5}$$

and, as stated above, we see that the field ϕ thus has no effect on the equilibrium statistical mechanics of the field ψ.

We now consider the dynamics of the fields. We take local diffusive model B dynamics for the field ψ and non-conserved model A dynamics for the field ϕ

$$\frac{\partial \psi(\mathbf{x}, t)}{\partial t} + \mathbf{v} \cdot \nabla \psi(\mathbf{x}, t) = D\nabla^2 \frac{\delta H}{\delta \psi(\mathbf{x})} + \sqrt{2DT} \nabla \cdot \boldsymbol{\eta}_1(\mathbf{x}, t) \tag{5.6}$$

$$\frac{\partial \phi(\mathbf{x}, t)}{\partial t} = -\alpha \frac{\delta H}{\delta \phi(\mathbf{x})} + \sqrt{2\alpha T} \eta_2(\mathbf{x}, t). \tag{5.7}$$

71

The first equation corresponds to standard model B dynamics but with an advection term by a constant velocity field **v**. In Fig 5.1, we show the effect of that advection term in the presence of an interface. Since phase 1 is more diluted than phase 2, there are less particles which are driven at constant velocity **v**. The second equation has no advection term and is simple model A dynamics. In principle we can also treat the case where the dynamics of the field ϕ is also diffusive and thus of model B type, the analysis given here can be extended to this case but the analysis of the resulting equations is considerably more complicated. The use of model A dynamics for the solvent is justified by assuming that its dynamics is faster than that of the colloids and that the volume fraction can vary due to local conformational changes rather than diffusive transport.

The noise terms above are uncorrelated and Gaussian with zero mean, their correlation functions are given by

$$\langle \eta_{1i}(\mathbf{x}, t)\eta_{1j}(\mathbf{x}', t)\rangle = \delta_{ij}\delta(t - t')\delta(\mathbf{x} - \mathbf{x}') \tag{5.8}$$

$$\langle \eta_2(\mathbf{x}, t)\eta_2(\mathbf{x}', t)\rangle = \delta(t - t')\delta(\mathbf{x} - \mathbf{x}'), \tag{5.9}$$

and T is the temperature in units where $k_B = 1$. These dynamical equations are thus explicitly given by

$$\frac{\partial \psi(\mathbf{x}, t)}{\partial t} + \mathbf{v} \cdot \nabla \psi(\mathbf{x}, t) = D\nabla^2 [\frac{\delta H_1}{\delta \psi(\mathbf{x})} + \lambda(\phi(\mathbf{x}, t) + \psi(\mathbf{x}, t))] + \sqrt{2DT}\nabla \cdot \boldsymbol{\eta}_1(\mathbf{x}, t) \tag{5.10}$$

and

$$\frac{\partial \phi(\mathbf{x}, t)}{\partial t} = -\alpha\lambda[\phi(\mathbf{x}, t) + \psi(\mathbf{x}, t)] + \sqrt{2\alpha T}\eta_2(\mathbf{x}, t). \tag{5.11}$$

Taking the temporal Fourier transform, defined with the convention

$$\tilde{F}(\mathbf{x}, \omega) = \int_{-\infty}^{\infty} dt \exp(-i\omega t)F(\mathbf{x}, t), \tag{5.12}$$

we can eliminate the field $\tilde{\phi}$ which is given by

$$\tilde{\phi}(\mathbf{x}, \omega) = \frac{-\alpha\lambda\tilde{\psi}(\mathbf{x}, \omega) + \sqrt{2\alpha T}\tilde{\eta}_2(\mathbf{x}, \omega)}{i\omega + \alpha\lambda}, \tag{5.13}$$

this then gives the closed equation for $\tilde{\psi}$:

$$\left[1 - \frac{\lambda D\nabla^2}{i\omega + \alpha\lambda}\right]i\omega\tilde{\psi}(\mathbf{x}, \omega) + \mathbf{v} \cdot \nabla\tilde{\psi}(\mathbf{x}, \omega) = D\nabla^2\tilde{\mu}(\mathbf{x}, \omega) + \tilde{\zeta}(\mathbf{x}, \omega), \tag{5.14}$$

where

$$\mu(\mathbf{x}, t) = \frac{\delta H_1}{\delta \psi(\mathbf{x}, t)} \tag{5.15}$$

is the effective chemical potential associated with the field ψ and the noise term is given by

$$\tilde{\zeta}(\mathbf{x}, \omega) = \frac{\sqrt{2\alpha T}D\lambda}{i\omega + \alpha\lambda}\nabla^2\tilde{\eta}_2(\mathbf{x}, \omega) + \sqrt{2DT}\nabla \cdot \tilde{\boldsymbol{\eta}}_1(\mathbf{x}, \omega). \tag{5.16}$$

Inverting the temporal Fourier transform then gives the effective evolution equation

$$\frac{\partial \psi(\mathbf{x}, t)}{\partial t} - \lambda D\nabla^2 \int_{-\infty}^{t} dt' \exp(-\alpha\lambda(t - t'))\frac{\partial \psi(\mathbf{x}, t')}{\partial t} + \mathbf{v} \cdot \nabla\psi(\mathbf{x}, t) = D\nabla^2\mu(\mathbf{x}, t') + \zeta(\mathbf{x}, t). \tag{5.17}$$

5.1.2 Effective interface dynamics

Following Sec 1.2.2, we derive the dynamical equation for the interface $h(\mathbf{r})$, where

$$\psi(\mathbf{x}, t) = f(z - h(\mathbf{r}, t)) \tag{5.18}$$

and $f(z) \to \psi_2$ as $z \to -\infty$ and $f(z) \to \psi_2$ as $z \to \infty$, and we use the sharp interface aproximation

$$f'(z) = \Delta\psi\delta(z) \tag{5.19}$$

We also assume that the driving is in the $\mathbf{r} = (x, y)$. The dynamical evolution for the field ψ in Eq. (5.17) is first written as

$$\nabla^{-2}\left[\frac{\partial\psi(\mathbf{x}, t)}{\partial t} + \mathbf{v}\cdot\nabla\psi(\mathbf{x}, t)\right] - \lambda D\int_{-\infty}^{t} dt' \exp(-\alpha\lambda(t - t'))\frac{\partial\psi(\mathbf{x}, t')}{\partial t'} = D\mu(\mathbf{x}, t') + \nabla^{-2}\zeta(\mathbf{x}, t). \tag{5.20}$$

Using the relations (1.57) and (1.59), where $V(\psi(\mathbf{x})) = V(\psi(\mathbf{x})) - gz\psi(\mathbf{x})$, multiplying both sides by $f'(z - h(\mathbf{r}, t))$ and integrating over z as in Eq (??), we obtain

$$
\begin{aligned}
\int_{-\infty}^{\infty} dz f'(z - h(\mathbf{r}, t)\mu(\mathbf{x}, t) &= \kappa\nabla^2 h(\mathbf{r}, t)\int_{-\infty}^{\infty} dz\, f'(z - h(\mathbf{r}, t))^2 - \int_{-\infty}^{\infty} dz gz f'(z - h(\mathbf{r}, t)) \\
&= \kappa\nabla^2 h(\mathbf{r}, t)\int_{-\infty}^{\infty} dz'\, f'(z')^2 - \int_{-\infty}^{\infty} dz' g(z' + h(\mathbf{r}, t)) f'(z') \\
&= \kappa\nabla^2 h(\mathbf{r}, t)\int_{-\infty}^{\infty} dz'\, f'(z')^2 - \Delta\psi g h(\mathbf{r}, t). \tag{5.21}
\end{aligned}
$$

By using the Cahn-Hilliard estimate of the surface tension (1.41), we thus find

$$\int_{-\infty}^{\infty} dz f'(z - h(\mathbf{r}, t)\mu(\mathbf{x}, t) = \sigma[\nabla^2 h(\mathbf{r}, t) - m^2 h(\mathbf{r}, t)] \tag{5.22}$$

where $m^2 = \Delta\psi g/\sigma$.

We now carry out the same operation on the left hand side of Eq. (5.20). First we have

$$
\begin{aligned}
\nabla^{-2}\frac{\partial\psi(\mathbf{x}, t)}{\partial t} + \mathbf{v}\cdot\nabla\psi(\mathbf{x}, t) + \lambda D\int_{-\infty}^{t} dt' \exp(-\alpha\lambda(t - t'))\frac{\partial\psi(\mathbf{x}, t')}{\partial t'} &= \\
-\nabla^{-2}f'(z - h(\mathbf{r}, t))[\frac{\partial h(\mathbf{r}, t)}{\partial t} + \mathbf{v}\cdot\nabla h(\mathbf{r}, t)] + \lambda D\int_{-\infty}^{t} dt' \exp(-\alpha\lambda(t - t'))f'(z - h(\mathbf{r}, t'))\frac{\partial h(\mathbf{r}, t')}{\partial t'} \\
\approx -\nabla^{-2}f'(z)\frac{\partial h(\mathbf{r}, t)}{\partial t} + \mathbf{v}\cdot\nabla h(\mathbf{r}, t)] + \lambda D\int_{-\infty}^{t} dt' \exp(-\alpha\lambda(t - t'))f'(z)\frac{\partial h(\mathbf{r}, t')}{\partial t'} \tag{5.23}
\end{aligned}
$$

where in the last line above we have neglected terms quadratic in h. Note that the neglecting of these additional terms is not strictly justified, they could potentially induce non-perturbative effects which render the surface fluctuations non-Gaussian. However we see here that the first order computation we carry out tends to reduce fluctuations with respect to equilibrium or non-driven interfaces and so if the equilibrium theory can be described by an equation which is linear in height fluctuations, it seems physically reasonable to assume that the the approximation also holds for the driven interface. Again, we multiply the above by $f'(z)$ and integrate over z.

Putting this all together we obtain

$$\Delta\psi^2\int d\mathbf{r} G(0, \mathbf{r} - \mathbf{r}')[\frac{\partial h(\mathbf{r}, t)}{\partial t} + \mathbf{v}\cdot\nabla h(\mathbf{r}, t)] + \frac{\sigma\lambda D}{\kappa}\int_{-\infty}^{t} dt' \exp(-\alpha\lambda(t - t'))\frac{\partial h(\mathbf{r}, t')}{\partial t'} =$$
$$\sigma[\nabla^2 h(\mathbf{r}, t) - m^2 h(\mathbf{r}, t)] + \xi(\mathbf{r}, t) \tag{5.24}$$

where $G = -\nabla^{-2}$, or more explicitly

$$\nabla^2 G(z - z', \mathbf{r} - \mathbf{r}') = -\delta(z - z')\delta(\mathbf{r} - \mathbf{r}') \tag{5.25}$$

The noise term ξ is given by

$$\xi(\mathbf{r}, t) = \int_{-\infty}^{\infty} dz f'(z - h(\mathbf{r}, t))\nabla^{-2}\zeta(\mathbf{x}, t). \tag{5.26}$$

Now, as the equations of motion have been derived to first order in h and we wish to recover the correct equilibrium statistics for the non-driven system, we ignore the h dependence in the noise and make the approximation

$$\xi(\mathbf{r}, t) \approx \int_{-\infty}^{\infty} dz f'(z)\nabla^{-2}\zeta(\mathbf{x}, t). \tag{5.27}$$

The correlation function of this noise is most easily evaluated in terms of its Fourier transform with respect to space and time defined by

$$\hat{F}(\mathbf{q}, \omega) = \int dt d\mathbf{r} \exp(-i\omega t - i\mathbf{q} \cdot \mathbf{r})F(\mathbf{r}, t). \tag{5.28}$$

Using the relations Eqs. (1.41) and (5.19) one can show that

$$\langle \hat{\xi}(\mathbf{q}, \omega)\hat{\xi}(\mathbf{q}', \omega')\rangle = 2T(2\pi)^d \delta(\omega + \omega')\delta(\mathbf{q} + \mathbf{q}')\left[\frac{\sigma}{\kappa}\frac{\alpha D^2\lambda^2}{\omega^2 + \alpha^2\lambda^2} + \frac{D\Delta\psi^2}{2q}\right] \tag{5.29}$$

In full Fourier space the equation of motion for the field ψ then reads

$$\left[i(\omega + \mathbf{q} \cdot \mathbf{v})\frac{\Delta\psi^2}{2q} + \frac{D\sigma\lambda}{\kappa}\frac{i\omega}{\alpha\lambda + i\omega}\right]\hat{h}(\mathbf{q}, \omega) = -D\sigma(q^2 + m^2)\hat{h}(\mathbf{q}, \omega) + \hat{\xi}(\mathbf{q}, \omega) \tag{5.30}$$

From this, the full Fourier transform of the correlation function of the interface height is given by

$$\hat{C}(\mathbf{q}, \omega) = 2TD\frac{\left[\frac{\Delta\psi^2}{2q}(\omega^2 + \alpha^2\lambda^2) + \frac{\sigma\alpha D\lambda^2}{\kappa}\right]}{\left|i[\frac{\alpha\lambda\Delta\psi^2}{2q}(\omega + \mathbf{q} \cdot \mathbf{v}) + \frac{\lambda\sigma D}{\kappa}\omega + D\sigma(q^2 + m^2)\omega] + [\alpha\lambda D\sigma(q^2 + m^2) - \frac{\Delta\psi^2}{2q}\omega(\omega + \mathbf{q} \cdot \mathbf{v})]\right|^2} \tag{5.31}$$

Using the above we can extract the equal time height-height correlation function in the steady states. Its spatial Fourier transform can shown to be given by

$$\tilde{C}_s(\mathbf{q}) = \frac{1}{2\pi}\int d\omega \hat{C}(\mathbf{q}, \omega) \tag{5.32}$$

This integral has the same form as

$$I(f(\omega)) = \int \frac{d\omega}{2\pi}\frac{f(\omega)}{\left|i(A\omega + B) + (C - D\omega - E\omega^2)\right|} \tag{5.33}$$

so we see that the integral we need to evaluate can be written in the form

$$I = aI(\omega^2) + bI(1) \tag{5.34}$$

The calculation of Eq. (5.32) can be carried out in the presence of a forcing term on the height profile in order to compute the response function for the surface which has a denominator of the form

$$Den = i(A\omega + B) + (C - D\omega - E\omega^2) \tag{5.35}$$

and due to causality the above only has poles in the upper complex plane (due to the convention of Fourier transforms used here). Consequently we find that

$$\int \frac{d\omega}{2\pi} \frac{1}{i(A\omega + B) + (C - D\omega - E\omega^2)} = 0 \tag{5.36}$$

as one may close the integration contour in the lower half of the complex plane. Taking the real and imaginary part of Eq. (5.36) leads to

$$CI(1) - DI(\omega) - EI(\omega^2) = 0 \tag{5.37}$$

$$AI(\omega) + BI(1) = 0 \tag{5.38}$$

Using this we can express $I(\omega^2)$ as a function of $I(1)$, and explicitly we have

$$I(\omega^2) = \frac{I(1)}{E} [C + \frac{DB}{A}] \tag{5.39}$$

To evaluate $I(1)$ we now use

$$I(1) = -\text{Im} \int \frac{d\omega}{2\pi} \frac{1}{A\omega + B} \frac{1}{i(A\omega + B) + (C - D\omega - E\omega^2)} \tag{5.40}$$

The integrand above has no poles in the lower half of the complex plane but has a *half pole* at $\omega = -B/A$ on the real axis, thus using standard complex analysis we find

$$I(1) = \frac{1}{2(CA + BD - \frac{EB^2}{A})} \tag{5.41}$$

Then after some laborious, but straightforward algebra, we obtain that

$$\tilde{C}_s(\mathbf{q} = T \frac{\left(2D\sigma q(\kappa[q^2 + m^2] + \lambda) + \alpha\kappa\lambda\Delta\psi^2\right)^2 + \kappa^2\Delta\psi^4(\mathbf{q}\cdot\mathbf{v})^2}{\sigma[q^2 + m^2]\left(2Dq\sigma(\kappa[q^2 + m^2] + \lambda) + \alpha\kappa\lambda\Delta\psi^2\right)^2 + \kappa\left(\kappa\sigma[q^2 + m^2] + \lambda\sigma\right)\Delta\psi^4(\mathbf{q}\cdot\mathbf{v})^2} \tag{5.42}$$

In the absence of driving, *i.e.* when $\mathbf{v} = \mathbf{0}$ we recover the equilibrium correlation function

$$\tilde{C}_s(\mathbf{q}) = \tilde{C}_{eq}(\mathbf{q}) = \frac{T}{\sigma[q^2 + m^2]}, \tag{5.43}$$

here we see that $1/m = \xi_{eq}$ is the so called capillary length, which is the equilibrium correlation length of the height fluctuations. We also notice that the correlation function for wave vectors perpendicular to the driving direction is simply the equilibrium one.

If we write $C_s(\mathbf{q}) = T/H_s(\mathbf{q})$ we can interpret $H_s(\mathbf{q})$ as an effective quadratic Hamiltonian for the height fluctuations, it is thus given by

$$H_s(\mathbf{q}) = \sigma[q^2 + m^2] + \frac{\kappa\lambda\sigma\Delta\psi^4(\mathbf{q}\cdot\mathbf{v})^2}{\left(2D\sigma q(\kappa[q^2 + m^2] + \lambda) + \alpha\kappa\lambda\Delta\psi^2\right)^2 + \kappa^2\Delta\psi^4(\mathbf{q}\cdot\mathbf{v})^2} \tag{5.44}$$

For small q we find

$$H_s(\mathbf{q}) = \sigma m^2 + \sigma q^2(1 + \frac{v^2\cos^2(\theta)}{\alpha^2\lambda\kappa}), \tag{5.45}$$

where θ is the angle between the wave vector $\mathbf{q}$ and the direction of the driving. This thus gives a direction dependent surface tension

$$\sigma_s(\theta) = \sigma(1 + \frac{v^2\cos^2(\theta)}{v_0^2}) \tag{5.46}$$

where we have introduced the intrinsic velocity $v_0 = \sqrt{\alpha^2 \lambda \kappa}$ which depends on the microscopic *dynamical* quantity α associated with the model A dynamics of the field ϕ, as well as the microscopic static quantities κ (which generates the surface tension) and λ the coupling between the field ψ and ϕ. This appearance of dynamical and static quantities that are otherwise hidden in equal time correlation functions in equilibrium is already implicit in the works of Onsager [114] where it is used to compute the conductivity of Brownian electrolytes and the explicit expressions were derived using stochastic density functional theory in [121]. We also note that the universal thermal Casimir effect between model Brownian electrolyte systems driven by an electric field exhibits similar features, developing a dependency on both additional static and dynamical variables with respect to the equilibrium case [127]

However for this small q expansion we see that the microscopic quantities D, the diffusion constant of the field ϕ, and the order parameter jump $\Delta\psi$ do not appear.

From the above, we see that in the direction of the driving the surface tension increases and the fluctuations of the surface are thus suppressed. We may also write

$$H_s(\mathbf{q}) = \sigma_s(\theta)[q^2 + m_e^2(\theta)], \tag{5.47}$$

with

$$m_s^2(\theta) = \frac{m^2}{1 + \frac{v^2 \cos^2(\theta)}{v_0^2}}, \tag{5.48}$$

this corresponds to a correlation length

$$\xi_s = \xi_{eq}\sqrt{1 + \frac{v^2 \cos^2(\theta)}{v_0^2}}, \tag{5.49}$$

and we see that it is increased in the direction of the driving.

As we have just remarked that the above results appear to be independent of the order parameter jump $\Delta\psi$ and the diffusion constant D, however the next order correction to H_s for small q is given by

$$H_s(\mathbf{q}) = \sigma_s(\theta)[q^2 + m_e^2(\theta)] - \frac{4Dq\sigma^2(\lambda + \kappa m^2)(\mathbf{q}\cdot\mathbf{v})^2}{\alpha^3 \kappa^2 \lambda^2 \Delta\psi^2}, \tag{5.50}$$

and so the small $\mathbf{q}$ expansion breaks down at $\Delta\psi = 0$, indeed one can see that the system has exactly the equilibrium correlation function when $\Delta\psi = 0$.

In the limit of large q we see that the effective Hamiltonian is given, to leading order, by the original equilibrium Hamiltonian and so the out of equilibrium driving has no effect on the most energetic modes of the system.

The results here predict that for unconfined surfaces the long range height fluctuations are described by an isotropic form of capillary wave theory with an anisotropic surface tension which is largest in the direction of driving. Numerical simulations of driven lattice gases in two dimensions [125] show a more drastic change upon driving and find $C_s(q) \sim 1/q^{.66}$ and thus a strong deviation from capillary wave theory.

5.1.3 A model of active interfaces

We can apply the results derived in the previous section to analyse a simple model for surfaces formed between two phases of active colloids. Activity is modelled by assuming that the colloidal field ψ has a temperature different to that of the solvent field ϕ. This models the effect that activity leads to enhanced colloidal diffusivity over and above the Brownian motion of particles due to thermal fluctuations [113].

In the absence of any driving the dynamical equations for the field ψ and ϕ become

$$\frac{\partial \psi(\mathbf{x}, t)}{\partial t} = D\nabla^2 \frac{\delta H}{\delta \psi(\mathbf{x})} + \sqrt{2DT_1} \nabla \cdot \boldsymbol{\eta}_1(\mathbf{x}, t) \qquad (5.51)$$

$$\frac{\partial \phi(\mathbf{x}, t)}{\partial t} = -\alpha \frac{\delta H}{\delta \phi(\mathbf{x})} + \sqrt{2\alpha T_2} \eta_2(\mathbf{x}, t). \qquad (5.52)$$

Following the same arguments as above we find that

$$\hat{C}(\mathbf{q}, \omega) = 2D \frac{\left[T_1 \frac{\Delta \psi^2}{2q} (\omega^2 + \alpha^2 \lambda^2) + T_2 \frac{\sigma \alpha D \lambda^2}{\kappa} \right]}{\left| i\omega[\frac{\alpha \lambda \Delta \psi^2}{2q} + \frac{\lambda \sigma D}{\kappa} + D\sigma(q^2 + m^2)] + [\alpha \lambda D\sigma(q^2 + m^2) - \frac{\Delta \psi^2}{2q} \omega^2] \right|^2}. \qquad (5.53)$$

The equal time steady state height fluctuations thus have correlation function

$$\tilde{C}_s(q) = \frac{T_1}{\sigma(q^2 + m^2)} \left[1 - (1 - \frac{T_2}{T_1}) \frac{\lambda \sigma}{\kappa} \frac{1}{\frac{\alpha \lambda \Delta \psi^2}{2Dq} + \frac{\lambda \sigma}{\kappa} + \sigma(q^2 + m^2)} \right]. \qquad (5.54)$$

We see, again, that the inclusion of a non-equilibrium driving changes the statistics of height fluctuations and leads to a steady state that depends on both dynamical variables D and α as well as static ones $\Delta\psi$, λ and κ that remain hidden in the equilibrium case. This phenomenon is again seen in the behavior of the universal thermal Casimir force between Brownian conductors held at different temperatures [128].

If we assume strong activity we can take the limit $T_1 \gg T_2$, in this case we find

$$\tilde{C}_s(q) = \frac{T_1}{\sigma(q^2 + m^2)} \frac{\frac{\alpha \lambda \Delta \psi^2}{2Dq} + \sigma(q^2 + m^2)}{\frac{\alpha \lambda \Delta \psi^2}{2Dq} + \frac{\lambda \sigma}{\kappa} + \sigma(q^2 + m^2)}. \qquad (5.55)$$

Interpreted in terms of an effective Hamiltonian for an equilibrium system at the temperature T_1 the above gives

$$H_s(q) = \sigma(q^2 + m^2) \left[1 + \frac{\lambda \sigma}{\kappa} \frac{q}{\frac{\alpha \lambda \Delta \psi^2}{2D} + q\sigma(q^2 + m^2)} \right]. \qquad (5.56)$$

psi In the case of an unconfined interface (where there is no gravitational effect on the surface fluctuations) *i.e.* $m = 0$ we see that for small q

$$H_s(q) \approx \sigma q^2 + \frac{2D\sigma^2}{\kappa \alpha \Delta \psi^2} q^3. \qquad (5.57)$$

We see that the effective surface tension is not modified but a reduction of fluctuations due to the presence of the term in q^3 arises. As in the case of a driven system, we see that the large q behavior of the effective Hamiltonian is given by the equilibrium case where $T = T_1 = T_2$.

In the case where the interface is confined, we see that for small q one obtains

$$H_s(q) \approx \sigma m^2 \left[1 + \frac{2D\sigma}{\kappa \alpha \Delta \psi^2} q \right], \qquad (5.58)$$

and thus at the largest length scales of the problem there is a qualitative departure from capillary wave behavior induced by activity, and the correlation length of height fluctuations at the largest length scales is given by

$$\xi_a = \frac{2D\sigma}{\kappa \alpha \Delta \psi^2}. \qquad (5.59)$$

The above result should be compared with that obtained in [124] for systems with anisotropic thermal white noise, which breaks detailed balance and mimics random driving of the system parallel to the interface; for free interfaces it was found that $C_s(q) \sim 1/q$.

5.1.4 Conclusion

We have presented a model to analyse the effect of uniform driving on the dynamics of the interface in a two phase system. In order to generate a non-equilibrium state a second *hidden* order parameter was introduced. This models the behaviour of a local or solvent degree of freedom which is not influenced by the driving field. In this way, we obtain out of equilibrium interface fluctuations which are described by Gaussian statistics as found in the experimental study of [19]. The agreement with this experimental study also extends to qualitative agreement with the increase of the effective surface tension in the direction of driving and also an increase in the correlation length of the height fluctuations with respect to a non-driven equilibrium interface. However, we note that numerical simulations of a sheared Ising interface [72, 104] also reveal a reduction of interface fluctuations but the lateral correlation length is found to be reduced.

The basic idea underlying this study would be interesting to apply to a number of possible variants of this model, for instance both the dynamics of the main field ϕ and the solvent field φ could be varied. To make a direct link with driven colloidal interfaces one should study model H type dynamics for the main field ϕ and other variants for the dynamics of the solvent field φ could also be considered.

As mentioned above, in lattice based models driving induces non-equilibrium states even in the simple Ising lattice gas. A model analogous to that studied here can be formulated in a lattice based systems using the Hamiltonian

$$H = -J \sum_{(ij)} S_i S_j (1 + \sigma_{(ij)}), \tag{5.60}$$

where $S_i = \pm 1$ are Ising spins at the lattice sites i, and $\sigma_{(ij)} = \pm 1$ are Ising like dynamical solvent variables associated with the lattice links (ij). The static partition function is given by

$$Z = \text{Tr}_{\sigma_{ij}, S_i} \exp \left[\beta J \sum_{(ij)} S_i S_j (1 + \sigma_{(ij)}) \right], \tag{5.61}$$

and the trace over the solvent variables can be trivially carried out to give

$$Z = \text{Tr}_{S_i} \left(\exp \left[\beta J \sum_{(ij)} S_i S_j \right] \prod_{(ij)} 2 \cosh(\beta J S_i S_j) \right) = [2 \cosh(\beta J)]^L \text{Tr}_{S_i} \exp(\beta J \sum_{(ij)} S_i S_j), \tag{5.62}$$

where L is the number of links on the lattice of the model. We thus see that the underlying effective static model is precisely the zero field Ising model.

This model can then be driven in a number of ways, for instance using conserved Kawasaki dynamics for the Ising spins to model diffusive dynamics in the presence of a uniform driving field parallel to the surface between the two phases at a temperature below the ferromagnetic ordering temperature T_c. The dynamics of the Ising spins on the lattice links can be given by non-conservative single spin flip, for instance Glauber, dynamics to keep the analogy with the continuum model discussed in the paper but diffusive dynamics or indeed a mixture of diffusive and non-conserved dynamics could be implemented. It would be interesting to see to what extent this modification of the driven lattice gas model affects the non-equilibrium driven states that arise.

It is also clear that this lattice model can be used to simulate the effect of activity where the Ising spins S_1 corresponding to the colloid field undergo Kawasaki dynamics at the temperature T_1 where as the link variables $\sigma_{(ij)}$ undergo single spin flip non-conserved dynamics at the temperature T_2.

5.2 Driven SOS model

In the previous section, coupling of a model B field with a model A one was done in order to break the Galilean transformation, leading to out-of-equilibrium steady state. In lattice based numerical simulations, the invariance is broken because of the discrete-time nature of the algorithm. In a SOS model

under Kawasaki dynamics, the implementation of a constant driving flow is as follows. From the configuration C we choose a configuration C′ as explained is Sec 2.2.2, meaning we chose a random site i and a nearest neighboor $i \pm 1$ to which give one of its particles. Under a flow, the difference of energy between both states is

$$\Delta E_d = \Delta E_{eq} \pm v \tag{5.63}$$

where v is the intensity of the drive, and the sign depends on the direction of the flow . For example, if the flow goes to the right, then every configuration which moves a particle to the right will have an additional energy $+v$, while if the particle goes against the flow, it will have an additional energy $-v$.

Implementing a shear $v|L/2 - y|$ as in Fig 1.10 is tricky, because it requires to know the height of the particle, and thus have access to bulk information. In SOS models, we consider that only the particle at the interface moves and changes height accordingly to the interface's height of the neighbooring site. The vertical movement of the particle, couple to the horizontal one, is what makes the SOS model different to the Ising one, and physical arguments forbids the use h_i, h_{i+1} or even the average $\frac{h_i + h_{i+1}}{2}$ as the shear contribution might be zero depending of the configuration, even though it should always be present.

Under periodic boundary conditions, the direction of the flow should not alter the steady state. The average total energy has thus to be an even function with respect to the drive v, ie

$$\langle E(v) \rangle = \langle E(-v) \rangle \tag{5.64}$$

and same goes for the surface tension $\sigma(v)$. From Eq (1.41) and (1.43), we have the surface tension

$$\sigma(v) = \int_{-\infty}^{\infty} dz J \left(\frac{d \tanh\left(\frac{z}{\xi_\perp(v)}\right)}{dz} \right)^2 = \int_{-\infty}^{\infty} dz J \frac{1}{\cosh^4(\frac{x}{\xi_\perp(v)}) \xi_\perp^2} \tag{5.65}$$

where $\xi_\perp(v)$ is the interfacial correlation length. This interface width has the same qualitative behaviour as the interface width $\langle w \rangle = \sqrt{\langle h^2 \rangle - \langle h \rangle^2}$.

In Fig 5.2 we show the interface width and the surface tension with respect to the drive computed through Kawasaki dynamics. The first thing we notice is that the interface width increases with the imposed driving in an almost linear way, as does the mean height of wind generated waves with respect to the wind surface velocity [129]. The second thing we notice is that there are a change of regime at $v = 2J$ and $v = 4J$, with a net change in the derivative. The change of energy ΔE has values in $[-4, -2, 0, 2, 4]$, so we see that there are three regimes : the weak driving regime for $v < 2J$, the middle regime for $2J < v < 4J$ where some moves with adding energy to the system are always accepted, and the strong driving regime for $v > 4J$ where all moves adding energy are accepted, ending with a saturation when the bond energy becomes negligible with respect to the driving.

While this result is in direct contradiction with Eq. (3.1) in the model C and Ising simulations [72, 104] where the surface tension increases with v, we provide no formal physical theory explaining why there is a diference between those two interface models.
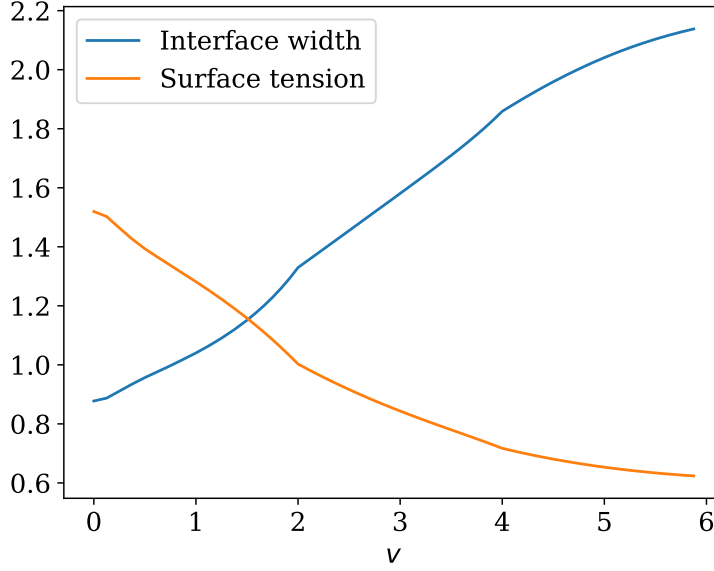
Figure 5.2: Interface width $w = \sqrt{\langle h^2 \rangle - \langle h \rangle^2}$ and surface tension σ computed from the integral (5.65) with respect to the drive v, with $L' = 256$, $L = 200$, $\langle h \rangle = 4.5$, and $\beta = J = 1$ for $5 \cdot 10^7$ MC steps.

5.3 Driven POP model

5.3.1 Conserved diffusive dynamics

We now study a system of two particle types A and B, where one is a a solvent and the other one a particle in suspension, for example. Assuming Brownian dynamics for the particles, the stochastic density functional equations for the continuum fields n_A and n_B are given by

$$\frac{\partial n_A(x)}{\partial t} = \frac{\partial}{\partial x} \beta D_A n_A(x) \frac{\partial}{\partial x} \frac{\delta H}{\delta n_A(x)} + \frac{\partial}{\partial x} \sqrt{2 D_A n_A(x)} \eta_A(x, t) \tag{5.66}$$

and

$$\frac{\partial n_B(x)}{\partial t} = \frac{\partial}{\partial x} \beta D_B n_B(x) \frac{\partial}{\partial x} \frac{\delta H}{\delta n_B(x)} + \frac{\partial}{\partial x} \sqrt{2 D_B n_B(x)} \eta_B(x, t) \tag{5.67}$$

where D_A and D_B are the diffusion constants of the particles. The noise terms are independent , zero mean, spatiotemporal Gaussian white noise with

$$\langle \eta_A(x, t) \eta_A(x', t') \rangle = \langle \eta_B(x, t) \eta_B(x', t') \rangle = \delta(x - x') \delta(t - t'). \tag{5.68}$$

As we are interested in what happens when one of the species is driven, we add a term

$$H_D = -\int dx x f n_A(x) \tag{5.69}$$

to the Hamiltonian, this corresponds to a force which pushes the particles of type A to the right. We also assume periodic boundary conditions, and thus a current will exist in the resulting steady state. This introduces term in the equation for $n_A(x)$ which becomes

$$\frac{\partial n_A(x)}{\partial t} + \frac{\partial}{\partial x} D_A \beta f n_A(x) = \frac{\partial}{\partial x} \beta D_A n_A(x) \frac{\partial}{\partial x} \frac{\delta H}{\delta n_A(x)} + \frac{\partial}{\partial x} \sqrt{2 D_A n_A(x)} \eta_A(x, t). \tag{5.70}$$

It is important to note that in the absence of the particles of type B, the resulting equation for the field $n_A(x, t)$ can be rendered independent of the force f via the Galilean transformation

$$n(x, t) = n(x - vt, t) \tag{5.71}$$

where $v = D_A \beta f$ is the induced drift on the particles of type A. Note that the Galilean invariance can also be broken if the force f acts on both particle types but the diffusion coefficients D_A and D_B are different.

We now expand the deterministic part of the two equations to first order in the density fluctuations about its mean value and the noise terms to zeroth order. This approximation respects detailed balance for the effective quadratic Hamiltonian and has been used with accuracy in a wide variety of contexts. The resulting dynamics of of a model B and Fourier transforming in space gives

$$\frac{\partial \tilde{\Phi}(k, t)}{\partial t} = -\beta \tilde{A}(k)\Phi(k, t) + \tilde{\eta}(k, t), \tag{5.72}$$

where

$$\Phi(k, t) = \begin{pmatrix} \tilde{\phi}_A(k, t) \\ \tilde{\phi}_B(k, t) \end{pmatrix} \tag{5.73}$$

The noise correlation function is given by

$$\langle \tilde{\eta}^T(k, t)\tilde{\eta}(k', t') \rangle = 4\pi \tilde{R}(k)\delta(t - t')\delta(k + k') \tag{5.74}$$

where

$$\tilde{R}(k) = 2 \begin{pmatrix} D_A \overline{n}_A k^2 & 0 \\ 0 & D_B \overline{n}_B k^2 \end{pmatrix}, \tag{5.75}$$

and

$$\tilde{A}(k) = \sigma \begin{pmatrix} D_A \overline{n}_A k^2(k^2 + m_A^2) - i\frac{D_A k f}{\sigma} & D_A \overline{n}_A k^4 \\ D_B \overline{n}_B k^4 & D_B \overline{n}_B k^2(k^2 + m_B^2) \end{pmatrix} \tag{5.76}$$

The Fourier transform steady state correlation function matrix defined by

$$\langle \tilde{\Phi}^T(k)\tilde{\Phi}(k') \rangle = 2\pi\delta(k + k')\tilde{C}(k) \tag{5.77}$$

is then given by the solution to the Lyapounov equation

$$\tilde{A}(k)\tilde{C}(k) + \tilde{C}(k)\tilde{A}^T(-k) = 2T\tilde{R}(k) \tag{5.78}$$

Solving this we find that

$$\tilde{C}_{hh}(k) = \frac{T}{\sigma} \frac{k^2(m_A^2 + m_B^2)(D_A \overline{n}_A[k^2 + m_A^2] + D_B \overline{n}_B[k^2 + m_B^2])^2 + \frac{f^2}{\sigma^2}D_A^2(2k^2 + m_A^2 + m_B^2)}{k^2(D_A \overline{n}_A[k^2 + m_A^2] + D_B \overline{n}_B[k^2 + m_B^2])^2(m_A^2 m_B^2 + k^2(m_A^2 + m_B^2)) + \frac{f^2}{\sigma^2}D_A^2(k^2 + m_A^2)(k^2 + m_B^2)}. \tag{5.79}$$

In the equilibrium or non-driven system where $f = 0$ the above formula yields the static result Eq. (4.25). Of particular interest is the strong driving limit where we find that as $f \to \infty$ the result

$$\tilde{C}_{hh}(k) = \frac{T}{\sigma} \left[\frac{1}{k^2 + m_A^2} + \frac{1}{k^2 + m_B^2} \right] \tag{5.80}$$

The effect of strong driving is to decouple the fluctuations of n_A and n_B and we see that the total height fluctuation is that of the sum two independent interfaces. The height variance is then given by

$$\langle h^2 \rangle_s = \frac{T}{2\sigma m_d} \tag{5.81}$$

where

$$m_d = \frac{m_A m_B}{m_A + m_B} \tag{5.82}$$

From this we find that

$$\frac{\langle h^2 \rangle_s}{\langle h^2 \rangle_{eq}} = \frac{m_A + m_B}{\sqrt{m_A^2 + m_B^2}}. \tag{5.83}$$

We also see that, as m_A and m_B are positive, the fluctuations in limit of infinite driving are always larger than in the equilibrium state.

Imagine now that the B particles constitute the bottom layer and that $D_B \ll D_A$ this mimics the solid on solid dynamics where only the top layer of the particles participate in the dynamics. This gives

$$\tilde{C}_{hh}(k) = \frac{T}{\sigma} \frac{k^2(m_A^2 + m_B^2)(\overline{n}_A[k^2 + m_A^2])^2 + \frac{f^2}{\sigma^2}(2k^2 + m_A^2 + m_B^2)}{k^2(\overline{n}_A[k^2 + m_A^2])^2(m_A^2 m_B^2 + k^2(m_A^2 + m_B^2)) + \frac{f^2}{\sigma^2}(k^2 + m_A^2)(k^2 + m_B^2)}. \tag{5.84}$$

Assuming the A layer is thinner that the B layer so $m_B \ll m_A$ gives

$$\tilde{C}_{hh}(k) = \frac{T}{\sigma} \frac{k^2 m_A^2(\overline{n}_A[k^2 + m_A^2])^2 + \frac{f^2}{\sigma^2}(2k^2 + m_A^2)}{k^2(\overline{n}_A[k^2 + m_A^2])^2(m_A^2 m_B^2 + k^2 m_A^2) + \frac{f^2}{\sigma^2}(k^2 + m_A^2)(k^2 + m_B^2)}. \tag{5.85}$$

which simplifies to give

$$\tilde{C}_{hh}(k) \quad = \quad \frac{T}{\sigma} \frac{k^2 m_A^2(\overline{n}_A[k^2 + m_A^2])^2 + \frac{f^2}{\sigma^2}(2k^2 + m_A^2)}{(k^2 + m_A^2)(k^2 + m_B^2)[(n_A^2 m_A^2 k^2(k^2 + m_A^2) + \frac{f^2}{\sigma^2}]} \tag{5.86}$$

$$\tilde{C}_{hh}(k) \quad = \quad \frac{T}{\sigma} \frac{1}{k^2 + m_B^2} + \frac{T}{\sigma} \frac{\frac{f^2}{\sigma^2}k^2}{(k^2 + m_A^2)(k^2 + m_B^2)[(n_A^2 m_A^2 k^2(k^2 + m_A^2) + \frac{f^2}{\sigma^2}]} \tag{5.87}$$

$$= \quad \frac{T}{\sigma} \left[\frac{1}{(k^2 + m_B^2)} + \frac{f^2}{\sigma^2 \overline{n}_A^2 m_A^2} \frac{k^2}{(k^2 + m_A^2)(k^2 + m_B^2)(k^4 + m_A^2 k^2 + \frac{f^2}{\sigma^2 n_A^2 m_A^2})} \right] \tag{5.88}$$

The height fluctuations are then given by

$$\langle h^2 \rangle = \frac{T}{2\sigma m_B} + \frac{T}{2\sigma} \frac{f^2}{\sigma^2 \overline{n}_A^2 m_A^2} \frac{m_A + m_B + m_+ + m_-}{(m_A + m_B)(m_+ + m_B)(m_- + m_B)(m_A + m_+)(m_A + m_+)(m_+ + m_-)}, \tag{5.89}$$

where

$$m_{\pm} = \sqrt{\frac{m_A^2 \pm \sqrt{m_A^4 - \frac{4f^2}{\sigma^2 n_A^2 m_A^2}}}{2}} \tag{5.90}$$

5.3.2 Non conserved dynamics

We now consider the case where the particles of type B are in contact with a reservoir of the same particles in a vapour phase. To model this we modify the dynamics of the B phase by introducing a component of non-conserved dynamics for these particles

$$\frac{\partial n_B(x)}{\partial t} = \frac{\partial}{\partial x} \beta D_B n_B(x) \frac{\partial}{\partial x} \frac{\delta H}{\delta n_B(x)} + \frac{\partial}{\partial x} \sqrt{2D_B n_B(x)} \eta_B(x, t) - K_B \beta \frac{\delta H}{\delta n_B(x)} + \sqrt{2K_B} \eta_B'(x, t), \tag{5.91}$$

here if $\eta'_\mathrm{B}(x,t)$ is a new spatio-temporal white noise independent of the others, the undriven system obeys detailed balance. Now the average value of the n_B is determined by taking the average in the steady state. As the system is invariant under translation, the average of the first diffusive term on the right-hand-side is zero and so we find

$$\langle\frac{\delta\mathrm{H}}{\delta n_\mathrm{B}(x)}\rangle = 0, \tag{5.92}$$

where the averaging is over the system in the steady state. Again invariance by translation in space can be applied to write

$$\langle\frac{\partial\mathrm{V}(n_\mathrm{A},n_\mathrm{B})}{\partial n_\mathrm{A}}\rangle = 0 \tag{5.93}$$

Here we have $\mathrm{V}(n_\mathrm{A},n_\mathrm{B}) = \mathrm{U}(n_\mathrm{A}) + \mathrm{U}(n_\mathrm{B})$ where $\mathrm{U}(x) = Tx(\ln(x)-1) - \mu x$ and so expanding about $\overline{n}_\mathrm{A}$ we find to second order that

$$\langle\mathrm{U}'(\overline{n}_\mathrm{A}) + \mathrm{U}''(\overline{n}_\mathrm{A})\phi_\mathrm{A} + \frac{1}{2}\mathrm{U}'''(\overline{n}_\mathrm{A})\phi_\mathrm{A}^2\rangle = 0, \tag{5.94}$$

the equation to first order gives

$$\mathrm{U}'(\overline{n}_\mathrm{A}) = 0 \tag{5.95}$$

which gives $\overline{n}_\mathrm{A} = n_m$ where n_m is the value for which U attains its minimum. However if we keep the next order term we find

$$\mathrm{U}'(\overline{n}_\mathrm{A}) + \frac{1}{2}\mathrm{U}'''(\overline{n}_\mathrm{A})\langle\phi_\mathrm{A}^2\rangle = 0. \tag{5.96}$$

If the renormalization of the average value of $\overline{n}_\mathrm{A}$ is assumed to be small we can write

$$\overline{n}_\mathrm{A} = n_m + \delta, \tag{5.97}$$

which gives

$$\delta = -\frac{1}{2}\frac{\mathrm{U}'''(n_m)}{\mathrm{U}''(n_m)}\langle\phi_\mathrm{A}^2\rangle. \tag{5.98}$$

For the (entropic) potential in question here we have

$$\delta = \frac{1}{2n_m}\langle\phi_\mathrm{A}^2\rangle, \tag{5.99}$$

we thus see that the average height of the interface is increased due to fluctuations. The non-equilibrium fluctuations are stronger an thus the height increases under driving.

5.4 Conclusions

Bibliography

[1] L. Landau and E. Lifchitz. *Physique théorique - T9 Physique Statistique*. Éditions Mir Moscou. 1990. xi, 4

[2] Nigel Goldenfeld. *Lectures on Phase Transitions and the Renormalization Group*. CRC Press, 1 edition, March 2018. xi, 15, 64

[3] Andrea Gambassi. The Casimir effect: From quantum to critical fluctuations. *Journal of Physics: Conference Series*, 161:012037, April 2009. xi, 39, 42, 60

[4] Martin Niss. History of the Lenz-Ising Model 1920–1950: From Ferromagnetic to Cooperative Phenomena. *Archive for History of Exact Sciences*, 59(3):267–318, March 2005. xi, 14, 24, 61

[5] D. B. Abraham and A. Martin-Löf. The transfer matrix for a pure phase in the two-dimensional Ising model. *Communications in Mathematical Physics*, 32(3):245–268, September 1973. xi, 16, 20, 24

[6] G. H. Gilmer and P. Bennema. Simulation of Crystal Growth with Surface Diffusion. *Journal of Applied Physics*, 43(4):1347–1360, April 1972. xi, 18, 24, 61, 67

[7] D. J. Amit and Victor Martin Mayor. *Field theory, the renormalization group, and critical phenomena: graphs to computers*. World Scientific, Singapore ; New Jersey, 3rd ed edition, 2005. xi, 40

[8] Takeo Matsubara. A New Approach to Quantum-Statistical Mechanics. *Progress of Theoretical Physics*, 14(4):351–378, October 1955. xi, 39, 42, 60

[9] Alan J. Bray, Andrea Cavagna, and Rui D. M. Travasso. Interface fluctuations under shear. *Physical Review E*, 64(1):012102, June 2001. xii, xiii, 9, 22, 70

[10] M. E. J. Newman and G. T. Barkema. *Monte Carlo Methods in Statistical Physics*. Oxford University Press, Oxford, New York, February 1999. xii, 24, 25, 27, 34, 61, 67

[11] O. Vasilyev, A. Gambassi, A. Maciołek, and S. Dietrich. Universal scaling functions of critical Casimir forces obtained by Monte Carlo simulations. *Physical Review E*, 79(4), April 2009. xii, 31, 34

[12] David Lopes Cardozo, Hugo Jacquin, and Peter C. W. Holdsworth. Critical Casimir forces in a magnetic system: An experimental protocol. *Physical Review B*, 90(18), November 2014. xii, 32, 33, 34, 60

[13] Kimball A. Milton. *The Casimir effect: Physical manifestation of zero-point energy*. World Scientific Pub, 1st edition, 2001. xii

[14] H. B. G. Casimir. On the attraction between two perfectly conducting plates. *Royal Netherlands Academy of Arts and Sciences,*, 51(7):793–498, 1948. xii, 35, 37, 60

[15] I M Lifshits and A M Kosevich. On the theory of magnetic susceptibility of metals at low temperatures. *Zh. Eksp. Teor. Fiz.*, 53(6):730–742, 1955. xii, 38, 60

[16] Vladimir Privman. Finite-Size Properties of the Angle-Dependent Surface Tension of Rough Interfaces. *Physical Review Letters*, 61(2):4, 1988. xii, 42, 45, 60

[17] David S Dean, Paul Gersberg, and Peter C W Holdsworth. The effect of driving on model C interfaces. *Journal of Statistical Mechanics: Theory and Experiment*, 2020(3):033206, March 2020. xiii, 69

[18] P. C. Hohenberg and B. I. Halperin. Theory of dynamic critical phenomena. *Reviews of Modern Physics*, 49(3):435–479, July 1977. xiii, 1, 6, 24, 66, 70

[19] Didi Derks, Dirk G. A. L. Aarts, Daniel Bonn, Henk N. W. Lekkerkerker, and Arnout Imhof. Suppression of Thermally Excited Capillary Waves by Shear Flow. *Physical Review Letters*, 97(3), July 2006. xiii, 22, 23, 24, 69, 70, 78

[20] Mésocentre de Calcul Intensif Aquitain. https://redmine.mcia.fr/projects/mcia. xiii, 25

[21] Paul Gersberg. Github with all my programs, 2020. https://github.com/Bulbille/Curta. xiii, 25

[22] A. J. Bray. Theory of phase-ordering kinetics. *Advances in Physics*, 43(3):357–459, June 1994. 1, 24

[23] Lars Onsager. Crystal Statistics. I. A Two-Dimensional Model with an Order-Disorder Transition. *Physical Review*, 65(3-4):117–149, February 1944. 2, 15

[24] J. A. Tuszyński, R. Paul, and R. Chatterjee. Exact solutions to the time-dependent Landau-Ginzburg model of phase transitions. *Physical Review B*, 29(1):380–386, January 1984. 6

[25] John W Cahn and John E Hilliard. Free Energy of a Nonuniform System. I. Interfacial Free Energy. *The Journal of Chemical Physics*, 28(2):11, February 1958. 6, 7, 24

[26] Y. Hennequin, D. G. A. L. Aarts, J. H. van der Wiel, G. Wegdam, J. Eggers, H. N. W. Lekkerkerker, and Daniel Bonn. Drop Formation by Thermal Fluctuations at an Ultralow Surface Tension. *Physical Review Letters*, 97(24), December 2006. 7

[27] Javier Atencia and David J. Beebe. Controlled microfluidic interfaces. *Nature*, 437(7059):648–655, September 2005. 7

[28] H. W. Diehl, D. M. Kroll, and H. Wagner. The interface in a Ginsburg-Landau-Wilson model: Derivation of the drumhead model in the low-temperature limit. *Zeitschrift fur Physik B Condensed Matter and Quanta*, 36(4):329–333, December 1980. 8

[29] Alan J. Bray, Andrea Cavagna, and Rui D. M. Travasso. Interface fluctuations, Burgers equations, and coarsening under shear. *Physical Review E*, 65(1), December 2001. 9, 22, 70

[30] S. F. Edwards and D. R. Wilkinson. The Surface Statistics of a Granular Aggregate. *Proceedings of the Royal Society of London. Series A, Mathematical and Physical Sciences*, 381(1780):17–31, 1982. 11, 24, 61

[31] Timothy Halpin-Healy and Yi-Cheng Zhang. Kinetic roughening phenomena, stochastic growth, directed polymers and all that. Aspects of multidisciplinary statistical mechanics. *Physics Reports*, 254(4-6):215–414, March 1995. 11, 61

[32] Raja Paul, Sanjay Puri, and Heiko Rieger. Domain growth in Ising systems with quenched disorder. *Physical Review E*, 71(6), June 2005. 11

[33] David A. Huse. Corrections to late-stage behavior in spinodal decomposition: Lifshitz-Slyozov scaling and Monte Carlo simulations. *Physical Review B*, 34(11):7845–7850, December 1986. 13

[34] Martin Niss. History of the Lenz–Ising Model 1950–1965: from irrelevance to relevance. *Archive for History of Exact Sciences*, 63(3):243, May 2009. 14, 24, 61

[35] Rajan Gupta, Jerry DeLapp, George G. Batrouni, Geoffrey C. Fox, Clive F. Baillie, and John Apostolakis. Phase Transition in the 2 D XY Model. *Physical Review Letters*, 61(17):1996–1999, October 1988. 14

[36] Michel Le Bellac, Fabrice Mortessagne, and G George Batrouni. *Equilibrium and Non-Equilibrium Statistical Thermodynamics*. Cambridge University Press, 2004. 14, 24

[37] Michael Aizenman. Proof of the Triviality of ϕ d 4 Field Theory and Some Mean-Field Features of Ising Models for d > 4. *Physical Review Letters*, 47(1):1–4, July 1981. 14

[38] L.J. de Jongh and A.R. Miedema. Experiments on simple magnetic model systems. *Advances in Physics*, 23(1):1–260, January 1974. 15

[39] W.P. Wold. The Ising Model and Real Magnetic Materials. *Brazilian Journal of Physics*, 30(4):794–810, December 2000. 15

[40] Hironobu Ikeda and Kinshiro Hirakawa. Neutron scattering study of two-dimensional Ising nature of K2CoF4. *Solid Sate Communications*, 14:529–532, November 1973. 15

[41] Jiirg Frohlich. On the triviality of $\lambda\varphi4$ theories and the approach to the critical point in D>4 dimensions. *Nuclear Physics B*, 200:281–296, August 1981. 15

[42] A L Talapov and H W J Blöte. The magnetization of the 3D Ising model. *Journal of Physics A: Mathematical and General*, 29(17):5727–5733, September 1996. 15

[43] Tobias Preis, Peter Virnau, Wolfgang Paul, and Johannes J. Schneider. GPU accelerated Monte Carlo simulation of the 2D and 3D Ising model. *Journal of Computational Physics*, 228(12):4468–4477, July 2009. 15

[44] J. Stecki, A. Maciol/ek, and K. Olaussen. Magnetization profiles of the planar fluctuating interface in a d=2 Ising strip. *Physical Review B*, 49(2):1092–1103, January 1994. 16

[45] Howard L. Richards, M. A. Novotny, and Per Arne Rikvold. Numerical transfer-matrix study of surface-tension anisotropy in Ising models on square and cubic lattices. *Physical Review B*, 48(19):14584–14598, November 1993. 16

[46] D. B. Abraham and P. Reed. Interface profile of the Ising ferromagnet in two dimensions. *Communications in Mathematical Physics*, 49(1):35–46, February 1976. 16, 61

[47] Robert H. Swendsen. Roughening transition in the solid-on-solid model. *Physical Review B*, 15(2):689–692, January 1977. 17, 61

[48] J. M. J. van Leeuwen and H. J. Hilhorst. Pinning of a rough interface by an external potential. *Physica A: Statistical Mechanics and its Applications*, 107(2):319–329, June 1981. 17

[49] M Elwenspoek and J P van der Eerden. Kinetic roughening and step free energy in the solid-on-solid model and on naphthalene crystals. *Journal of Physics A: Mathematical and General*, 20(3):669–678, February 1987. 18

[50] M. R. Wilby, D. D. Vvedensky, and A. Zangwill. Scaling in a solid-on-solid model of epitaxial growth. *Physical Review B*, 46(19):12896–12898, November 1992. 18, 61

[51] David Boal. Mechanics of the Cell: Second edition. page 624, 2012. 18

[52] G Gompper and D. M Kroll. Steric Interactions in Multimembrane Systems: A Monte Carlo Study. *Europhysics Letters (EPL)*, 9(1):59–64, May 1989. 18

[53] Michael E Fisher. Walks, walls, wetting, and melting. *Journal of Statistical Physics*, 34(5/6):63, October 1983. 18

[54] V. Privman and N. M. Švrakić. Transfer-Matrix Spectrum for Systems with Interfaces. *Physical Review Letters*, 62(6):633–636, February 1989. 18

[55] Yup Kim, D. K. Park, and Jin Min Kim. Conserved growth in a restricted solid-on-solid model. *Journal of Physics A: Mathematical and General*, 27(15):L533, 1994. 18

[56] I. Vaysburd. Critical RSOS models in external fields. *Nuclear Physics B*, 446(3):387–404, July 1995. 18

[57] H. J. F. Knops. Exact Relation between the Solid-on-Solid Model and the XY Model. *Physical Review Letters*, 39(12):766–769, September 1977. 18

[58] Grégory Schehr and Satya N. Majumdar. Universal asymptotic statistics of maximal relative height in one-dimensional solid-on-solid models. *Physical Review E*, 73(5):056103, May 2006. 18

[59] Robert H. Swendsen. Monte Carlo studies of the interface roughening transition. *Physical Review B*, 15(11):5421–5431, June 1977. 18

[60] Aleksander L. Owczarek and Thomas Prellberg. Exact solution of the discrete (1+1)-dimensional SOS model with field and surface interactions. *Journal of Statistical Physics*, 70(5-6):1175–1194, March 1993. 18

[61] Satya N. Majumdar and Alain Comtet. Airy Distribution Function: From the Area Under a Brownian Excursion to the Maximal Height of Fluctuating Interfaces. *Journal of Statistical Physics*, 119(3-4):777–826, May 2005. 18

[62] Martin Siegert and Michael Plischke. Scaling behavior of driven solid-on-solid models with diffusion. *Journal de Physique I*, 3(6):1371–1376, June 1993. 20, 61

[63] Paul A Pearce and Katherine A Seaton. Exact solution of cyclic solid-on-solid lattice models. *Annals of Physics*, 193(2):326–366, August 1989. 20

[64] A. Girot, J. Petit, R. Saiseau, T. Guérin, H. Chraibi, U. Delabre, and J. P. Delville. Conical Interfaces between Two Immiscible Fluids Induced by an Optical Laser Beam. *Physical Review Letters*, 122(17), May 2019. 22

[65] Didi Derks, Hans Wisman, Alfons van Blaaderen, and Arnout Imhof. Confocal microscopy of colloidal dispersions in shear flow using a counter-rotating cone–plate shear cell. *Journal of Physics: Condensed Matter*, 16(38):S3917–S3927, September 2004. 22

[66] Ludovic Berthier and Jean-Louis Barrat. Nonequilibrium dynamics and fluctuation-dissipation relation in a sheared fluid. *The Journal of Chemical Physics*, 116(14):6228–6242, April 2002. 22

[67] Ludovic Berthier and Jean-Louis Barrat. Shearing a Glassy Material: Numerical Tests of Nonequilibrium Mode-Coupling Approaches and Experimental Proposals. *Physical Review Letters*, 89(9), August 2002. 22

[68] Kwan-tai Leung and John L. Cardy. Field theory of critical behavior in a driven diffusive system. *Journal of Statistical Physics*, 44(3-4):567–588, August 1986. 22

[69] Alan J Bray and Andrea Cavagna. Coarsening dynamics of a nonconserved field advected by a uniform shear flow. *Journal of Physics A: Mathematical and General*, 33(33):L305–L311, August 2000. 22

[70] Marine Thiébaud and Thomas Bickel. Nonequilibrium fluctuations of an interface under shear. *Physical Review E*, 81(3), March 2010. 22, 70

[71] Thomas HR Smith. *Driven interfaces in the Ising model*. PhD thesis, University of Bristol, 2010. 22

[72] Thomas H. R. Smith, Oleg Vasilyev, Douglas B. Abraham, Anna Maciołek, and Matthias Schmidt. Interfaces in Driven Ising Models: Shear Enhances Confinement. *Physical Review Letters*, 101(6):067203, August 2008. 22, 24, 61, 78, 80

[73] Thomas H R Smith, Oleg Vasilyev, Douglas B Abraham, Anna Maciołek, and Matthias Schmidt. Interfaces in confined Ising models: Kawasaki, Glauber and sheared dynamics. *Journal of Physics: Condensed Matter*, 20(49):494237, December 2008. 22, 69, 70

[74] V. Privman and N. M. Švrakić. Asymptotic degeneracy of the transfer matrix spectrum for systems with interfaces: Relation to surface stiffness and step free energy. *Journal of Statistical Physics*, 54(3-4):735–754, February 1989. 24

[75] Nicholas Metropolis and S. Ulam. The Monte Carlo Method. *Journal of the American Statistical Association*, 44(247):335–341, September 1949. 25, 34, 61, 64, 67

[76] S. Wansleben and D. P. Landau. Monte Carlo investigation of critical dynamics in the three-dimensional Ising model. *Physical Review B*, 43(7):6006–6014, March 1991. 26

[77] Roy J. Glauber. Time-Dependent Statistics of the Ising Model. *Journal of Mathematical Physics*, 4(2):294–307, February 1963. 27, 34

[78] Kyozi Kawasaki. Diffusion Constants near the Critical Point for Time-Dependent Ising Models. I. *Physical Review*, 145(1):224–230, May 1966. 29, 34

[79] Martin Ankerl. Fast random bool in C++. https://martin.ankerl.com/2018/12/08/fast-random-bool/. 33

[80] Richard Feynman. Feynman Lectures on Physics, Mainly Electromagnetism and Matter., 1963. 35

[81] Cosima Stubenrauch and Regine von Klitzing. Disjoining pressure in thin liquid foam and emulsion films—new concepts and perspectives. *Journal of Physics: Condensed Matter*, 15(27):R1197–R1232, July 2003. 36

[82] B. Carazza and G. P. Guidetti. The Casimir Electron Model. *Archive for History of Exact Sciences*, 35(3):273–279, 1986. 37

[83] Timothy H. Boyer. Quantum Electromagnetic Zero-Point Energy of a Conducting Spherical Shell and the Casimir Model for a Charged Particle. *Physical Review*, 174(5):1764–1776, October 1968. 37

[84] Kimball A. Milton, Lester L. DeRaad, and Julian Schwinger. Casimir self-stress on a perfectly conducting spherical shell. *Annals of Physics*, 115(2):388–403, October 1978. 37

[85] M. E. Bowers and C. R. Hagen. Casimir energy of a spherical shell. *Physical Review D*, 59(2), December 1998. 37

[86] Julian Schwinger, Lester L DeRaad, and Kimball A. Milton. Casimir Effect in Dielectrics. *Annals of Physics*, pages 1–23, 1978. 38

[87] J. Schwinger. Casimir energy for dielectrics. *Proceedings of the National Academy of Sciences*, 89(9):4091–4093, May 1992. 38

[88] S.M. Rytov, Yu A. Kravtsov, and V.I. Tatarskii. *Principles of Statistical Radiophysics Vol 3*. Elements of Random Fields. Springer, Berlin, 1989. 38, 60

[89] N.G. Van Kampen, B.R.A. Nijboer, and K. Schram. On the macroscopic theory of Van der Waals forces. *Physics Letters A*, 26(7):307–308, February 1968. 38

[90] B W Ninham and V A Parsegian. van der Waals Forces. 10:18, 1970. 38

[91] A. Gambassi, A. Maciołek, C. Hertlein, U. Nellen, L. Helden, C. Bechinger, and S. Dietrich. Critical Casimir effect in classical binary liquid mixtures. *Physical Review E*, 80(6), December 2009. 42

[92] H. Kleinert. *Path Integrals in Quantum Mechanics, Statistics, Polymer Physics, and Financial Markets*. World Scientific, Singapore, 5th edition, 2009. 42

[93] Claude Cohen-Tannoudji, Bernard Diu, and Franck Laloë. *Mécanique quantique*, volume 1. EDP-Sciences, 2018. 44

[94] J R Albright. Integrals of products of Airy functions. *Journal of Physics A: Mathematical and General*, 10(4):485–490, April 1977. 48

[95] Rodrigo Bissacot and Leandro Cioletti. Phase Transition in Ferromagnetic Ising Models with Non-uniform External Magnetic Fields. *Journal of Statistical Physics*, 139(5):769–778, June 2010. 52

[96] R. A. Guyer. Sine-Gordon chain as a model for a two-dimensional interface. *Physical Review B*, 20(10):4375–4381, November 1979. 54, 56, 61

[97] N. M. Švrakić, V. Privman, and D. B. Abraham. Finite-size corrections for inclined interfaces in two dimensions: Exact results for Ising and solid-on-solid models. *Journal of Statistical Physics*, 53(5-6):1041–1059, December 1988. 54, 58, 60

[98] V. Privman and N. M. Švrakić. Finite-size scaling for the restricted solid-on-solid model of the two-dimensional wetting transition. *Physical Review B*, 37(7):3713–3715, March 1988. 54

[99] G.H. Gilmer and P. Bennema. Computer simulation of crystal surface structure and growth kinetics. *Journal of Crystal Growth*, 13-14:148–153, May 1972. 61, 67

[100] H H. Müller-Krumbhaar. Kinetic Gaussian model. *Zeitschrift für Physik B*, 25:287–292, 1976. 61

[101] C.F. Baillie, W. Janke, and D.A. Johnston. Solid on solid on fluid lattices. *Physics Letters B*, 318(3):424–432, December 1993. 61

[102] B Schmittmann and R.K.P Zia. Driven diffusive systems. An introduction and recent developments. *Physics Reports*, 301(1-3):45–64, July 1998. 61, 70

[103] Melanie Müller and Gernot Münster. Profile and Width of Rough Interfaces. *Journal of Statistical Physics*, 118(3-4):669–686, February 2005. 61

[104] Thomas H. R. Smith, Oleg Vasilyev, Anna Maciołek, and Matthias Schmidt. Lateral transport of thermal capillary waves. *EPL (Europhysics Letters)*, 89(1):10006, 2010. 61, 69, 70, 78, 80

[105] H. N. V. Temperley. Statistical mechanics and the partition of numbers II. The form of crystal surfaces. *Mathematical Proceedings of the Cambridge Philosophical Society*, 48(4):683–697, October 1952. 61, 67

[106] T. W. Burkhardt. Localisation-delocalisation transition in a solid-on-solid model with a pinning potential. *Journal of Physics A: Mathematical and General*, 14(3):L63, 1981. 62

[107] S. T. Chui and John D. Weeks. Pinning and roughening of one-dimensional models of interfaces and steps. *Physical Review B*, 23(5):2438–2441, March 1981. 62, 67

[108] C. K. Wang, J. J. Seaborg, and S. P. Lin. Instability of multi-layered liquid films. *Physics of Fluids*, 21(10):1669, 1978. 64

[109] M. Bonizzi and R.I. Issa. On the simulation of three-phase slug flow in nearly horizontal pipes using the multi-fluid model. *International Journal of Multiphase Flow*, 29(11):1719–1747, November 2003. 64

[110] Andrea Crisanti, Massimo Falcioni, Antonello Provenzale, Paolo Tanga, and Angelo Vulpiani. Dynamics of passively advected impurities in simple two-dimensional flow models. *Physics of Fluids A: Fluid Dynamics*, 4(8):1805–1820, August 1992. 66

[111] W. Dieterich, P. Fulde, and I. Peschel. Theoretical models for superionic conductors. *Advances in Physics*, 29(3):527–605, June 1980. 66

[112] Sheldon Katz, Joel L. Lebowitz, and Herbert Spohn. Nonequilibrium steady states of stochastic lattice gas models of fast ionic conductors. *Journal of Statistical Physics*, 34(3-4):497–537, February 1984. 66, 70

[113] A. Y. Grosberg and J.-F. Joanny. Nonequilibrium statistical mechanics of mixtures of particles in contact with different thermostats. *Physical Review E*, 92(3), September 2015. 66, 76

[114] Lars Onsager, Hemmer P.C., and Holden H. *The Collected Works of Lars Onsager: With Commentary*, volume 17. World Scientific, world scientific series in 20th century physics edition, 1996. 69, 76

[115] J. Dzubiella, G. P. Hoffmann, and H. Löwen. Lane formation in colloidal mixtures driven by an external field. *Physical Review E*, 65(2), January 2002. 69

[116] J Chakrabarti, J Dzubiella, and H Löwen. Dynamical instability in driven colloids. *Europhysics Letters (EPL)*, 61(3):415–421, February 2003. 69

[117] J. Chakrabarti, J. Dzubiella, and H. Löwen. Reentrance effect in the lane formation of driven colloids. *Physical Review E*, 70(1), July 2004. 69

[118] K. R. Sütterlin, A. Wysocki, A. V. Ivlev, C. Räth, H. M. Thomas, M. Rubin-Zuzic, W. J. Goedheer, V. E. Fortov, A. M. Lipaev, V. I. Molotkov, O. F. Petrov, G. E. Morfill, and H. Löwen. Dynamics of Lane Formation in Driven Binary Complex Plasmas. *Physical Review Letters*, 102(8), February 2009. 69

[119] T Glanz and H Löwen. The nature of the laning transition in two dimensions. *Journal of Physics: Condensed Matter*, 24(46):464114, November 2012. 69

[120] Katherine Klymko, Phillip L. Geissler, and Stephen Whitelam. Microscopic origin and macroscopic implications of lane formation in mixtures of oppositely driven particles. *Physical Review E*, 94(2), August 2016. 69

[121] V. Démery and D. S. Dean. The conductivity of strong electrolytes from stochastic density functional theory. *Journal of Statistical Mechanics: Theory and Experiment*, 2016(2):023106, 2016. 69, 76

[122] Alexis Poncet, Olivier Bénichou, Vincent Démery, and Gleb Oshanin. Universal Long Ranged Correlations in Driven Binary Mixtures. *Physical Review Letters*, 118(11), March 2017. 69

[123] D S Dean, I T Drummond, and R R Horgan. Renormalization of drift and diffusivity in random gradient flows. *Journal of Physics A: Mathematical and General*, 29(24):7867–7879, December 1996. 69

[124] R K P Zia and K T Leung. Interfacial correlation and dispersion in a non-equilibrium steady state system. *Journal of Physics A: Mathematical and General*, 24(24):L1399–L1404, December 1991. 70, 77

[125] K T Leung and R K P Zia. Anomalous interfacial correlations in non-equilibrium anisotropic systems. *Journal of Physics A: Mathematical and General*, 26(16):L737–L741, August 1993. 70, 76

[126] Marine Thiébaud, Yacine Amarouchene, and Thomas Bickel. Nonlinear Brownian dynamics of interfacial fluctuations in a shear flow. *Journal of Statistical Mechanics: Theory and Experiment*, 2014(12):P12011, December 2014. 70

[127] David S. Dean, Bing-Sui Lu, A. C. Maggs, and Rudolf Podgornik. Nonequilibrium Tuning of the Thermal Casimir Effect. *Physical Review Letters*, 116(24), June 2016. 76

[128] B.-S. Lu, D. S. Dean, and R. Podgornik. Out-of-equilibrium thermal Casimir effect between Brownian conducting plates. *EPL (Europhysics Letters)*, 112(2):20001, October 2015. 77

[129] N. Maat, C. Kraan, and W. A. Oost. The roughness of wind waves. *Boundary-Layer Meteorology*, 54(1-2):89–103, January 1991. 80